Model-based and data-driven approaches to complex systems: novel methods for psychology

Italian National Ph.D. Program in Autonomous Systems

ACADEMIC DISCIPLINE: SYSTEMS AND CONTROL ENGINEERING (IINF-04/A)

Final Dissertation

Model-based and Data-driven Approaches to Complex Systems: Novel Methods for Psychology

---

by

Eleonora Vitanza

Administrative Headquarters:

Politecnico di Bari – Department of Electrical and Information Engineering

Hosting University:

University of Siena – Department of Information Engineering and Mathematics

Referees:

Prof. Fernando A. López Hernández

Prof. Han L. J. Van Der Maas

Supervisors:

Prof. Chiara Mocenni

Prof. Domenico Prattichizzo

Coordinator of Ph.D Program

Prof. Mariagrazia Dotoli

Course no. 38, 01/11/2022-31/10/2025

LIBERATORIA PER L'ARCHIVIAZIONE DELLA TESI DI DOTTORATO

Al Magnifico Rettore
del Politecnico di Bari

Il/la sottoscritto/a Vitanza Eleonora nato/a a Catania il 29/10/1996
residente a San Giovanni La Punta (CT) in via Etna 11/A e-mail eleonoravitanza@gmail.com
iscritto al 3° anno di Corso di Dottorato di Ricerca in Autonomous Systems ciclo 38 ed essendo stato ammesso a sostenere l'esame finale con la prevista discussione della tesi dal titolo:
Model-based and Data-driven Approaches to Complex Systems: Novel Methods for Psychology

---

DICHIARA

1) di essere consapevole che, ai sensi del D.P.R. n. 445 del 28.12.2000, le dichiarazioni mendaci, la falsità negli atti e l'uso di atti falsi sono puniti ai sensi del codice penale e delle Leggi speciali in materia, e che nel caso ricorressero dette ipotesi, decade fin dall'inizio e senza necessità di nessuna formalità dai benefici conseguenti al provvedimento emanato sulla base di tali dichiarazioni;
2) di essere iscritto al Corso di Dottorato di ricerca in Autonomous Systems ciclo 38, corso attivato ai sensi del "*Regolamento dei Corsi di Dottorato di ricerca del Politecnico di Bari"*, emanato con D.R. n.286 del 01.07.2013;
3) di essere pienamente a conoscenza delle disposizioni contenute nel predetto Regolamento in merito alla procedura di deposito, pubblicazione e autoarchiviazione della tesi di dottorato nell'Archivio Istituzionale ad accesso aperto alla letteratura scientifica;
4) di essere consapevole che attraverso l'autoarchiviazione delle tesi nell'Archivio Istituzionale ad accesso aperto alla letteratura scientifica del Politecnico di Bari (IRIS-POLIBA), l'Ateneo archivierà e renderà consultabile in rete (nel rispetto della Policy di Ateneo di cui al D.R. 642 del 13.11.2015) il testo completo della tesi di dottorato, fatta salva la possibilità di sottoscrizione di apposite licenze per le relative condizioni di utilizzo (di cui al sito http://www.creativecommons.it/Licenze), e fatte salve, altresì, le eventuali esigenze di "embargo", legate a strette considerazioni sulla tutelabilità e sfruttamento industriale/commerciale dei contenuti della tesi, da rappresentarsi mediante compilazione e sottoscrizione del modulo in calce
(Richiesta di embargo);
5) che la tesi da depositare in IRIS-POLIBA, in formato digitale (PDF/A) sarà del tutto identica a quelle **consegnate**/inviate/da inviarsi ai componenti della commissione per l'esame finale e a qualsiasi altra copia depositata presso gli Uffici del Politecnico di Bari in forma cartacea o digitale, ovvero a quella da discutere in sede di esame finale, a quella da depositare, a cura dell'Ateneo, presso le Biblioteche Nazionali Centrali di Roma e Firenze e presso tutti gli Uffici competenti per legge al momento del deposito stesso, e che di conseguenza va esclusa qualsiasi responsabilità del Politecnico di Bari per quanto riguarda eventuali errori, imprecisioni o omissioni nei contenuti della tesi;
6) che il contenuto e l'organizzazione della tesi è opera originale realizzata dal sottoscritto e non compromette in alcun modo i diritti di terzi, ivi compresi quelli relativi alla sicurezza dei dati personali; che pertanto il Politecnico di Bari ed i suoi funzionari sono in ogni caso esenti da responsabilità di qualsivoglia natura: civile, amministrativa e penale e saranno dal sottoscritto tenuti indenni da qualsiasi richiesta o rivendicazione da parte di terzi;
7) che il contenuto della tesi non infrange in alcun modo il diritto d'Autore né gli obblighi connessi alla salvaguardia di diritti morali od economici di altri autori o di altri aventi diritto, sia per testi, immagini, foto, tabelle, o altre parti di cui la tesi è composta.

Luogo e data Bari, 15/01/2026 Firma _____

Il/La sottoscritto, con l'autoarchiviazione della propria tesi di dottorato nell'Archivio Istituzionale ad accesso aperto del Politecnico di Bari (POLIBA-IRIS), pur mantenendo su di essa tutti i diritti d'autore, morali ed economici, ai sensi della normativa vigente (Legge 633/1941 e ss.mm.ii.),

CONCEDE

- al Politecnico di Bari il permesso di trasferire l'opera su qualsiasi supporto e di convertirla in qualsiasi formato al fine di una corretta conservazione nel tempo. Il Politecnico di Bari garantisce che non verrà effettuata alcuna modifica al contenuto e alla struttura dell'opera.
- al Politecnico di Bari la possibilità di riprodurre l'opera in più di una copia per fini di sicurezza, back-up e conservazione.

Luogo e data Bari, 15/01/2026 Firma _____

Eleonora Vitanza

Model-based and Data-driven Approaches to Complex Systems: Novel Methods for Psychology

Thesis submitted for the degree of Philosophiae Doctor

Italian National Ph.D. Program in Autonomous Systems
University of Siena

Tutor
Professor *Chiara Mocenni*
Co-tutor
Professor *Domenico Prattichizzo*

2026

The doctoral scholarship was funded by the European Union - Next Generation EU, Project ECS00000017 'Ecosistema dell'Innovazione' THE - Tuscany Health Ecosystem (Spoke 9: Robotics and Automation for Health).

Dissertation submitted for the degree of *Philosophiae Doctor*
Italian National Ph.D. Program in Autonomous Systems

Cycle:
38th

Administrative Headquarters:
Politecnico di Bari

Hosting University:
University of Siena

Title:
Model-based and Data-driven Approaches to Complex Systems: Novel Methods for Psychology

Ph.D Candidate:
Eleonora Vitanza, University of Siena (Siena, Italy)

Tutors:
Prof. Chiara Mocenni, University of Siena (Siena, Italy)
Prof. Domenico Prattichizzo, University of Siena (Siena, Italy)

Coordinator:
Prof. Engr. Mariagrazia Dotoli, Politecnico di Bari (Bari, Italy)

External Reviewers:
Prof. Fernando A. López-Hernández, Polytechnic University of Cartagena (Cartagena, Spain)
Prof. Han L. J. Van Der Maas, University of Amsterdam (Amsterdam, Netherlands)

Last version:
January 11, 2026

Abstract

This thesis explores both model-based and data-driven approaches to the analysis of complex systems, with a particular emphasis on innovative methodologies for the study of psychology. On the model-based side, the thesis investigates agent-based models and Markov models, presenting case studies in sustainability and climate change perception. These models illustrate how formal representations of interacting components can generate emergent phenomena and offer valuable insights into the dynamics of large-scale systems. On the data-driven side, the thesis examines machine learning techniques –clustering, prediction, classification– together with causal inference. Two empirical studies in extreme rainfall events analysis and air quality monitoring demonstrate how these methods identify complex patterns and improve predictive performance on longitudinal data. Recognizing that analyzing individual affect dynamics is key for understanding decision-making and human behavior, the methodological foundations previously developed are transferred to the field of psychology. First, a novel Markov model formalizes emotion regulation in individuals, with particular attention to the concept of egosyntonicity –the alignment between current and expected emotion– demonstrating that while it may provide short-term positive impacts, it may not always be beneficial in the long run. Second, a methodological pipeline is proposed for the study of mental disorders. Specifically, causal inference and machine learning are applied to longitudinal symptom data to capture nonlinear relationships among symptoms at both individual and group levels, and to improve the distinction between clinically similar disorders through complexity measures derived from time series. Overall, the findings suggest that complexity-rich methodologies provide a powerful framework for advancing research in psychology, and highlight a direction for computational social science—namely, linking idiographic affective dynamics to population-level models that instead often rely on reductionist assumptions.

The question is not whether intelligent machines can have any emotions, but whether machines can be intelligent without any emotions.
Marvin Minsky

Contents

List of Figures

List of Tables

Preface

This thesis is submitted in partial fulfillment of the requirements for the degree of *Philosophiae Doctor* in the Italian National Ph.D. Program in Autonomous Systems. The research was carried out between 2022 and 2025 at the Department of Information Engineering and Mathematics, University of Siena, under the supervision of Professor Chiara Mocenni and Professor Domenico Prattichizzo.

The dissertation reflects my interest in complex systems, combining both model-based and data-driven approaches applied to real-world scenarios, with novel applications in psychology and human behavior.

Academic visits to the University of Naples Federico II with Professor Pietro De Lellis and the University of Cartagena with Professor Manuel Ruiz Marín provided valuable collaborations and greatly enriched this experience.

This journey has been both professionally and personally rewarding, and I am grateful for the opportunities and challenges that shaped my growth as a researcher.

The list of publications written by the author is listed below.

List of Papers Written by the Author

International Journal Articles

[1] Vitanza, E., Dimitri, G. M., and Mocenni, C., "A multi-modal machine learning approach to detect extreme rainfall events in sicily," *Scientific Reports*, vol. 13, no. 1, p. 6196, 2023. DOI: 10.1038/s41598-023-33160-9.

[2] Socci, V., Vitanza, E., and Mocenni, C., "An agent-based model to foster citizens' sustainable behavior in the italian city of siena," *The European Physical Journal B*, vol. 98, no. 4, p. 72, 2025. DOI: 10.1140/epjb/s10051-025-00910-9.

[3] Dimitri, G. M., Parri, L., Vitanza, E., Pozzebon, A., Fort, A., and Mocenni, C., "Weair: Wearable swarm sensors for air quality monitoring to foster citizens' awareness of climate change," *Computer Standards & Interfaces*, vol. 94, p. 104 004, 2025. DOI: 10.1016/j.csi.2025.104004.

[4] Vitanza, E., Mocenni, C., and De Lellis, P., "Egosyntonicity and emotion regulation: A probabilistic model of valence dynamics," *Royal Society Open Science*, vol. 12, no. 9, p. 250 062, 2025. DOI: 10.1098/rsos.250062.

[5] Vitanza, E., De Lellis, P., Mocenni, C., and Marin, M. R., "Complex dynamics in psychological data: Mapping individual symptom trajectories to group-level patterns," *Behavior Research Methods*, 2025, Under review (minor revision). DOI: 10.48550/arXiv.2507.14161.

International Conference Proceedings

[6] Dimitri, G., Parri, L., Pozzebon, A., Vitanza, E., Fort, A., Mocenni, C., *et al.*, "Weair: Wearable swarm sensors for air quality monitoring to foster citizens' awareness of climate change," in *Proceedings of 2023 IEEE International Conference on Metrology for eXtended Reality, Artificial Intelligence and Neural Engineering*, IEEE, 2023, pp. 98–103. DOI: 10.1109/MetroXRAINE58569.2023.10405724.

[7] Vitanza, E., Dimitri, G., Bizzarri, F., Mocenni, C., *et al.*, "Investigating the impact of extreme rainfall events on individual perception of climate change," in *2023 International Symposium on Nonlinear Theory and Its Applications NOLTA2023*, 2023, pp. 202–205. DOI: 10.34385/proc.76.A5L-42.

Acknowledgements

First of all, I would like to express my deepest gratitude to my supervisors, Professors Chiara Mocenni and Domenico Prattichizzo, for this extraordinary opportunity for growth.

I extend my thanks to the DAUSY committee and the National Ph.D. Program in Autonomous Systems for providing me with this unique opportunity to grow as a researcher and as a person.

I also warmly thank Professor De Lellis for welcoming me in Naples and for being a constant and essential guide throughout this journey; Professor Ruiz Marin and his family for their extraordinary hospitality in Murcia; and Professor Pluchino for the stimulating conversations we've shared over the years.

I finally thank my family, friends and colleagues for all the support and encouragement they have given me over the years.

(in Italian) Desidero dedicare alcune righe alle persone ed esperienze che hanno reso questo viaggio così speciale. Affrontare questo dottorato è stata una sfida e una continua scoperta; in tre anni mi sembra di averne vissuti cento. Ho viaggiato tra Parigi, Como, Salvador de Bahia, Grosseto, Lipari, Exeter, Amsterdam; ognuno di questi viaggi mi ha segnato, sia a livello accademico che soprattutto umano. Ho poi abitato in quattro città totalmente diverse, assaporandone di ognuna ogni dettaglio, odore, sapore. Firenze, per l'aria di libertà che ho respirato e di cui avevo estremamente bisogno, perché in fondo "libertà è partecipazione"; Napoli, per avermi fatto vivere le esperienze più assurde della mia vita, tanto in positivo quanto in negativo, ed avermi fatto realizzare che "basta 'na jurnata 'e sole". Murcia, ed in generale la Spagna, per avermi fatto sentire più a casa che mai. Siena, per tutte le sfide che nel corso degli anni mi ha messo davanti e grazie alle quali sono cresciuta.

Ringrazio la mia famiglia, le radici che ogni giorno mi aiutano a costruire una vita serena, entusiasmante e felice: mia madre Rosa, per aver capito nel profondo; mio padre Salvo, per aver sentito nel profondo; mio fratello Andrea, per esserci sempre; i miei zii e cugini, per il supporto costante ad ogni mio viaggio ed avventura.

Un sentito grazie:

Al Dr. Cappellini, per avermi insegnato la differenza tra resistenza e resa.

A Rossana, per essere stata al mio fianco in questo cammino tortuoso.

A Emilia, per essere la sorella che non ho avuto.

A Giorgio, per gli audiolibri già fatti e per quelli che verranno.

Ai miei amici sparsi per il mondo: Sabrina, Giuliana, Modica, Michele, Zinna, Paola, Camilla, Naomi; per esserci stati sempre.

Ai miei amici e coinquilini di Firenze Cristina, Marco e Sara, per tutti i bei momenti condivisi e per l'aria di casa che siamo riusciti a creare.

Ad Andrea Giusti, alla sua famiglia, e a Susy, per avermi accolto con calore nella loro bellissima casa napoletana in uno dei momenti più bui: vi sarò per sempre grata.

A Piero, per essere stato il maestro di cui avevo bisogno, al tempo giusto nel luogo giusto.

A Manolo, por enseñarme a trabajar disfrutando y a disfrutar trabajando.

A Martina e la sua famiglia, per avermi fatta sentire finalmente un po' parte di Siena.

A Barbara, per avermi accolta e formata con pazienza ed entusiasmo nella critica figura di docente.

Ai miei colleghi Vittoria, Riccardo e Iacopo, per aver condiviso con me questo percorso così sfidante, sostenendoci a vicenda. Al mio collega Pierluigi, per aver condiviso la parte finale di questo percorso.

A Ruffi, per avermi insegnato che l'amore non ha nulla a che fare con il merito.

A me, per aver capito; per aver sentito.

Introduction

Chapter 1

Introduction to Complex Systems

What makes a system complex, and why should we care? Complex systems are broadly defined as systems composed of many interacting components, whose collective behavior cannot be easily inferred from the properties of the individual parts, exhibiting emergence, feedback loops, nonlinearity, and adaptive behavior [1], [2]. Interest in this field has grown rapidly since the late 20th century when theory, data, and computation started to reinforce one another: nonlinear dynamics and chaos revealed how simple deterministic rules can generate irregular, unpredictable trajectories [3]; agent-based and rule-based modeling provided computational laboratories for controlled simulation studies of adaptation, emergence and collective dynamics [4]; and network science offered a unifying language to map and analyze interdependence in biology, technology, and society [5]. From ecosystems and neural circuits to the internet, financial markets, and epidemic processes, researchers have documented nonlinearity, path dependence, and critical phenomena that defy purely reductionist approaches [6].

An essential feature of complex systems is that they are dynamical: their macroscopic patterns emerge from micro-level interactions unfolding over multiple, often entangled time scales, and the current state of the system is dependent on its past states. Thus, in order to study and model complex systems, time must be taken into account [7]. A complex-systems view is based on three primitives: (i) a networked substrate that specifies who interacts with whom (possibly weighted, multilayer, and time-varying); (ii) interaction rules that couple components through feedbacks and nonlinearities; and (iii) explicitly dynamical evolution, typically operating far from equilibrium [8], [9]. Building on these primitives, two broad methodological strategies emerge: model-based and data-driven.

Model-based approaches assume specific mechanisms that generate data (e.g., deterministic or stochastic differential equations, agent-based rules, conservation laws). They offer interpretability, counterfactual reasoning, and principled extrapolation when theory is approximately correct; but they can suffer from misspecification and identifiability issues [10]. Data-driven approaches instead prioritize predictive performance from observations, using flexible methods (e.g., kernel methods, deep and graph neural networks, causal inference). They excel when mechanisms are unknown and data are abundant, but may generalize poorly out of distribution and offer limited insight [11]. Choice depends on purpose and regime: model-based approaches are preferable when prior knowledge and interpretability are crucial or data are scarce; data-driven approaches are preferable when complexity overwhelms first-principles modeling or when rapid, accurate prediction is paramount.

The complexity science perspective has proved fruitful in diverse domains. In biology, network and dynamical views explain stability and fragility in ecological communities and mutualisms, as well as modular motifs in gene regulation [12]. In physics, complex-systems tools illuminate critical phenomena, self-organization, and synchronization, linking microscopic interactions to macroscopic laws [13]. In economics and finance, production and financial networks mediate aggregate fluctuations and systemic risk, complementing traditional equilibrium models [14]. In computer science and engineering, principles of distributed interaction underpin swarm intelligence, consensus, and resilient coordination in large-scale cyber-physical systems [15].

1.1 Motivation

Complexity science has also reshaped how we study human behavior, especially at the social or group-level [16]. Network models, opinion dynamics, and collective decision-

making have clarified how local interactions scale up to population-level patterns such as cascades, polarization, and coordination [17]. By contrast, the individual level has received comparatively less sustained attention in the complex-systems canon, despite long-standing calls to bridge scales [18].

As an example, cognition itself is naturally framed as a complex system. Rather than a linear pipeline, cognitive function emerges from the nonlinear interaction of perception, memory, attention, affect, and action across multiple time scales [19], [20]. Network neuroscience further supports this view: flexible, transient coalitions of brain regions (modules, hubs, and motifs) coordinate via metastable dynamics to support adaptive behavior [21], [22]. Such systems can display sudden reorganizations—insight, affective shifts, or breakdowns—consistent with dynamical transitions and early-warning signals [23], [24]. Moreover, affect and behavior exhibit inertia, feedback, and context sensitivity at short time scales. These properties indicate that affective and behavioral processes are fundamentally nonstationary [25].

Methodologically, model-based tools (e.g., dynamical systems, Markov models, agent-based models) provide interpretable hypotheses about mechanisms and permit counterfactuals; yet, idiographic dynamical models remain underdeveloped, reflecting both the historical scarcity of data sufficient for rigorous validation and the lack of connection with the individual-level qualitative theories to guide modeling when such data are unavailable.

Data-driven tools (e.g., regression, decision trees, clustering, dimensionality reduction, neural networks) exploit high-dimensional observations for prediction and discovery. Nevertheless, data at the necessary temporal resolution have historically been scarce, and empirical work has tended to privilege between-person aggregates over within-person dynamics [26].

Traditional reductionist approaches in the social sciences often compress individuals into static points, averaging across time or across people. Such simplifications overlook the feedbacks, memory, and transient episodes that are intrinsic to human dynamics. In other words, reductionism filters out precisely the nonlinear and context-sensitive features that define complex behaviors. From a complex-systems perspective, however, the individual is not noise to be averaged away but a dynamical unit whose trajectories matter. Capturing these idiographic dynamics is conceptually indispensable: without it, the bridge between micro-level processes and macro-level phenomena remains incomplete. Additionally, mobile sensing and digital traces have recently made it feasible to collect dense, longitudinal records of feelings and behaviors, enabling the investigation of idiographic dynamics at scale [27]. These considerations motivate the contributions of this thesis detailed section 1.3.

1.2 Complex Systems in Psychology

The complex-systems and network-oriented view has recently gained particular traction in psychology. Denny Borsboom and colleagues, for example, have proposed conceptualizing mental disorders as emergent properties of interacting symptoms rather than as manifestations of latent disease entities [28]. In this framework, symptoms such as insomnia, fatigue, and low mood are not merely passive indicators but active components of a network that influence one another bidirectionally over time, potentially leading to self-sustaining pathological states. Building on this foundation, recent contributions extend network models toward within-person dynamics and individual tailoring, moving beyond cross-sectional associations.

To study psychological phenomena as processes, the first step is to capture measurements over time, for instance through experience sampling methods (ESM) or ecological momentary assessment (EMA). These methods provide dense longitudinal data, making it possible to investigate bridges between syndromes or to develop methods that explicitly target moment-to-moment dependencies at the individual level [29], [30].

Emotions represent a paradigmatic example of dynamical processes: they participate in an adaptive feedback loop in which situations shape perception, perception elicits emotions, and emotions drive actions that reconfigure subsequent situations. Affective states fluctuate across multiple time scales and display inertia and context-sensitive feedback. Capturing these moment-to-moment changes is essential for explaining micro-level psychological phenomena. In this vein, Ryan et al. present a generative model of emotion dynamics, formalizing the link from situations to emotional responses within individuals [31].

It is important to emphasize, however, that these psychological and affective frameworks complement, rather than replace, neuroscientific perspectives [32]. In fact, while the underlying neural mechanisms provide the biological substrate for cognition and emotion, the complex systems approach to psychology highlights an additional level of description: the emergent patterns of interaction among psychological components themselves. This systems-level perspective offers valuable insights into how mental phenomena can arise, stabilize, and transform within individuals over time.

Despite rapid progress, much remains to be done. Open problems include formalizing theoretical psychological frameworks through mathematical modeling, achieving reliable causal identification and validation of relationships among symptoms, connecting group and individual-level structures, and establishing robust reporting and replication standards [33], [34]. These open problems frame the contributions detailed in the next section.

1.3 Contributions

This thesis advances the study of complex systems through two main complementary contributions. On the one side, it investigates model-based and data-driven methods across domains where complexity science is already a recognized lens. On the other side, it focuses on psychological dynamics, a comparatively underexplored area, applying state-of-the-art methodologies at the individual level and bridging to group-level inference.

The first part deepens both model-based and data-driven approaches through four case studies, selecting the most suitable mathematical tools case by case. It addresses the following research questions:

- **RQ1:** What is the role of citizens and their knowledge, opinions, awareness and experience on sustainability?
- **RQ2:** How do individuals' perceptions of climate change evolve over time, and what factors drive these trajectories?
- **RQ3:** Can extreme rainfall areas be detected by clustering spatio-temporal rainfall data?
- **RQ4:** Can a swarm of wearable air-quality sensors, integrated with neural networks, predict optimal geo-locations for monitoring?

The studies developed here first serve as a methodological training ground and second suggest that cognitive and affective components are integral to decision making and human behavior even in sustainability and climate contexts—thus motivating a shift to the study of psychological dynamics in the second part.

The second part targets the core contribution: applying complex-systems methodologies to psychological processes, combining model-based and data-driven analyses at the individual level and aggregating to the group-level. It addresses:

- **RQ5:** How emotions evolve over time, and how these processes can lead to adaptive or maladaptive patterns?
- **RQ6:** Is egosyntonicity invariably beneficial as a strategy for emotion regulation, or can it incur long-run costs?
- **RQ7:** Is it possible to infer individual-level nonlinear causal relationships among symptom time series?

- **RQ8:** Can idiographic findings be generalized to the group-level without erasing individual heterogeneity?
- **RQ9:** Can classification of mental disorders that share common symptoms be improved by leveraging complexity measures of symptom time series?

By focusing on temporal dynamics, this thesis aspires to provide a richer understanding of human affect and mental disorders as complex, adaptive systems, and to demonstrate how modern analytical tools can uncover hidden structures and transitions within these processes.

1.4 Outline

The thesis is organized into two main parts. Part I includes chapters 2 and 3 and illustrates how the model-based and data-driven approaches employed throughout the thesis can be utilized in testbed applications. Specifically, chapter 2 develops two model-based frameworks. First, an agent-based model grounded on graph theory and game theory explores the sustainability propensity of citizens on social networks over time, answering RQ1 [35]. Second, a Markov modeling approach is introduced to investigate individual differences in the perception of extreme rainfall events, with the goal of characterizing cognitive pathways that lead to adaptive or maladaptive responses, answering RQ2 [36]. Additional information about chapter 2 are provided in Appendix A.

Chapter 3 turns to data-driven studies. It employs machine learning to analyze patterns in extreme rainfall, assessing whether spatio-temporal clustering can detect areas prone to extreme events (RQ3) [37]. The chapter also introduces wearable swarm sensors for air-quality monitoring, integrating spatio-temporal data with neural networks to predict optimal geo-locations (RQ4) [38]. Supplementary details of the chapter are collected in Appendix B.

Part II includes chapters 4 and 5 and advances novel complex methodologies for psychology. Chapter 4 provides a model-based formalization of emotion-regulation dynamics by presenting a Markov model based on the concept of egosyntonicity [39]. This chapter addresses questions RQ5–RQ6.

Chapter 5 presents a data-driven pipeline for studying mental disorders, using Generalized Anxiety Disorder and Major Depressive Disorder as case studies. In particular, it applies modern state-of-the-art methods to recover nonlinear, individual-level causal relationships among symptom time series and then aggregates idiographic structures to the group-level, addressing RQ7 and RQ8. Finally, it evaluates whether disorders with overlapping symptoms can be classified by leveraging complex dynamics analysis (RQ9) [40]. This chapter is complemented by Appendix C.

Chapter 6 concludes the thesis, summarizing contributions, limitations, and avenues for future research.

I Model-based and Data-driven Approaches to Complex Systems

Chapter 2

Model-based Approaches to Complex Systems

II

Contents

Models are simplified representations of reality that help us understand, simulate, and predict the behavior of (complex) systems. While they necessarily abstract certain elements, they remain essential tools in both theoretical and applied research.

In this Chapter, I present a selection of model-based methods explored and applied during this thesis. The next section introduces two modeling approaches: agent-based models and Markov models. These are chosen for their flexibility and relevance in contexts involving human behavior and decision making. The following two sections explain two applications: an agent-based model on sustainable behavior (RQ1) and a Markov decision process addressing climate change perception (RQ2). These preliminary studies helped me prepare for the main contribution of this thesis on model-based approaches in the novel and sensitive domain of psychology, which is discussed in Chapter 4. This Chapter also has an associated Appendix A with additional material and details.

2.1 Model-based Methods

There are many ways to model complex systems. In this section, I focus on two widely used approaches: agent-based models and Markov models. These are selected based on their suitability for representing both individual and collective behavior in systems where decision making, interaction, probabilistic transitions, as well as temporal dynamics, play a key role. The goal here is not to provide an exhaustive review of all model-based methods but to give an overview of those most relevant to the work carried out in this thesis.

2.1.1 Agent-based Models

Agent-based modeling is a computational modeling technique used to study the collective behavior of complex systems, such as groups of individuals or autonomous decision making agents interacting with each other and their environment. An agent-based model (ABM) is thus a particular type of model where agents are represented as autonomous and unique entities endowed with certain attributes and make decisions on some issue according to specific behavioral rules.

The agents of an ABM generally exhibit adaptive behavior, since they regulate their actions and decisions according to their current states, those of other agents, and of the environment. Hence, in agent-based modeling, instead of describing a system from a macroscopic level as we do with approaches using differential equations, we describe the system from a microscopic level by defining its individual agents in a bottom-up approach [41]–[44]. Consequently, an ABM allows both to understand how a system's behavior at the macroscopic level derives from the behaviors of individual agents at the microscopic

level and to grasp how the behaviors of individual agents are affected by the behavior of the system as a whole.

Additionally, while related to multi-agent systems in AI, ABMs typically prioritize explanatory and exploratory modeling of social or natural phenomena over task-oriented coordination or control, and are often less focused on optimality or centralized goals [45].

The main benefit of agent-based modeling is the ability to capture the emerging phenomena resulting from the interactions of individual entities with each other and with the environment [43]. Very often the patterns emerging at the macro-level depend on how individuals make decisions at the micro-level [46]. Therefore, representing human decision making, which can be defined as the cognitive process of making a choice from a number of alternative actions [47], in ABM is of primary importance.

ABMs are particularly well-suited for contexts in which heterogeneity among agents plays a significant role, where interactions are local or nonlinear, and where adaptation or learning influences behavior over time. They are also effective in settings requiring an explicit representation of space—through lattices, continuous fields, or geographic information systems (GIS)—or dynamic interaction networks that evolve as agents interact.

A basic ABM architecture consists of agents, an environment, and a scheduling mechanism. Agents are typically characterized by static attributes (such as age, type, or preferences in the case of individuals), an internal dynamic state, and often a memory of past experiences. The environment, which may be spatially explicit or abstract, shapes the context in which agents perceive and act. Interactions among agents may occur directly, or through network structures—static or dynamic—that define who can interact with whom. Stochasticity is commonly introduced in perception, behavior, or outcomes, and is usually controlled through the use of random seeds to ensure reproducibility.

Ultimately, agent-based models are particularly useful for exploring "what-if" scenarios. They give researchers the ability to test how varying assumptions or interventions could generate different results, especially in contexts where analytical solutions are difficult to obtain.

We now focus on the case in which the agents of the model are individuals. The decision making process of individuals can be described in many ways, depending on the context and the considered application. In DeAngelis and Diaz [48] the authors provide an overview of some of the ways in which decisions can be embedded in ABMs: from the use of simple logical rules (if-then) to more sophisticated learning mechanisms via neural networks and genetic algorithms. Decision making can also depend on social norms, peer influence, imitation, noisy perception and limited attention. Agents often operate under partial or biased information, which further enriches the behavioral landscape.

Decision-making processes are often described by Game Theory (GT) and Evolutionary Game Theory (EGT) [49], [50]. GT is a mathematical field dedicated to the study of social interactions between rational individuals whose decisions are interdependent, that is, the outcome of their choices depends not only on their own decisions but also on those of all the others [51]. EGT is an application of GT combining the principles of biological evolution with the analysis of strategic interactions [52]. Both GT and EGT have been recognized to be particularly suitable in modeling decision making processes, especially for the study of social interactions among rational individuals whose decisions are interdependent [51]. For instance, cooperation has been widely formulated and analyzed in the context of EGT [53]. The Prisoners' Dilemma (PD) game has been employed as a metaphor for examining cooperation among selfish individuals [54], while the Stag-Hunt (SH) and Hawk-Dove (HD) games represent herding and anti-herding mechanism, respectively [55], [56]. Further details about GT and games are available in Appendix A.

Another crucial point in ABMs is the integration of empirical data during either initialization, calibration, verification, or validation. Finally, the documentation and reproducibility of ABMs are supported by established standards such as the ODD (Overview, Design concepts, Details) protocol, which provides a structured framework to describe the purpose, mechanisms, and implementation of the model in a transparent and replicable manner [57].

While agent-based models offer valuable insights in contexts where classical approaches fail — for instance, in systems with strong heterogeneity that cannot be easily represented by differential equations — they also present some limitations: they often rely on simplified behavioral rules, may require strong assumptions about decision-making processes, and can be difficult to validate against real-world data.

2.1.2 Markov Models

I now describe the key properties of Markov models, the second model-based approach used in this thesis alongside agent-based modeling. Markov models are mathematical frameworks that are used to describe systems that evolve over time in a probabilistic manner. They are particularly suited for modeling dynamical systems where the future state depends only on the current state. Moreover, they provide a simple yet effective way to study complex systems by capturing their stochastic and time-dependent behavior.

In this section, we first introduce Markov chains, which model transitions between discrete states with fixed probabilities. We then move to Markov Decision Processes (MDPs), which extend this framework by incorporating actions and rewards, enabling the modeling of decision making under uncertainty.

These models are widely used thanks to their interpretability and flexibility in capturing stochastic dynamics across a variety of domains.

Markov Chains

Markov chains provide a rich framework for studying many discrete event systems (DES) of practical interest, ranging from gambling and the stock market to the design of high-tech computer systems and communication networks [58].

The main characteristic of Markov chains is that their stochastic behavior is described by transition probabilities of the form $P[X(t+1) = x' \mid X(t) = x]$ for all state values x, x'. Given these transition probabilities and a distribution for the initial state, it is possible — in principle— to determine the probability of being at any state at any time instant. However, in practice, this task can be very difficult, as it often involves the solution of complicated differential equations. Even though we would like to obtain general transient solutions, in most cases we have to settle for steady-state or stationary solutions, which describe the probability of being at any state in the long run only (after the system has been in operation for a sufficiently long period of time).

In a discrete-time Markov chain, events (and hence state transitions) are constrained to occur at discrete time instants $0, 1, 2, \ldots, t, \ldots$, thus forming a stochastic sequence $\{X_0, X_1, \ldots\}$ which is characterized by the Markov (memoryless) property:

$$P[X_{t+1} = x_{t+1} \mid X_t = x_t, X_{t-1} = x_{t-1}, \ldots, X_0 = x_0] = P[X_{t+1} = x_{t+1} \mid X_t = x_t] \quad (2.1)$$

Given the current state x_t, the value of the next state depends only on x_t and not on any past state. Moreover, the amount of time spent in the current state is irrelevant in determining the next state.

Definition 2.1.1 (*Markov chain*)

A Markov chain model is defined by:

1. *A state space X.*
2. *An initial state probability $p_0(x) = P[X_0 = x], \forall x \in X$.*
3. *Transition probabilities $p(x', x)$ where x is the current state and x' is the next state.*

□

Whenever the transition probability $p_{ij}(t)$ is independent of $t \quad \forall i, j \in X$, we obtain a homogeneous Markov chain.

The transition probability information for a discrete-time Markov chain is conveniently summarized in matrix form: $\boldsymbol{P} \equiv [p_{ij}],\ i, j = 0, 1, 2, \ldots$; observe that all elements of the i-th row in this matrix must always sum up to 1, since we are summing over all possible mutually exclusive events causing a transition from state i to some new state.

One of the main objectives of Markov chain analysis is the determination of probabilities of finding the chain at various states at specific time instants. We define state probabilities as $\pi_j(t) \equiv P[X_t = j]$. Accordingly, we define the state probability vector as a row vector $\boldsymbol{\pi}(t) = [\pi_0(t), \pi_1(t), \ldots]$, whose dimension is specified by the dimension of the state space X of the chain.

A discrete-time Markov chain model is completely specified if, in addition to the state space X and the transition probability matrix P, we also specify an initial state probability vector $\boldsymbol{\pi}(0) = [\pi_0(0), \pi_1(0), \ldots]$ which provides the probability distribution of the initial state, X_0, of the chain.

Transient analysis Once a Markov model is specified through X, P, and $\boldsymbol{\pi}(0)$, we can start addressing questions such as: What is the probability of moving from state i to state j in n steps? What is the probability of finding the chain at state i at time t? In answering such questions, we limit ourselves to given finite numbers of steps over which the chain is analyzed. This is what we refer to as transient analysis. Using the definitions of $\boldsymbol{\pi}(t)$ and $\boldsymbol{P}$ we get:

$$\boldsymbol{\pi}(t+1) = \boldsymbol{\pi}(t)\boldsymbol{P}, \quad t = 0, 1, \ldots, \tag{2.2}$$

which is equivalent to

$$\boldsymbol{\pi}(t) = \boldsymbol{\pi}(0)\boldsymbol{P}^t, \quad t = 1, 2, \ldots \tag{2.3}$$

Using such equations we can completely study the transient behavior of homogeneous discrete-time Markov chains.

In general, solving equations 2.2 or 2.3 to obtain $\boldsymbol{\pi}(t)$ for any t is not a simple task. As in classical system theory, where we resort to z-transform or Laplace transform techniques in order to obtain transient responses, a similar approach may be used here as well. The main result is that $\boldsymbol{P}^t$, which we need to calculate $\boldsymbol{\pi}(t)$ through equation 2.3, is the inverse z-transform of the matrix $[\boldsymbol{I} - z\boldsymbol{P}]^{-1}$, where $\boldsymbol{I}$ is the identity matrix.

Steady state analysis In steady state analysis we extend our inquiry to questions such as: What is the probability of finding a Markov chain at state i in the long run? By "long run" we mean that the system we are modeling as a Markov chain is allowed to operate for a sufficiently long period of time so that the state probabilities can reach some fixed values which no longer vary with time. This may or may not be achievable. Our study, therefore, centers around the quantities:

$$\pi_j = \lim_{t \to \infty} \pi_j(t), \tag{2.4}$$

where, $\pi_j(t) = P[X_t = j]$, and the existence of these limits is not always guaranteed. Thus, we need to address three basic questions:

1. Under what conditions do the limits in equation 2.4 exist?
2. If these limits exist, do they form a legitimate probability distribution, that is, $\sum_j \pi_j = 1$?
3. How do we evaluate π_j?

Definition 2.1.2 (*Steady state*)

If $\pi_j = \lim_{t\to\infty} \pi_j(t)$ exists for some state j, it is referred to as a steady-state, equilibrium, or stationary state probability. □

If $\pi_j = \lim_{t\to\infty} \pi_j(t)$ exists for all states j, then we obtain the stationary state probability vector $\boldsymbol{\pi} = [\pi_0, \pi_1, \dots]$. It is essential to keep in mind that the quantity reaching steady state is a state probability – not a state which of course remains a random variable.

It is often the case that after a long time period (i.e., large values of t) we have $\boldsymbol{\pi}(t+1) \approx \boldsymbol{\pi}(t)$. In other words, as $t \to \infty$ we get $\boldsymbol{\pi}(t) \to \boldsymbol{\pi}$, where $\boldsymbol{\pi}$ is the stationary state probability vector. This vector, if it exists, also defines the stationary probability distribution of the chain. Then, if indeed in the limit as $t \to \infty$ we get $\boldsymbol{\pi}(t+1) = \boldsymbol{\pi}(t) = \boldsymbol{\pi}$, we should be able to obtain $\boldsymbol{\pi}$ from equation 2.2 by solving a system of linear algebraic equations $\boldsymbol{\pi} = \boldsymbol{\pi}\boldsymbol{P}$, where the elements of $\boldsymbol{\pi}$ satisfy $\pi_j \geq 0$ and $\sum_j \pi_j = 1$.

Fortunately, as long as an irreducible Markov chain is not periodic, the limit of $\pi_j(t)$ as $t \to \infty$ always exists. The formal definitions and details can be found in Appendix A.

Theorem 2.1.1

In an irreducible aperiodic Markov chain the limits $\pi_j = \lim_{t\to\infty} \pi_j(t)$ always exist and they are independent of the initial state probability vector. □

Theorem 2.1.2

In an irreducible aperiodic Markov chain consisting of positive recurrent states a unique stationary state probability vector $\boldsymbol{\pi}$ exists such that $\pi_j > 0$ and $\pi_j = \lim_{t\to\infty} \pi_j(t) = \frac{1}{M_j}$, where M_j is the mean recurrence time of state j. The vector $\boldsymbol{\pi}$ is determined by solving:

$$\boldsymbol{\pi} = \boldsymbol{\pi}\boldsymbol{P}, \quad \sum_{all\ j} \pi_j = 1 \tag{2.5}$$

□

Note that every finite irreducible aperiodic Markov chain has a unique stationary state probability vector $\boldsymbol{\pi}$ determined through equation 2.5. In this case, obtaining $\boldsymbol{\pi}$ is simply a matter of solving a set of linear equations.

Thus, Markov chains offer both theoretical guarantees and computational tractability. Nevertheless, Markov chains have some limitations. First, the existence and uniqueness of steady states depend on relatively stringent conditions—such as irreducibility and aperiodicity—that may not always hold in empirical applications. Moreover, Markov chains rely on the assumption of memorylessness, which may lead to oversimplification of complex dynamics. This reflects a fundamental trade-off: compact representation versus structural information.

Markov Decision Processes

I now introduce the basics of Markov decision processes, which extend Markov chains by incorporating actions, rewards, and decision-making under uncertainty.

In order to introduce a Markov decision process related to a stochastic DES, three ingredients are needed: control actions taken when a state transition takes place, the cost (or reward) associated with such actions, and transition probabilities which may depend on control actions.

When a new state is entered, a control action u is selected from a known set U of possible control actions. There is a cost associated with the selection of a control action u at state i, and we denote this cost by $C(i, u)$. The nature of $C(i, u)$ plays a crucial role in the solution of the problems we will consider. The rule based on which control actions are chosen is called a policy. The only new element compared to Markov chain models is the fact that the transition probabilities $p_{ij}[u(i)]$ depend on the particular policy π that we wish to adopt. Our objective is to determine policies π which are "optimal" in some sense. Thus, we need to specify a cost criterion that we should seek to minimize (or a reward function that we want to maximize). There are several common forms of cost criteria, among which the total expected cost over a finite horizon, the total expected discounted cost over an infinite horizon, the total expected (undiscounted) cost over an

infinite horizon and the expected average cost. In any case, the cost $V_\pi(x_0)$ is specified with respect to a given initial state x_0, and the aim is to determine a policy π to minimize $V_\pi(x_0)$.

We can limit ourselves to discrete-time Markov chains, and, therefore, concentrate on a Markov chain $\{X_t\}$, $t = 0, 1, \ldots$ with transition probabilities $p_{ij}[u(i)]$, where the control actions $u(i)$ are determined according to a policy π. The process $\{X_t\}$ is what is commonly referred to as a Markov decision process (MDP).

Definition 2.1.3 (*Markov Decision Process*)

An MDP is a tuple $M = (S, U, P, C)$ where S is a finite set of possible states, U is a finite set of available control actions, $P : S \times S \times U \to [0, 1]$ is a transition probability function depending on current state and action chosen, and $C : S \times U \to R$ is a cost (or reward) function. □

As in Markov chains, in MDPs, the current state incorporates all the past of the Decision Maker (DM): it is the result of all their previous decisions, related outcomes, and experience gained.

We assume that at every state transition a cost $C(i, u)$ is incurred, where i is the state entered and u is a control action selected from a set of admissible actions U_i. Under a stationary policy π, the control u depends only on the state i. The next state is then determined according to transition probabilities $p_{ij}(u)$. We also assume that a discount factor δ, $0 < \delta < 1$, is given, and that an initial state is specified. We then define the cost criterion:

$$V_\pi(i) = \mathbb{E}_\pi \left[\sum_{t=0}^{\infty} \delta^t C(X_t, u_t) \right] \tag{2.6}$$

which is the total expected discounted cost accumulated over an infinite horizon, given the initial state i. Therefore, our Markov decision problem is to determine a policy π to minimize $V_\pi(i)$.

A fundamental solution technique for Markov decision problems is based on the concept of Dynamic Programming (DP) [59]. DP is guaranteed to converge to the optimal policy, however, due to the curse of dimensionality, it cannot be applied in high-dimensional problems. DP therefore provides the classical foundation for solving MDPs, although its direct use is restricted by computational intractability.

The rest of the Chapter is devoted to presenting two training applications of model-based approaches to complex systems. The first focuses on sustainable behavior by proposing an agent-based model, while the second applies a Markov decision process to the context of climate change. These studies served primarily as exploratory exercises, allowing me to gain familiarity with the methods before applying them to the main case study of the thesis, discussed in Chapters 4 and 5.

2.2 An Agent-based Model to Study Sustainable Behavior in the Italian City of Siena

This section summarizes and adapts the work presented in [35], which illustrates the development of an agent-based model aimed at investigating individual and collective patterns related to sustainable behavior (RQ1). This study is included as a methodological exercise that illustrates the potential of ABM in the analysis of sustainable behavior.

2.2.1 Introduction

What is the role of citizens and their knowledge, opinions, awareness and experience on climate change effects? Sustainable policies are more effective when supported by citizens' choices, for instance in the case of waste reduction. We thus focus on the micro-to-macro link between individual decisions and collective sustainability.

ABMs are particularly suitable in modeling environmental attitudes among people, as they represent complex systems where agents are autonomous entities interacting with each other and the environment [41]. ABMs have been widely applied to sociology and are powerful tools for examining agent-agent interaction and understanding how individual actions influence social outcomes [42]. This encourages the use of such models in the context of environmental sustainability, allowing to analyze how agent-agent and agent-environment interactions at the micro-level may or may not give rise to sustainable scenarios at the macro-level.

We build an ABM whose entities are residents of Siena (Tuscany, Italy). A survey (May–July 2023) collected attitudes toward climate change and sustainable practices; the dataset is used to parameterize the ABM and map five behavioral types.

Using (evolutionary) game-theoretic rules, we examine how cooperation— here interpreted as pro-environmental behavior—spreads and persists over time and space.

Preliminary survey results align with known patterns: the gap in climate awareness related to the educational level and the eco-gender gap phenomenon [60]–[64]. Surprisingly, results indicate that the youngest age class is not the most aware of climate change in Siena [65], [66]. The obtained dataset has been not only analyzed from a statistical point of view, but mainly used to tune our ABM on real local data. The model explores how these micro-level ingredients and network structure shape macro-level outcomes. The exploration of different scenarios suggest that the geographical and urbanistic features of the city itself may have a significant impact on this phenomenon.

2.2.2 Methods

Each agent chooses between two strategies at each iteration: cooperation (C) and defection (D), where cooperation is interpreted as pro-environmental behavior and vice versa.

We consider the iterated versions of three games, involving more than two players and multiple rounds: Prisoners' Dilemma (PD), Stag-Hunt (SH) and Hawk-Dove (HD). In the iterated version of (PD), an increase in the number of people cooperating proportionally raises the benefit for each of them. This assumption suggests that cooperation may lead to greater individual reward, thus encouraging players to cooperate with each other. For players who defect, their benefit is assumed to be given by an α factor multiplied by the number of people who cooperate, where the parameter $\alpha \in [0, 3]$ represents the benefit each player obtains from defection and it is called *defection-award*. This may reflect situations in which non-cooperators benefit from the actions of cooperators without contributing to the common good.

We identify five agent types through the survey, corresponding to the five games. Prisoners' Dilemma (PD), Stag-Hunt (SH) and Hawk-Dove (HD) players can change strategy at each iteration of the model and are called indifferent players. Activists (A) and deniers (D) agents always choose the same strategy at each time instant: cooperation (C) for the former and defection (D) for the latter.

Taking inspiration from an existing model, which explores how the behavior of agents positioned on a grid evolves as they play iterated (PD) with their neighbors [67], our model extends it by including also (SH), (HD), (A) and (D).

Specifically, results obtained from the survey enable us to both assess the climate awareness of the examined population and determine the number of agents in the sample belonging to each of the five categories (see Appendix A for details).

The purpose of the model is to understand under what conditions there is diffusion of sustainable practices among citizens.

Model Setup

The ABM is initially developed in a theoretical case, called the Basic Model, in which we assign to the agents all the attributes obtained from the survey except for the geographical position on the map of Siena. Thereafter, the ABM is fully adapted to our case study, the so called Siena model, in which the agents are georeferenced on the map of the city.

The Basic model simulates the behavior over sustainable practices of individuals living in a city with a prototypical regular structure. The ABM contains a total number of $N = 324$ agents positioned to form a 2-dimensional lattice of size 18×18. The agents in the model do not move and interactions among agents are represented by links.

All the agents belong to one of the five classes and never change it, thus having: 33 (A), 15 (D), 197 (PD), 45 (SH) and 34 (HD). The strategy selection of each player at each time step is described using colors (further details in Appendix A).

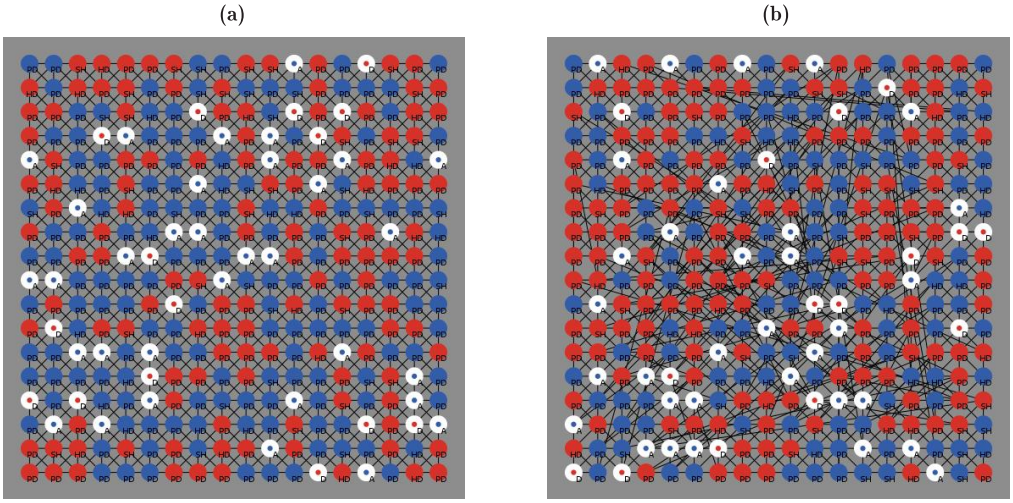

Figure 2.1: Basic model depicted at time $t = 0$ with $ic = 50\%$. (a) regular lattice; (b) small-world network. The type of each agent is represented by a label A, D, PD, SH or HD. Each agent of type (PD), (SH) and (HD) is initialized either as a cooperator (blue node) or a defector (red node). Activists (A) and deniers (D) are represented by white nodes with a blue and red central dot, respectively.

According to the survey, each agent in the model has discrete variables of *age*, *gender*, *educational level*, *awareness* $\in [1, 10]$ and *kind* $\in \{(\text{A}), (\text{D}), (\text{PD}), (\text{SH}), (\text{HD})\}$. The values of these variables are randomly initialized for each agent so that the percentages of each category found in the survey are fulfilled. Each agent has also associated the continuous variable *score*, which is assumed initially equal to 0 and free to change over time. In particular, let i be the i-th agent and let *total-cooperators* (tc) denote the total number of cooperating agents connected to agent i in the graph. Then, its *score* is updated according to the following rule [67]:

$$score(i) = \begin{cases} tc & \text{if agent } i \text{ cooperates} \\ \alpha \cdot tc & \text{if agent } i \text{ defects} \end{cases}, \tag{2.7}$$

where α is the *defection-award* parameter.

There are two other parameters in the model: *initial-cooperation* ($ic \in [0, 100]$), which establishes the percentage of cooperating indifferent agents at the initial time $t = 0$, and *SW-rewiring-prob* ($SW_{rp} \in [0, 1]$), the rewiring probability used to build a small-world graph starting from the regular lattice.

Specifically, we consider two different scenarios: a 2-dimensional regular lattice where each agent is connected to its 1-distance neighbors, obtained with $SWrp = 0$ (see Figure 2.1a); a small-world (SW) graph obtained from the regular one using a rewiring algorithm inspired by Watts and Strogatz's model and obtained with $SWrp = 0.05$ (see Figure 2.1b) [68]. In the first case we assumed to have a perfectly regular city or neighborhood where only geographical proximity connections are considered in the decision making process. In the second case, SW networks also consider social networks (e.g., friendships), and are therefore more suitable to represent social phenomena [69], [70].

Once the model has been set to its initial configuration, it is ready for execution. At each iteration, all players make their decision based on the interactions with others and the game they play. Specifically:

- (PD) players select the same strategy as the agent with maximum score among their neighbors.
- (SH) players select the same strategy as the majority of their neighbors.
- (HD) players select the opposite strategy with respect to the majority of their neighbors.
- (A) players choose always to cooperate independently of the neighbors' decisions.
- (D) players choose always to defect independently of the neighbors' decisions.

In the Siena model, many of the aspects described in the Basic model remain essentially the same. The agents, however, are now georeferenced on the map of the city of Siena [71], [72].

Each player, in addition to the variables described in the Basic model, has also the variables *terzo*, *location*, *lat* and *long*: *terzo* indicates the neighborhood of the city of Siena where agents live; *location* reports the address of residence; *lat* and *long* specify latitude and longitude of agents (see Figure 2.2) for the new setting).

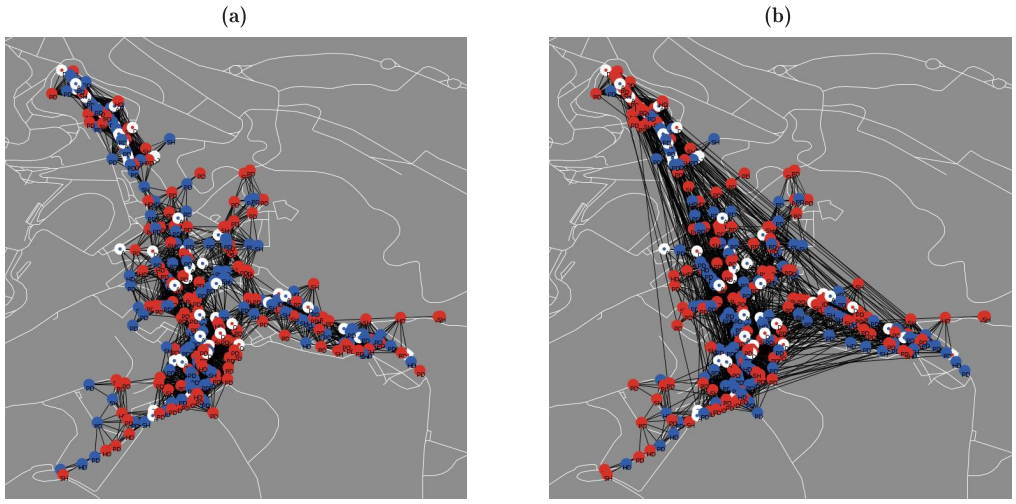

Figure 2.2: Siena model at time $t = 0$ with $ic = 50\%$. The white lines represent Siena's road network, while the black ones are the links between nodes. (a) geographic graph; (b) small-world (SW) graph.

Again we consider two scenarios: a geographical network, obtained with $SWrp = 0$, whose links represent Siena's neighborhoods within a radius of 120 m (see Figure 2.2a); a SW network, obtained leveraging the rewiring algorithm used in the Basic model with $SWrp = 0.05$ (see Figure 2.2b). Further details on the model variables can be found in Appendix A.

2.2.3 Results

Basic model simulations are examined in the two scenarios of the regular lattice and the SW network case. For each topology we perform many simulations to study the effect of changing the parameters ic and α. We find that the cooperation dynamics in the long run is independent from the value assumed by ic in our setting.

Referring instead to parameter α, we have that in the regular lattice, prevalence of cooperative behavior is observed for $\alpha \in [0, 1.34]$, conversely defection prevails for $\alpha \in (1.34, 3]$, as shown in Figure 2.3, where the two examples with $\alpha = 0.8$ and $\alpha = 1.7$ allow one to observe the differences. Thus, global scenarios of sustainability or unsustainability are observed in these cases. Note that the dominant type of agent in our sample is represented by (PD) players, who are the only ones whose decisions depend on α.

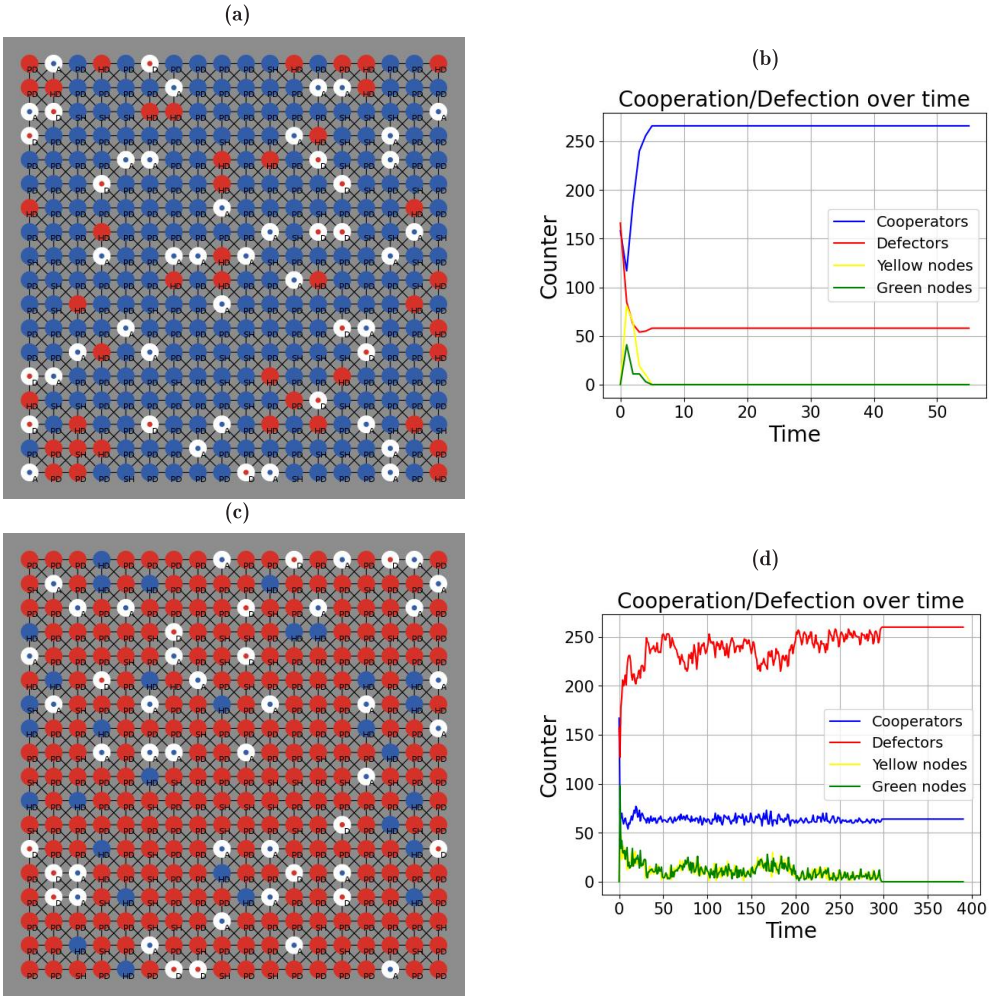

Figure 2.3: Regular lattice scenario. Top row: $\alpha = 0.8$; bottom row: $\alpha = 1.7$. **(a)**: Pattern at final time with $\alpha = 0.8$; **(b)**: Cooperation/Defection over time with $\alpha = 0.8$; **(c)**: Pattern at final time with $\alpha = 1.7$; **(d)**: Cooperation/Defection over time with $\alpha = 1.7$.

For the SW network, the overall dynamic remains almost the same. The key difference that is observed lies in the threshold for α at which there is a behavioral change from the cooperative to the defecting dynamics. We find prevalence of cooperation for $\alpha \in [0, 1.38]$ and defection for $\alpha \in (1.38, 3]$, enabling us to conclude that the SW network slightly facilitates the diffusion of cooperation compared to the regular one.

Siena model simulations are analyzed in the two scenarios of the geographical and the SW network. The cooperation dynamics is again independent of the value assumed by *ic* in the long run and depends only on α. As in the Basic model, either with the geographical or SW network, by varying the value of α from 0 to 3, the graph changes from cooperation to defection. Specifically, for the geographical network scenario, we observe prevalence of cooperation if $\alpha \in [0, 1]$ and defection if $\alpha \in (1, 3]$, while for the SW network scenario we get the prevalence of cooperation if $\alpha \in [0, 1.12]$ and defection if $\alpha \in (1.12, 3]$. Figure 2.4 shows two examples of the final patterns with $\alpha = 0.8$ and $\alpha = 1.7$, respectively. Similarly to the Basic model, we find that the SW network slightly facilitates the diffusion of cooperation compared to the geographical one.

It is evident from the results that the presence of a SW network slightly promotes the spread of cooperative behavior, according also to the results found by the authors in Masuda and Aihara [73], where it has been analyzed how cooperation emerges in the spatial prisoners' dilemma played in a range of networks, from regular to random, and

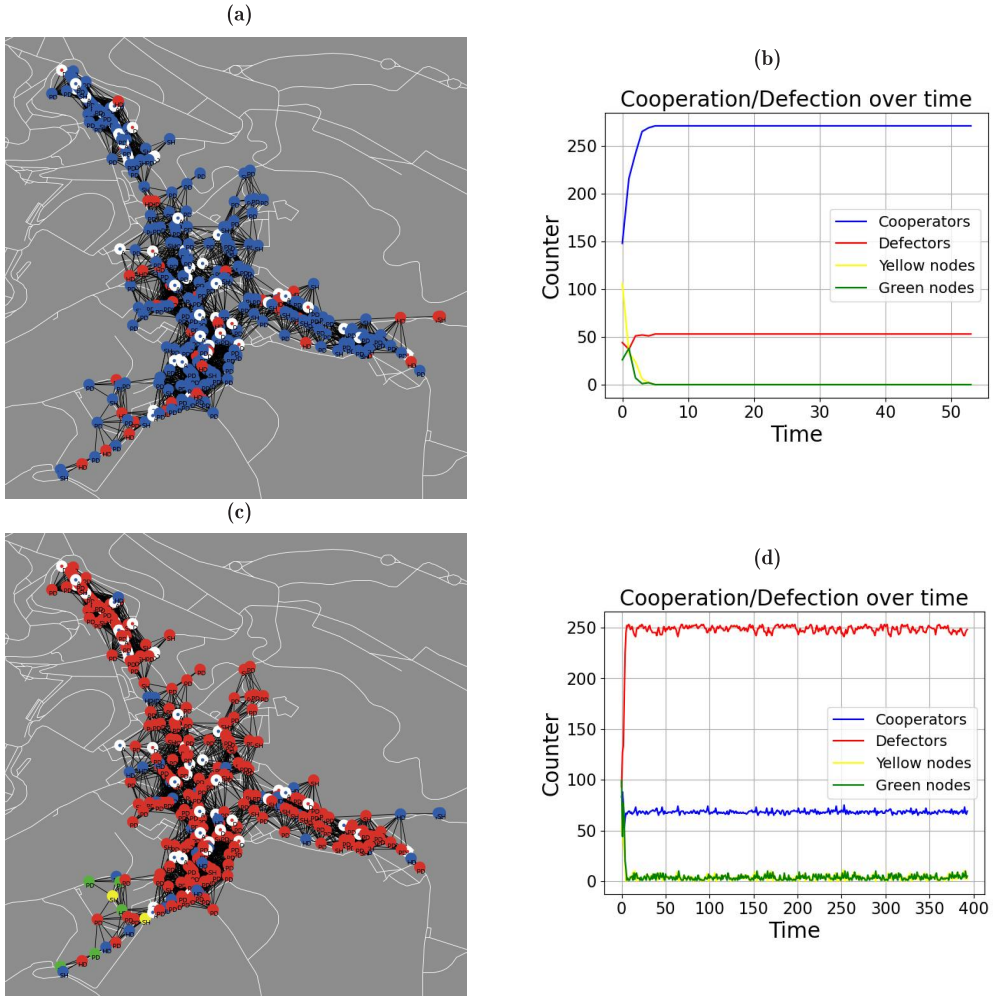

Figure 2.4: Geographical network scenario. Top row: $\alpha = 0.8$; bottom row: $\alpha = 1.7$. **(a)**: Pattern at final time with $\alpha = 0.8$; **(b)**: Cooperation/Defection over time with $\alpha = 0.8$; **(c)**: Pattern at final time with $\alpha = 1.7$; **(d)**: Cooperation/Defection over time with $\alpha = 1.7$.

where it has been proved that the SW topology is the optimal one for the spread of cooperation. Similarly, in both the Basic and Siena models, the range of α values over which cooperative behavior prevails expands when the structure is switched to a SW network.

Table 2.1: Threshold α_1 for parameter α indicating the transition from cooperation to defection in the Basic and Siena models across regular (R), geographical (G), and small-world (SW) network scenarios.

Basic model	**Siena model**
(R) $\alpha_1 = 1.34$	(G) $\alpha_1 = 1.00$
(SW) $\alpha_1 = 1.38$	(SW) $\alpha_1 = 1.12$

We denote by α_1 the critical threshold of α that separates cooperation from defection. In Table 2.1 we report the values of the threshold α_1 to highlight the differences between a regular city and the network of Siena. The threshold $\alpha_1 = 1$ obtained in the Siena case is significantly smaller than the one obtained in the regular case, $\alpha_1 = 1.34$. This means that the range of α where there is prevalence of cooperation is much smaller in the case of Siena. The same observation can be derived when comparing the two SW network scenarios. In fact, the threshold $\alpha_1 = 1.12$ obtained in the Siena (SW) model is again

significantly lower than the threshold $\alpha_1 = 1.38$ achieved in the Basic (SW) model. These results imply that the diffusion of cooperative behavior is more difficult in the city of Siena than in a regular one, thus opening interesting questions regarding the impact of urban structure on sustainable behaviors of citizens.

2.2.4 Discussion

We surveyed 324 residents of Siena's historical center to both map climate awareness and parameterize our geo-referenced ABM. Education emerges as the strongest predictor of awareness [60], [62]; women report higher concern than men (eco-gender gap) [64], [74]. We observe, unexpectedly, lower awareness in the 14–25 group than in the 25–60 groups. These patterns suggest targeted initiatives for youth and for low-awareness areas. Complete details of survey results are reported in Appendix A.

The survey informed five behavioral types mapped to evolutionary games; the ABM was then developed to study dynamics not inferable from cross-sectional data. Two main findings follow: first, adding small-world ties fosters cooperation relative to purely geographic neighborhoods; second, the real topology of Siena promotes cooperation less than an ideal regular lattice. Taken together, these findings indicate that the diffusion of cooperative behavior is more difficult in Siena's historical center than in an idealized regular city, raising important questions about how urban morphology shapes the sustainability practices of its residents.

Finally, our results suggest interesting policy implications. The parameter defection-award must be kept below the critical threshold α_1 to have a prevalence of cooperation and consequently to promote sustainable behaviors among citizens. This may be achieved through the design of tailored economic incentives together with targeted educational and informational measures.

Limitations and future directions

The main limitation of our ABM concerns the fact that the specific features of each citizen (age, gender, educational level) as well as climate awareness obtained from the survey in our ABM are only used as labels and do not influence decision making. Next steps include modeling awareness as an actual driver of individual choices, exploring richer agent sets (e.g., tourists), incorporating multilayer ties (e.g., work, hobbies), scaling the simulation from 324 to the full resident population, and replicating the study in other urban contexts. Another possible direction is to evaluate targeted interventions by embedding "special" influence nodes (e.g., activists or bots) in the social network; preliminary results suggest that increasing (SH) agents enlarges the cooperation regime.

More broadly, agent-based models often rely on simplified behavioral rules or assumptions of strategic rationality that may not be realistic in contexts involving individual cognition and internal psychological states. This limitation motivated the adoption, in the main application of Chapter 4, of a Markov modeling approach, which is better suited to represent the probabilistic evolution of mental states over time.

2.3 A Markov Decision Process to Study the Individual Perception of Climate Change

This section summarizes and adapts the work presented in [36], which focuses on the construction of a Markov decision process model to represent how individuals evaluate and react to climate-related risks over time (RQ2). The aim is to formalize uncertainty and transitions between individual perceptions or attitudes.

2.3.1 Introduction

What shapes individuals' perception of climate change over time? In this application we explore the concept of *climatic awareness*, which refers to the evolution over time

of individual perception of climate change. To illustrate this concept, we propose an extension of a mathematical model of awareness based on Markov decision processes, taking into account high-frequency rainfall data recorded in Sicily between 2009 and 2021 [37], [75]. We focus on understanding how individuals develop their awareness over time and what factors influence this process. Moreover, since climatic data and in particular rainfall time series are generally nonlinear and unpredictable [76], [77], we intend to study the effects of such nonlinearities in human perception and decisions, particularly in the individual awareness dynamics.

Markov decision processes (MDPs) are particularly suitable for this purpose as they provide a structured way to model decision making under uncertainty, where actions, states, and transitions can reflect both environmental signals and internal cognitive processes.

We model the behavior of intuitive (I) and analytical (A) individuals, driven by "tacit knowledge" and quantitative analysis, respectively. We study the effects of extreme events on their perception of climate change, identifying the *Climate Aware* individuals -capable of processing cross-cutting information- and the *Climate Susceptible* individuals- more sensitive to external events. We also focus on the model parameters, looking for transition values that could discriminate between the two categories.

2.3.2 Methods

This section is divided into two parts: the first describes the Markov decision process model, and the second outlines the data used for its implementation.

The MDP Model

We adopt the MDP model introduced in [75] to study how climatic factors shape individual awareness and decisions. Below, I briefly outline its main components and structure.

First, we consider a finite discrete time horizon $\{1, 2 \dots, T\}$, where each time instant t corresponds to a moment of making a relevant decision, i.e. a decision which need some kind of reasoning process and is not purely automatic.

At each time instant, the individual experiences a particular state $s_t \in S = [0, 1]$, where S is the state space representing the finite set of available states. The state s_t reflects the individual level of awareness, i.e. the capacity to make aware choices at a certain time instant t.

Moreover, the individual is required to make an action/choice $u_t \in U = [0, 1]$ at each time instant t, where U represents the finite set of available actions. The decision is made by taking into account the outcomes they will receive throughout the finite time horizon T. In particular, the action or choice variable ranges from a fully intuitive decision ($u_t = 0$) to a fully analytic decision ($u_t = 1$), reflecting the dual-process framework described by Kahneman [78].

Each individual can be provided with a policy, which is a function $\pi : S \times T \to U$ prescribing to the individual the action to perform given their current state s_t at time t. The policy drives the choice to perform at each time instant: $u_t = \pi(s_t, t)$. Such choice leads to two results: the individual receives a reward, and their state evolves to a possibly new state.

We define the reasoning propensity parameter $p_r \in [0, 1]$ as a value characteristic of the single individual which represents their attitude in processing information about the decision problem, taking values in a continuum between the two extreme attitudes called intuitive ($p_r = 0$) and analytical ($p_r = 1$), assuming in this way that both are always involved, with different amounts, in any decision, according to the dichotomy largely adopted in dual process theories and economics [78].

The state s_t of the DM evolves according to a non-deterministic dynamics, ruled by:

$$s_{t+1} = f(s_t, u_t, w_t) = s_t + w_t(u_t), \tag{2.8}$$

where the future level of awareness of the individual depends on the current state s_t, the choices u_t, and it is subjected to some uncertainty represented by a stochastic variable $w_t \in W$. w_t varies according to a transition probability function $P : S \times U \times S \to [0, 1]$ such that $P(s, u, s') = Pr(s_{t+1} = s' \mid s_t = s,\ u_t = u)$, representing the probability to move from state s to state s' by selecting an action u.

In particular, by assuming that from a state s_t there exist only three possibilities: $s_t + z, s_t$ and $s_t - z$, with z a fixed step size, the function P represents, accordingly, three components specifying *Forward* $P^F(u_t)$, *Stationary* $P^S(u_t)$, and *Backward* $P^B(u_t)$ probabilities, which depend on the specific decision u_t. Thus, the stochastic variable w_t is:

$$w_t = \begin{cases} z & \text{with probability } P^F(u_t) \\ 0 & \text{with probability } P^S(u_t) \\ -z & \text{with probability } P^B(u_t) \end{cases}$$

The three probabilities are defined as follows:

- $P^S(u_t) = k \quad \forall\, u_t \in U$, with k a fixed constant value.
- $P^B(u_t) = 1 - \left[P^F(u_t) + P^S(u_t)\right]$
- $P^F(u_t) = p_r\, P^F_{analytical}(u_t) + (1 - p_r)\, P^F_{intuitive}(u_t)$.

Specifically, $P^F_{analytical}(u_t)$ has the absolute minimum in $u_t = 0$, and the absolute maximum in the interval $(0.5, 1)$, while $P^F_{intuitive}(u_t)$ has the absolute minimum in $u_t = 1$, and the absolute maximum in the interval $(0, 0.5)$. Thus, $P^F_{intuitive}$ is maximal for fully intuitive decisions ($u_t = 0$), and $P^F_{analytical}$ is maximal for fully analytical ones ($u_t = 1$). Furthermore, each individual has a specific reasoning propensity parameter p_r and, consequently, a different forward probability.

The reward function $r : S \times S \times U \to R$ is a stochastic function where $r(s, s', u)$ gives the reward incurred by the agent by performing the action u from state s and transitioning to state s'.

According to the assumption of the model that awareness is related to the individual's well-being, the reward function incorporates a positive dependence on the current level of awareness s_t. On the other hand, the reward function must incorporate the costs of data acquisition and elaboration to find possible solutions to a given problem. Therefore, the more the decision implies analytical reasoning the more resources it needs in terms of time, personal energy, and monetary resources. Mathematically, the higher u_t the more analytical the reasoning of the DM, and so the more resources consumed:

$$r_t(s_t, u_t) = \alpha_b s_t - \alpha_c u_t, \tag{2.9}$$

where α_b and α_c weight the benefits of a given state s and the costs of a given decision u at time t.

The objective value function the individual has to maximize in the set of available decisions u, reads as follows:

$$V_t = \left(r_t(s_t, u_t) + \sum_{\tau=t+1}^{T} \delta^\tau \mathbb{E}\left[r_\tau(s'_\tau, u_\tau)\right] \right), \tag{2.10}$$

where the expected value $\mathbb{E}$ of the reward for future states takes into account an external stochastic source of uncertainty.

The future discount δ of an expected reward is the weight the individual assigns to the next state with respect to the present one. Specifically, $0 \leq \delta \leq \delta_{\max}$: when $\delta = 0$, the future is not considered, then the higher the value of δ, the higher the weight given by the agent to the future.

Moreover, the value $r_T(s_t)$ at final time T is fixed and depends exponentially on the state so as to drive the system dynamics towards higher states. Then, the maximization problem is solved through an algorithm of backward induction, starting from the last value and reconstructing step by step the sequence of the optimal decisions until the initial time.

Data

We refer to the RSE dataset (the Rainfall Sicily Extreme dataset) introduced in [37], which will be described in Chapter 3. The dataset is composed by geographical rainfall records with a 10 minutes periodicity from 2009 to 2021, provided by SIAS, the Servizio Informativo Agrometeorologico Siciliano. Without loss of generality, we reduce the dataset dimensionality by computing the moving average with step 10 of the time series, grouped by days.

Figure 2.5, for instance, reports the data used for the station gauges of Catania (panel **a**) and Palermo (panel **b**), where extreme values can be noticed in the case of Catania in 2021.

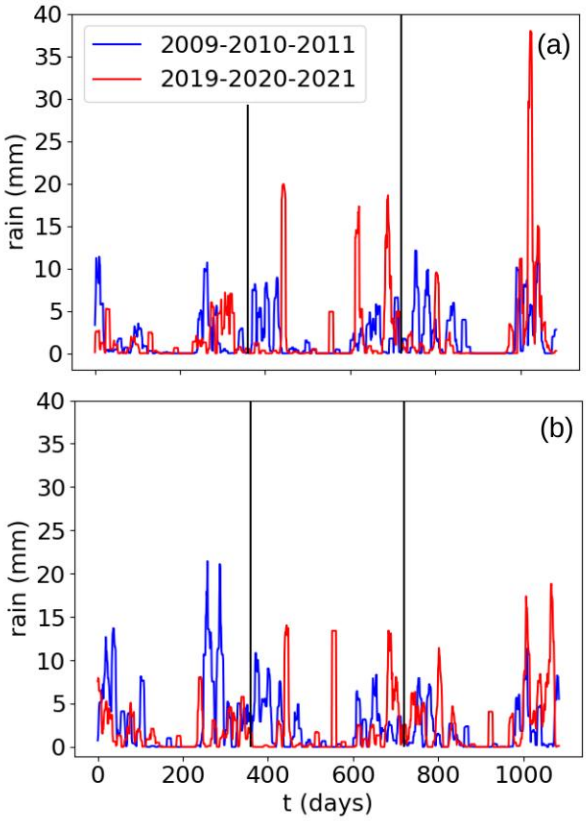

Figure 2.5: Moving average of step 10 of daily rainfall events. **(a)**: Catania. **(b)**: Palermo.

In this study, the MDP problem is solved by considering each instant t as a single day. Moreover, we replace parameter δ with a time-dependent function $\delta(t)$, consisting of the corresponding rainfall measurement at time t, in order to analyze how extreme rainfall events influence decisions in the context of climate change. Specifically, this value corresponds to the average of the data recorded in the previous 10 days, assuming that individuals process what they experienced with a certain delay. The underlying idea is that more extreme or unstable conditions may influence how individuals perceive and value future outcomes.

2.3.3 Results

According to the theoretical model described in section 2.3.2, we found a baseline configuration of the parameters to perform the numerical simulations. Moreover, several Sicilian sites have been considered, including Augusta, Catania, Palermo and Siracusa for the years 2009 and 2021. Data show that the year 2021 involved extreme events in all cases except Palermo, while the year 2009 did not present extreme events in any

location [37]. As explained in section 2.3.2, we performed the simulations by replacing the constant parameter δ with the real rainfall measurements from the RSE dataset.

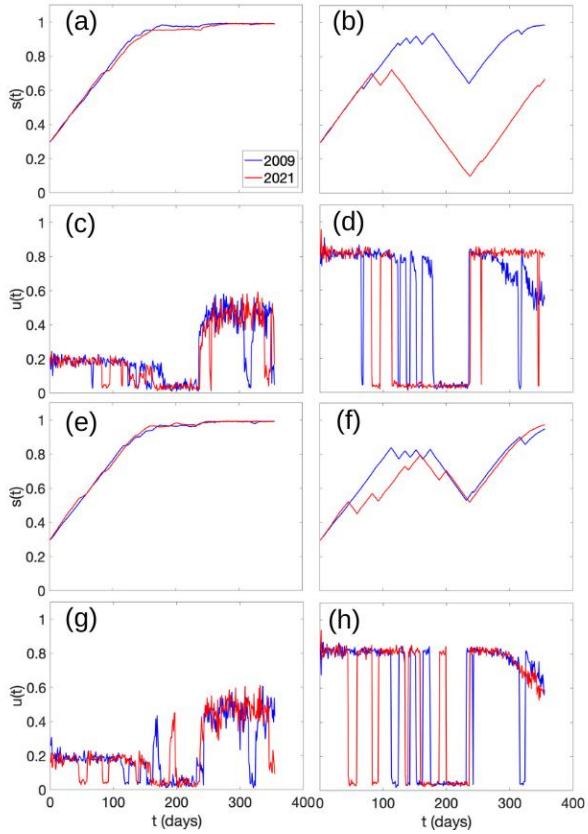

Figure 2.6: Temporal comparison: 2009 and 2021. **Catania-Palermo**. State dynamics of (I) **(a)-(e)** and (A) **(b)-(f)** individuals. Decision over time of (I) **(c)-(g)** and (A) **(d)-(h)** individuals.

In Figure 2.6, we show the evolution over time of both the state s_t, i.e. the awareness, and decisions u_t of the two types of individuals investigated in this study for Catania (panel **a** to panel **d**) and Palermo (panel **e** to panel **h**). Panels **a** and **e** refer to the intuitive individual (I) ($p_r = 0.3$), who, regardless of the experiences, manages to increase their awareness to the maximum value. Consistently with the model, in panels **c** and **g**, the decision is intuitive, thus allowing the (I) individual to increase the transition probability towards higher states (for both Catania and Palermo in both years). Panels **b** and **f** refer to the analytical individual (A) ($p_r = 0.7$), who, on the contrary, turns out to be very susceptible to external events. In panel **b** regarding Catania, in fact, there is a significant difference between the blue line (2009) and the red line (2021). This occurs because, as seen in Figure 2.5, the 2021 rainfall events in Catania were significantly more intense than in 2009. Similarly, in panel **f** a small difference between the two years is present, as the rainfall events in Palermo are not so different from each other (Figure 2.5).

In the cases of (A) individuals, decisions are optimal for high values of u_t, then when the associate decisions are low, the state may drop dramatically, such as in the central days of panels **d** and **h**).

The (A) individual, therefore, seems to be very sensitive to extreme rainfall events: the more intense the events, the more their state decreases, as if such individuals are excessively upset by the presence of extraordinary events. We could therefore say that (I) individuals are more autonomous, unconditioned, and capable of assimilating and processing information. On the other hand, the (A) individuals result very sensitive to their direct experiences and reactive to the data observed. In conclusion, we are able to identify two characters that react differently to extreme rainfall events: the Climate Aware (CA) and the Climate Susceptible (CS) individuals.

As mentioned before, we extended our analysis to other cities, in particular to Augusta and Siracusa. Moreover, we studied the sensitivity of the p_r parameter by performing additional extensive simulations. The goal of this further analysis is to find a critical threshold for p_r separating the two observed attitudes.

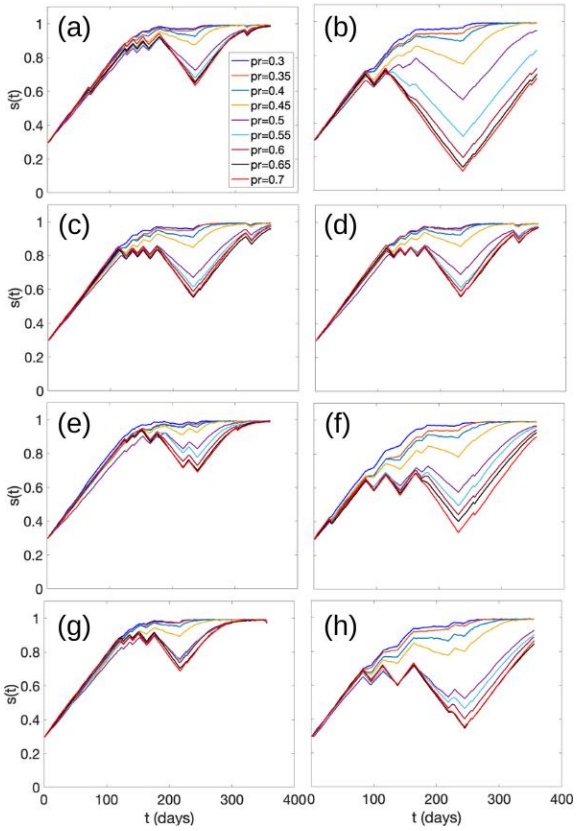

Figure 2.7: From $p_r = 0.3$ (CA) to $p_r = 0.7$ (CS) with step 0.05. **2009/2021**. Catania **(a)-(b)** Palermo **(c)-(d)** Augusta **(e)-(f)** Siracusa **(g)-(h)**.

Figure 2.7 reports the dynamics of individuals in all the considered locations. The parameter p_r varies in the interval [0.3,0.7] with a step of 0.05, where the minimum and the maximum values of the interval represent two prototypical (CA) and (CS) individuals, respectively. The figure rows correspond to different cities (Catania, Palermo, Augusta and Siracusa), while the columns refer to the years 2009 (no extreme events) and 2021 (mostly extreme events), respectively, according to the findings in [37]. We notice that in 2009 the changing of p_r affects slightly the individual behavior, while stronger changes in the dynamics are observed in 2021 for the locations of Catania, Augusta and Siracusa, where extreme events occurred. The case of Palermo, where only moderate differences in the dynamics are also observed for 2021, confirms this result. In conclusion, the individual sensitivity to rainfall events grows by increasing p_r, and it happens more abruptly when considering extreme locations. This suggests the presence of a critical transition from (CA) to (CS) individuals, occurring approximately at $p_r = 0.45$.

2.3.4 Discussion

The model presented in this application first confirms the results obtained in [37] and described below in Chapter 3. Indeed, in all of the locations clustered as extreme in Vitanza, Dimitri, and Mocenni [37], the critical transition from Climate Aware to Climate Susceptible individuals is more evident.

In addition, the results suggest that effective policy actions should regard mainly (CS) individuals, trying to bring them below the critical transition of the p_r parameter.

The determination of factors changing the inferential propensity parameter p_r can be supported by attitude surveys on the local population, considering both specific and universal factors. In fact, on the one hand, each country has its own unique features [60] and national and regional programs must be adapted. On the other hand, educational attainment is the single strongest predictor of climate change awareness worldwide [60].

In conclusion, the literature suggests that the considered reasoning propensity parameter p_r will be certainly related to the individual's basic education, the climate literacy, and the understanding of the micro to macro interactions mechanisms influencing climate change. Therefore, acting on those factors may produce a change in the p_r parameter, thus allowing individuals to pass from (CS) to (CA) attitude.

Preliminary results showed that changing the time horizon may affect the local dynamics: individual behavior depends on the length of the time horizon considered, suggesting and confirming that age and life expectancy influence the individual choices.

Limitations and future directions

This work has several limitations. The model is intentionally simple: transitions and rewards are stylized, the discount term $\delta(t)$ is specified ad hoc, and the parameter tuning is minimal. Validation is limited and potential confounders are not taken into account. On the data side, the focus on a single region, time period, and extreme rainfall events restricts generalizability. These limitations highlight directions for future research, particularly to enhance model reliability and external validity. Still, the goal of this application was mainly exploratory: to become familiar with Markov models and test their potential in decision-making contexts under uncertainty. A refined use of Markov models will be proposed in Chapter 4.

Chapter 3

Data-driven Approaches to Complex Systems

Contents

Data play a crucial role in understanding complex systems, especially when theoretical models are hard to specify or validate. Data-driven methods allow us to extract patterns, infer structure, and make predictions directly from observations, often without assuming strong prior models. These techniques are particularly useful when dealing with high-dimensional, noisy, or heterogeneous data, as is often the case in real-world systems.

In this Chapter, I present a selection of data-driven methods explored and applied during this thesis. The next section introduces two main approaches: machine learning—both unsupervised (e.g., clustering) and supervised (e.g., bagged trees)—and causal inference (e.g., the PC algorithm and its extensions). These methods are selected for their ability to capture hidden structures, classify complex patterns, and identify potential causal relationships among data, especially in domains involving human behavior or cognition. The following two sections provide applications for these approaches: a multi-modal machine learning framework to detect extreme rainfall events in Sicily (RQ3), and a wearable sensor study focused on air quality monitoring using swarm-based data collection (RQ4). These preliminary studies helped me prepare for the main application of this thesis on data-driven approaches in the novel and sensitive domain of psychology, which is discussed in Chapter 5. This Chapter also has an associated Appendix B with additional material and details.

3.1 Data-driven Methods

There are many ways to extract knowledge from data in complex systems. In this section, I focus on two widely used data-driven approaches: machine learning and causal inference. These are selected based on their ability to deal with high-dimensional longitudinal data, uncover nonlinear patterns, and infer relationships in settings where traditional modeling may fail. The goal here is not to provide an exhaustive review of all data-driven methods, but to give an overview of those most relevant to the work carried out in this thesis.

3.1.1 Machine Learning

Clustering

Clustering is an unsupervised machine learning methodology [79], [80]. Its goal is to detect groups of observations sharing similar characteristics. More precisely, it consists in the partitioning of a dataset into subsets, so that the data in each subset are characterized by a higher similarity than elements in different sets, according to some defined distance measure.

Two main types of clustering techniques can be defined: methods in which the number of clusters needs to be established a priori, as, for instance, the K-Means algorithm [81],

and algorithms in which, instead, the number of clusters is inherently estimated during the optimization phase, such as the Affinity Propagation [82].

K-Means

K-means clustering is an unsupervised learning algorithm that groups data points into k clusters based on their similarity. Unlike supervised learning, which relies on labeled examples, k-means is used with unlabeled data to uncover hidden patterns or structure.

Given a chosen number of clusters k, and using Euclidean distance to measure similarity, the algorithm proceeds as follows:

1. Initialization: Randomly select k cluster centroids.
2. Assignment: Assign each data point to the nearest centroid, forming clusters.
3. Update: Recompute each centroid as the mean of the points assigned to it.
4. Repeat: Iterate steps 2–3 until the centroids stop changing (converge) or a maximum number of iterations is reached.

The goal is to partition the dataset into k clusters so that points within each cluster are more similar to one another than to points in other clusters. K-means is popular because it is simple, efficient, and often effective in practice.

Affinity Propagation

Affinity Propagation (AP), introduced by Frey and Dueck in 2007 [82], and its extension to Hierarchical Affinity Propagation [83], are nowadays becoming extremely popular due to their simplicity, general applicability, and performance and have been succesfully applied to several contexts in research [84]–[86].

AP takes as input the measures of similarity between pairs of data points, and simultaneously considers all of them as potential exemplars. The number of clusters does not need to be defined in advance, indeed the algorithm is based on the hypothesis that the so called "real-valued messages" are exchanged between data points until a high-quality set of exemplars, together with the corresponding clusters, gradually emerges.

The algorithm requires two inputs parameters [82]:

- Similarities $s(i,k)$ between data points, representing how similar a point is to be another one's exemplar. If there is no similarity between two points, as in this case they cannot belong to the same cluster, this similarity can be omitted or set to -∞ depending on the implementation.
- Preferences $s(k,k)$, indicating each data point's suitability to be an exemplar. Since some prior information which points could be favored for being an exemplar can be available, it can be represented through preferences.

Similarity is usually defined starting from the negative Euclidean distance or the Pearson correlation coefficient, depending on the considered situation.

If all data points are supposed to be equally suitable as exemplars, the preferences should be set to a common value, such as for example the median of the input similarities, thus resulting in a moderate number of clusters, or their minimum, thus resulting in a small number of clusters [82].

Each iteration step of the optimization performance is composed by 2 main message-passing steps:

1. Computing responsibilities:

$$r(i,k) \leftarrow s(i,k) - \max_{k' \text{ s.t. } k' \neq k} \{a\,(i,k') + s\,(i,k')\}\,, \tag{3.1}$$

where $s(i,k)$ and $s(i,k')$ are similarities, while $a(i,k')$ are availabilities.

2. Computing availabilities

$$a(i,k) \leftarrow \min\left\{0, r(k,k) + \sum_{i' \text{ s.t. } i' \notin \{i,k\}} \max\{0, r(i',k)\}\right\}, \tag{3.2}$$

where $r(k,k)$ are the self-responsibilities, while $r(i',k)$ are general responsibilities. To limit the influence of strong incoming positive responsibilities, the total sum is lower bounded, so that it cannot be negative.

The "self-availability", $a(k,k)$ is updated differently, as follows:

$$a(k,k) \leftarrow \sum_{i' \text{ s.t } i' \neq k} \max\{0, r(i',k)\}. \tag{3.3}$$

The way for calculating how suitable a point is for being an exemplar is that it is favored more if the initial preference was higher, but the responsibility gets lower when there is a similar point that considers it as a good candidate, so there is a 'competition' between the two, until one of the two options is chosen in some iteration. The above procedure may be terminated after a fixed number of iterations, after changes in the messages fall below a threshold, or after the local decisions stay constant for a given number of iterations [82].

Prediction

Artificial Neural Networks (ANN) are flexible and powerful tools for prediction tasks, especially when the data exhibit complex and non-linear relationships. Due to their ability to approximate arbitrary functions [87], ANN have become a standard choice for forecasting and regression problems in various domains, from economics to energy systems [88], [89]. Techniques such as backpropagation and gradient-based optimization have made these architectures particularly effective in capturing hidden patterns in data [90].

Classification

Beyond regression and forecasting, ANN are widely used for classification problems, where the goal is to assign an observation to one of several predefined categories [91]. Nevertheless, ANN are not the only option for classification: established algorithms such as Support Vector Machines (SVM), Random Forests, and other ensemble methods often perform well, particularly with smaller datasets [92], [93].

Bagged Tree

An example of an ensemble method is Bagging (Bootstrap Aggregating), introduced by Breiman [94], [95], [96]. The core idea is to generate multiple decision trees on bootstrap samples of the training data and aggregate their predictions. This approach reduces variance and improves prediction stability compared to a single tree, resulting in a more robust model that is less sensitive to noise in the data. Specifically, the model works in three steps: (1) random sampling with replacement creates diverse training sets, (2) individual decision trees are trained independently on these samples, and (3) predictions are aggregated via majority voting.

3.1.2 Causal Inference

Causal inference aims at uncovering cause–effect relationships from observational or experimental data, moving beyond mere associations. The overarching goal is to reconstruct the underlying causal structure that governs a system, thereby enabling more accurate predictions and meaningful interventions. Among the most established approaches to causal discovery are constraint-based methods, such as the PC algorithm, and structural equation models (SEM), traditionally employed in the social and behavioral

sciences [97], [98]. In addition, other methods such as Vector Autoregression (VAR) and information-theoretic approaches such as Transfer Entropy (TE) have been widely adopted, particularly in economics, neuroscience, and complex systems research [99], [100].

Structural Equation Models

Structural equation modeling (SEM) is a way to describe how several variables relate to one another at the same time. It joins a measurement part, which links observed indicators (e.g., questionnaire items or test scores) to underlying unobserved concepts (latent variables), with a structural part that states how those concepts influence each other. By modeling measurement error explicitly, SEM provides cleaner estimates of the relations among the latent variables. Models are typically estimated with maximum likelihood or robust variants, using simple constraints to fix the scale of each latent variable. Overall fit is judged with statistics and residual checks (such as chi-square, CFI, RMSEA, SRMR), together with the substantive plausibility of the estimated paths. SEM also supports comparisons between competing models and extensions to multiple groups or longitudinal data. Importantly, good fit does not by itself prove causation; causal claims depend on study design and assumptions [101].

Typically, SEM path modeling assesses contemporaneous relationships among variables. However, many real mechanisms have sequential dependencies, connections estimated from solely contemporaneous path models may be biased. In complement, VAR modeling assesses lagged relationships while neglecting to account for contemporaneous relationships among variables. Each approach could be improved by simultaneous consideration of both the contemporaneous and lagged effects. Kim, Zhu, Chang, *et al.* [102] recently offered a solution which combines SEM path and VAR modeling into a "unified SEM" [103].

Vector Autoregression

Vector Autoregression (VAR) is a classical linear modeling framework used to capture temporal dependencies among multiple interrelated time series [99]. In a VAR model of order p, each scalar variable is modeled as a linear combination of its own past values and the past values of all other variables in the system; that is,

$$\mathbf{X}_t = \mathbf{A}_1\mathbf{X}_{t-1} + \mathbf{A}_2\mathbf{X}_{t-2} + \cdots + \mathbf{A}_p\mathbf{X}_{t-p} + \boldsymbol{\epsilon}_t,$$

where $\mathbf{X}_t \in \mathbb{R}^k$ is a k-dimensional vector of variables at time t, $\mathbf{A}_i$ are $k \times k$ coefficient matrices representing lagged dependencies, and $\boldsymbol{\epsilon}_t$ is a vector of white noise residuals, typically assumed to be multivariate Gaussian.VAR assumes linearity, and that the residuals have constant variance over time, and is therefore sensitive to violations of these assumptions. Although it can effectively capture linear lagged relationships between symptoms, it is inherently limited in modeling the complex and nonlinear dynamics that often characterize psychological time series. These limitations reduce its reliability for idiographic real data, where trajectories are short, noisy, and rarely conform to the statistical regularities required by VAR [104].

Transfer Entropy

Transfer Entropy (TE) is a nonlinear, model-free measure of directed information transfer between time series, rooted in Shannon's information theory [100]. It quantifies how much knowing the past of a source variable X_i reduces uncertainty about the future of a target variable X_j, beyond the information already contained in X_j's own past. Formally, the TE from X_i to X_j is defined as:

$$TE_{X_i \to X_j} = H(X_j^t \mid X_j^{t-1}) - H(X_j^t \mid X_j^{t-1}, X_i^{t-1}),$$

where $H(\cdot)$ denotes Shannon entropy. A positive TE value implies that including the past of X_i improves the prediction of X_j^t, suggesting a potential directional influence from

X_i to X_j. Conversely, if $TE_{X_i \to X_j} = 0$, then X_i^{t-1} provides no additional information about X_j^t beyond what is already captured by X_j^{t-1}. In practice, entropy is estimated via discretization of the time series and computation of empirical joint probabilities. This approach, however, becomes unreliable when dealing with high-dimensional or short time series—a common limitation in idiographic real data. Furthermore, the need to discretize continuous variables may obscure subtle, non-linear dependencies and introduce bias. Although TE does not assume linearity or Gaussianity, its data-hungry nature limits its practical utility for single-subject analyses with relatively few observations [105].

Peter Clark Algorithm

The PC algorithm is one of the most widely used constraint-based methods for causal structure learning [97]. It operates in two main phases: the skeleton phase and the orientation phase.

In the skeleton phase, the algorithm identifies the undirected structure of the graph by iteratively testing conditional independences between variables. Different conditional independence tests can be employed depending on the data characteristics, such as linear tests (partial correlation) or nonlinear tests (conditional mutual information, CMI). This phase is sensitive to several statistical factors:

- *Sample size*, which constrains the statistical power of the tests;
- *Significance level*, chosen by the researcher and affecting the rate of false positives and negatives;
- *Cardinality of the conditioning set*, which is automatically optimized by the PC algorithm;
- *Effect size*, i.e., the magnitude of the conditional dependence $I(X;Y|S)$.

In the orientation phase, the algorithm applies logical rules (e.g., orientation of v-structures and propagation rules) to direct the edges, resulting in a partially directed acyclic graph (PDAG).

Despite its popularity, the PC algorithm has well-known limitations. First, it may erroneously remove true links (false negatives). For example, let $P(X) \to X_{t-\tau} \to Y_t \leftarrow P(Y)$. If we condition on $P(X)$, the conditional mutual information $I(X;Y|S)$ may decrease, whereas if we condition on $P(Y)$, $I(X;Y|S)$ may increase, potentially leading to the erroneous removal of a true dependency.

Conversely, the PC algorithm may fail to remove spurious links (false positives). For instance, suppose $X_{t-\tau} \to X_t$ (strong autocorrelation) and $X_{t-1} \to Y_t$. Conditioning on X_{t-2} could erroneously eliminate the true link $X_{t-1} \to Y_t$, while at the same time introducing a spurious link $X_{t-2} \to Y_t$.

These limitations highlight the sensitivity of the PC algorithm to effect size, sample size, and autocorrelation, motivating the development of improved approaches such as PCMCI+, which specifically addresses these shortcomings [106].

PCMCI+ Algorithm

To uncover causal relationships in multivariate time series, the PCMCI+ algorithm is a state-of-the-art method designed to infer both lagged and contemporaneous causal links in high-dimensional, autocorrelated, and potentially nonlinear datasets [107]. PCMCI+ is an optimized extension of the original PCMCI framework [106]. PCMCI itself combines the PC algorithm [97]— a constraint-based method for causal structure learning— with an independence testing strategy tailored to time series data. PCMCI+ enhances this framework by refining the selection of conditioning sets for independence testing, thereby reducing false positives through a more robust pruning strategy.

We start by illustrating the PCMCI algorithm for causal discovery given the time series $y_1(t), \ldots, y_N(t)$ of the stochastic processes $Y_1(t), \ldots, Y_N(t)$, for $t = 1, \ldots, T$. The

PCMCI seeks the lagged dependencies between a target variable $Y_i(t)$ and a source variable $Y_j(t-\tau)$, with j possibly also equal to i, and $\tau \leq \tau_{\max}$ being a positive integer representing the lag. A graphical representation of a lagged dependency is a directed edge from the source to the target variable, with a label indicating the lag τ. We denote the source j as the parent of the target i. For all $\tau = 1, \ldots, \tau_{\max}$, the PCMCI is performed in two steps:

(PC_1) For each variable $Y_i(t)$, a superset of potential lagged causal parents $\mathcal{P}^\tau(Y_i(t))$ of $Y_i(t)$ is identified through an iterative procedure. At the first iteration, $\mathcal{P}^\tau(Y_i(t))$ is composed by all the variables that fail the (unconditional) statistical independence test with $Y_i(t)$ at a given significance level α, that is, checking $I(Y_j(t-\tau), Y_i(t)) < \alpha$, with I being the considered test statistic, see [106] for details. Then, at every successive iteration $p > 1$, the set $\mathcal{P}^\tau(Y_i(t))$ is pruned by conditioning the independence test on a set $\mathcal{S}$ composed of the top p strongest previously retained parents from $\mathcal{P}^\tau(Y_i(t)) \setminus \{Y_j(t-\tau)\}$, ranked according to their test statistic. At the end of the algorithm, a potential parent Y_j is retained in $\mathcal{P}$ if it is dependent of Y_i when conditioned on $\mathcal{P}^\tau(Y_i(t)) \setminus Y_j(t-\tau)$. Although this phase is designed to be sensitive and avoid false negatives, the resulting skeleton may still contain indirect or spurious connections. As discussed in [106], this is often due to limited statistical power, which depends on factors such as the sample size, the chosen significance level, the cardinality of the conditioning set, and the effect size—i.e., the magnitude of the conditional dependence measure $I(Y_i(t); Y_j(t-\tau)|\mathcal{S})$.

(MCI) In the second stage, PCMCI applies the so called Momentary Conditional Independence (MCI) test to each edge identified in the first phase. This test verifies whether $Y_i(t)$ remains dependent on $Y_j(t-\tau)$ when, in addition to $\mathcal{P}^\tau(Y_i(t)) \setminus \{Y_j(t-\tau)\}$, we also condition on the subset of the p_j strongest parents of $Y_j(t-\tau)$, with p_j being a free parameter of the algorithm. The MCI phase is specifically designed to eliminate false positives resulting from indirect or mediated pathways, while retaining true direct causal influences.

In its original formulation, PCMCI applies the MCI test only to lagged links. However, spurious or indirect links might appear also due to the presence of contemporaneous dependencies between variables. In this vein, the PCMCI+ algorithm, after performing a lagged conditioning phase as in the standard PCMCI, also includes a contemporaneous conditioning phase [107]. Once a more accurate skeleton has been obtained, PCMCI+ performs an orientation phase. This step is applied exclusively to contemporaneous links, as lagged links are naturally oriented by temporal order. Orientation is based on standard rules from the PC algorithm (the collider, propagation, and common child rule, see [107], which allow the algorithm to infer the direction of contemporaneous connections where possible.

Note that the PCMCI+ algorithm relies on standard assumptions from causal discovery theory. These include *faithfulness*, which assumes that all observed independencies correspond to the absence of edges in the true causal graph; the *Causal Markov Condition*, which states that each variable is independent of its non-effects (non-descendants) given its direct causes (parents); *causal sufficiency*, which assumes that all relevant variables are observed and there are no hidden confounders; and *stationarity*, meaning that the underlying causal mechanisms remain invariant over time.

Finally, we emphasize that a critical component of PCMCI+ is the conditional independence test employed. While linear methods like partial correlation are computationally efficient, they are limited in capturing nonlinear dependencies. To address this, we employed CMIknn [108], a non-parametric estimator of conditional mutual information (CMI) based on k-nearest neighbors. Given the random variables X, Y, a vector of random variables Z, and $p(x, y, z)$ their joint mass probability function, CMI is formally defined as

$$CMI := I(X; Y \mid Z) = \sum_{x,y,z} p(x, y, z) \log \left(\frac{p(x, y \mid z)}{p(x \mid z) p(y \mid z)} \right).$$

CMI quantifies the dependency between two variables X and Y, conditioned on Z, by estimating the reduction in uncertainty about Y when X is known, after accounting for Z. CMIknn provides a data-driven, distribution-free estimate of CMI, without assuming linearity, Gaussianity, or any specific parametric form. This makes CMIknn particularly suitable for complex time series, which often display nonlinear, noisy, and heterogeneous dynamics. Moreover, it is well-calibrated in finite-sample regimes and robust to a wide range of dependency structures. These features make it a flexible and powerful tool for uncovering meaningful, time-lagged variable interactions in high-dimensional and idiographic datasets. For instance, PCMCI+ has already shown promising results in biomedical domains, particularly in neuroscience. For example, it has been used to infer causal relationships between brain regions using hyperscanning EEG time series [109] and fMRI data [110], demonstrating its ability to extract meaningful temporal structures from complex biological signals.

3.2 A Multi-Modal Machine Learning Approach to Detect Extreme Rainfall Events in Sicily

This section summarizes and adapts the work presented in [37], which applies unsupervised machine learning — specifically the Affinity Propagation clustering algorithm — to detect local extreme rainfall events in Sicily (RQ3). The study serves as a training application of data-driven techniques, using high-frequency rainfall time series to identify anomalous patterns without relying on predefined labels.

3.2.1 Introduction

Is it possible to detect extreme rainfall events areas by clustering spatio-temporal data?

Extreme weather events, including intense rainfall, are becoming more frequent due to climate change [111]–[113]. Rising temperatures are contributing to shifts in precipitation intensity and frequency [114], [115], posing growing threats to vulnerable human and natural systems [116]. As a result, rainfall—especially in the Mediterranean—is now recognized as a key climatic variable, both as a scarce resource and as a driver of extreme events [117].

This growing concern has led to extensive investigations into regional rainfall patterns. In Sicily, studies have used methods such as Principal Component Analysis and clustering to identify homogeneous rainfall regions [118]–[120]. A key study by Bonaccorso and Aronica [121] applied L-moments and cluster analysis to reveal an increase in intense rainfall events after 2000, particularly in western Sicily, while eastern trends remain more localized and event-driven. Other research has pointed to a general decline in total rainfall across the region [122]. In this context, the heavy rainfall that hit eastern Sicily in late 2021 — nearly 300 mm of rain fell near Catania in just a few hours — highlights the urgency of localized detection tools. Such events are becoming increasingly frequent across the globe. Detecting extreme rainfall at the local scale is a key prerequisite for effective prevention and planning strategies.

In this study, we apply the Affinity Propagation clustering algorithm — grounded in machine learning — to identify extreme rainfall areas in Sicily. To our knowledge, this is the first time this technique is used for such a task. The analysis is based on a newly assembled high-frequency dataset ranging from 2009 to 2021. Weather indicators are then employed to validate the results, thus confirming the presence of recent anomalous rainfall events in eastern Sicily.

3.2.2 Methods

Data

The dataset used in this analysis consists of geographical rainfall records (mm) with a 10 minutes periodicity from 2009 to 2021, provided by SIAS, the Servizio Informativo

Agrometeorologico Siciliano. We consider six collections of datasets, as described in Table 3.1. C.A and C.B contain 13 datasets per station - one per year - with the original data and the weekly mean data, respectively. C.C and C.D include one full dataset per station - involving all the records from 2009 to 2021 - with the original data and the weekly mean data, respectively. C.A_s and C.B_s are subsets of C.A and C.B, respectively, since one station per time is considered, so that each of them includes 13 datasets.

Table 3.1: Dataset collections. The number of considered stations is 34, except for the Single stations Collections. * 52704 for leap years.

Name	Description	# Datasets per station	# Total datasets	# Records per dataset
C.A	Annual Collection	13	442	52560*
C.B	Annual Collection, Weekly mean	13	442	53
C.C	Full Collection	1	34	683713
C.D	Full Collection, Weekly mean	1	34	679
C.A_s	Single stations Collection	13	13	52560*
C.B_s	Single stations Collection, Weekly mean	13	13	53

The data preprocessing, described in Appendix B, leads to the selection of 34 stations out of the 96 available; their location across Sicily is reported in Figure 3.1.

Figure 3.1: Location of rainfall gauging stations in Sicily.

Clustering

We decide to use the Affinity Propagation (AP) clustering algorithm mainly because neither the number of clusters nor reliable initial centroids are known in this context. A detailed comparison with the well-established K-means method is reported in Appendix B, providing further support for this choice. The clustering analysis is performed on both high-frequency data (10-minute measurements) and weekly averages. Two main streams of experiments are explored:

1. *Geographical (or spacial) clustering*, consisting of grouping similar geographical stations together along different time horizons.

2. *Local (or temporal) clustering*, consisting of grouping similar years together on each single location.

For the first category, we run the algorithm four times, according to the four collections of datasets C.A, C.B, C.C and C.D of Table 3.1. In contrast, the second category involves C.A_s and C.B_s for each station. The algorithm is implemented with default hyper-parameters: *convergence_iter* is set to 15, meaning that convergence stops if the number of clusters does not change for 15 iterations; the *preference* value corresponds to the median of the input similarities; and the availabilities are initialized to zero, $a(i,k) = 0$. In addition, two similarity metrics are considered in the AP implementation: Euclidean distance and correlation.

We first conduct clustering using the Euclidean metric, which results in a principal large cluster and few smaller communities consisting of one element each. For this reason, we apply an iterated version of the AP algorithm in order to detect new geographical clusters, at first glance hidden by the anomalies. To this aim, the AP implementation is based on a particular multi-step structure:

1) AP is applied to the whole considered collection of datasets.
2) The exceptions found at level one from the data are removed, and the AP algorithm reiterated over the remaining datasets.
3) The process is repeated from Step 1.

We then consider correlation distance as an *affinity* metric of AP. In this case no multi-step procedure is needed.

In order to understand the rainfall phenomena that mostly characterize the clusters, several rainfall indicators over time series are introduced according to Glickman [123], as reported in Table 3.2. We assemble the original 10 minutes records according to specific needs: naturally an *hour* data includes six consecutive records summed up together, whereas a *day* consists of the sum of 144 consecutive data. We also compute the total number of rainy hours, where one hour is considered "rainy" if its amount of rain is higher than zero. Hence, some of the introduced indicators are the percentages of light (l), moderate (m), and heavy (h) rainy hours over the total. Moreover, we consider the absolute number of violent rainy hours v, which is not expressed in percentage since it represents very rare events.

To assess the presence of statistical differences between two identified communities, we apply the well-known Kruskal-Wallis test, whose details are reported in Appendix B [124]–[126]. It is applied to each indicator and to all the experiments described above, according to the following logical evaluation steps:

1) Fix an indicator i.
2) Run the clustering algorithm.
3) Create an array k with one element for cluster. Every element of k is in turn an array a_c, containing the indicator values of the stations belonging to that cluster.
4) Run the Kruskal-Wallis test on k.
5) If the p-value is less than 0.05: i is considered as characterizing for the clusters. Otherwise no.

3.2.3 Results

Geographical investigation

Results of this set of experiments are visualized in the Sicily maps of Figure 3.2, where the 34 stations with names or symbols colored according to their relative clusters are drawn. When the multi-step version of the algorithm is applied, different shapes for the points are used. Specifically, circle, squares and diamond markers represent clusters resulting from the first, second, and third iterations, respectively.

Table 3.2: Description of the Indicators.

Variable	Indicator	Description
wh	Wet hours (%)	Percentage of rainy hours over the total number of hours.
mh	Maximum per hour	Maximum amount of rain of the data series grouped by hours.
i	Intensity (mm/h)	Quotient between the total amount of rain and the number of wet hours.
t	Total rain	Total amount of rain in the time series.
mv	Maximum daily variation	Maximum rainfall variation between two consecutive days over the total time series.
wd	Wet days (%)	Percentage of rainy days over the total number of days.
md	Maximum per day	Maximum amount of rain of the data series grouped by days.
l	Light rain (%)	Percentage of light (0–2.5 mm) rainy hours over the total number of rainy hours.
m	Moderate rain (%)	Percentage of moderate (2.6–7.5 mm) rainy hours over the total number of rainy hours.
h	Heavy rain (%)	Percentage of heavy (7.6–50 mm) rainy hours over the total number of rainy hours.
v	Violent rain	Number of violent ($>$ 50 mm) rainy hours in the time series. Not reported in percentage since it represented very rare events.

Annual clustering

The results of the geographical clustering year by year for C.A and C.B, both with the Euclidean and Correlation similarities are included in the GitHub Repository. We hereby report the main results drawn from the several performed experiments:

- Euclidean metrics - C.A: in this case the annual results consist mostly of a principal cluster (at most two) and some anomalous stations. Continuing in the years, a flow in anomalies that goes from western to eastern Sicily is detectable. We argue that anomalous clusters, consisting of a single station, are more prone to extreme events due to their strong location-dependent variability. This observation is validated through a case study for 2021, reported in Appendix B.
- Euclidean metrics - C.B: the reduction in the dataset size leads the clusters to be more uniform and refer to geographical divisions. However, there are some exceptions, mainly in the South-East Sicily, and in the neighborhood of *Palermo*. As in the previous case, this represents a trend on extreme events, more diffused in the East side of the island.
- Correlation metrics - C.A: in this case a geographical clustering pattern is obtained, identifying eastern and western Sicily. This is coherent with the fact that the Correlation metrics finds shape similarities and it is less sensitive to the micro-climatic differences.
- Correlation metrics - C.B: here the combination between dimensionality reduction and correlation metrics brings to a rough splitting of the island. The number of

clusters does not exceed three and often very far away stations are grouped together in the same cluster.

The results of the four settings for the year 2021 -reported in Appendix B- are in line with our initial research hypothesis, for which the anomalies correspond to *extreme* stations, as also confirmed by the Kruskal-Wallis test. Moreover, East Sicily emerges as the most *extreme* zone of the island, confirming the occurred events discussed in Levantesi [127]. Finally, the use of weekly averaged data (C.B) gives rise to balanced presence of both anomalies and territorial clusters in the Euclidean case.

Full clustering

We report here the full clustering results, obtained using C.C and C.D of Table 3.1. Similarly to the annual case, the use of Euclidean metrics brings to anomalies detection, by highlighting the presence of clusters composed by a unique site. We claim that the reason why anomalous clusters are independent lies on the fact that extreme events intensities are very different among sites [128]. Figure 3.2a shows the presence of one principal cluster and many anomalies, such as *Pedara*, *Augusta* and *Siracusa*. In contrast, Figure 3.2b reports different principal clusters - geographically distributed - and only one exception: *Pedara*.

In order to validate results, we carry out a case by case analysis. First of all, the full and the annual clustering results in the case of Euclidean metrics (C.A and C.C, respectively) are compared in Figure 3.2a by counting how many times the stations has been clustered as anomalous in the annual case. It turns out that the stations with an higher counter are the ones clustered as anomalies in the full case as well, except for *Catania*. In any case, Figure 3.2a confirms the results consistency, since East Sicily emerges as the most *extreme* side of the island.

The Kruskal-Wallis test is then applied to the full case. Among the characterizing indicators, *md* (Maximum per day) and h (Heavy rain (%)) are particularly relevant in the full case. Figures 3.2c and 3.2d show the *md* and h heatmaps in the full case, respectively. Several similarities among the maximum values of the indicators and the anomalies can be observed. Therefore, the *extreme* stations coincide with the anomalous clusters. Moreover, the *red* cluster in Figure 3.2b represents a cluster of *extreme* stations, confirmed by Figure 3.2d. In fact, apart for the anomaly of *Pedara*, these stations retain the highest values of the h indicator.

In conclusion, the different implemented experimental settings allow us to highlight several different aspects of extreme events. Certainly, the presence of these phenomena in eastern Sicily emerges both from the annual and the full clustering, especially when the Euclidean metrics is used as a similarity measure in the AP algorithm. On the other hand, the use of Correlation metrics brings to consider Sicily composed of two different climatic areas: West side and East side, as shown in Figure 3.3, where there are only two large clusters. Moreover, in this case no similarities between characterizing indicators and clusters are found (compare Figures 3.3a and 3.2c, Figures 3.3b and 3.2d).

Eventually, the clustering involving C.C with the use of the Euclidean metrics seems to be the most performing setting - among those tested - in finding extreme events; whereas, collection C.D results as the most suitable arrangement to obtain geographically uniform clusters.

To confirm the latter results, first we compare our C.D findings with previous works in literature, obtaining similar geographical distributions [121], [129], [130]. In fact, in those works - as well as in figure 3.2b - there is a geographical splitting of the region highlighting the North, West, Center, East, and South-East Sicilian sub-regions.
Moreover, we evaluated the Kruskal-Wallis test between the clusters and the altitudes of the rain gauges for both collections C.C and C.D. In the case of collection C.C, the p value related to the *altitude* turns out not to be characterizing for the clusters ($p = 0.31$). Differently, in the case of C.D collection, the related p value is 0.03, confirming that the *altitude* characterizes the clusters. This suggests that the weekly mean data show a

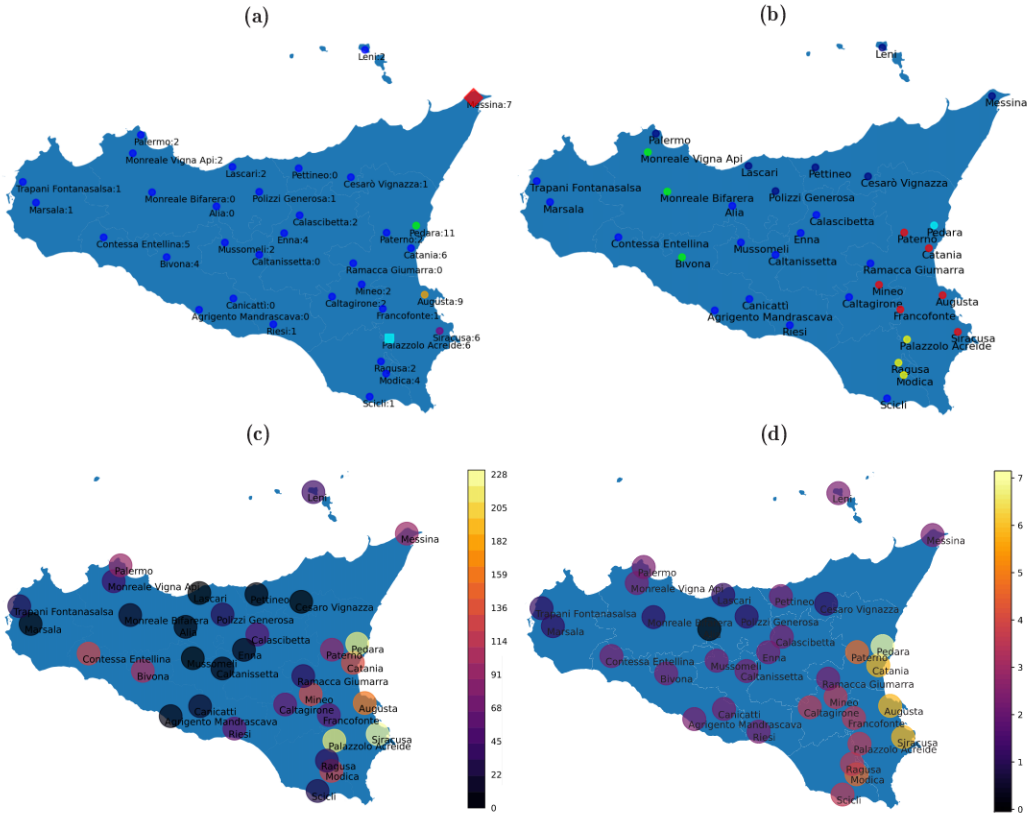

Figure 3.2: Full case - Euclidean metrics. In **(a)** and **(b)** different colors represent different clusters. Square and diamond points represent results from, respectively, the second and the third iteration of the algorithm. **(a)**: C.C. The principal cluster is reported in blue. The numbers indicate how many times the stations has been clustered as anomalous in the annual case. **(b)**: C.D. The five main clusters are reported in green, blue, dark blue, red and yellow. **(c)**: C.C. Maximum per day (md) heatmap. **(d)**: C.D. Heavy rain (%) (h) heatmap.

Figure 3.3: Full case - Correlation metrics. **(a)**: C.C. **(b)**: C.D. The two clusters are reported in red and blue in both the panels.

weak ability of representing extreme events, while they satisfactorily embed geographical aspects of the station gauges locations.

Local investigation

In the local case we investigate the temporal evolution of rainfall events. In particular, anomalous years in the entire observed period are detected. To this aim, the AP algorithm

is applied only to C.A_s and C.B_s, analyzing one station per time. As in the geographical investigation, we choose to use both the Euclidean and the Correlation metrics. In order to understand the most *anomalous* years, we count (over stations) how many times one year appears as exception when using the Euclidean distance. Figures 3.4a and 3.4b report in red the years counters in C.A_s and C.B_s, respectively. In both cases the most

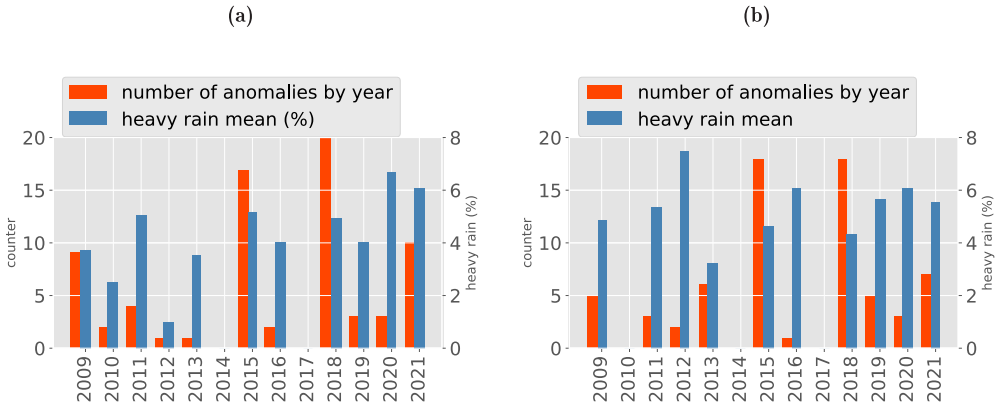

Figure 3.4: Anomalous years - Euclidean metrics. **(a)**: C.A_s. **(b)**: C.B_s. The heavy rain mean of the year y consists of the mean of the *heavy rain (%)* values for all the stations that cluster the year y as anomalous.

anomalous years are 2015 and 2018. This means for instance that 2018 is clustered as anomalous in about 20 over 34 stations for Euclidean distance and C.A_s. We also see that the 2021 counter increases after the years 2019 and 2020.

Figures 3.4a and 3.4b also report in blue the *heavy rain (%)* mean values. In this case, we fix a year y and we compute the mean of the *heavy rain (%)* values for all the stations that cluster the year y as anomalous, thus obtaining, for instance, that 2020 and 2021 have the highest mean values. Summarizing, in the case of C.A_s and Euclidean distance, an increasing trend on anomalous years is found concerning the heavy rain mean indicator (see Figure 3.4a in blue). On the other hand, in C.B_s and Euclidean distance, the trend is less detectable and the highest value of heavy rain mean is measured in 2012 (see Figure 3.4b in blue).

3.2.4 Discussion

This work presents several significant findings. East Sicily is increasingly becoming a protagonist of extreme events, both across the full period of recordings and in single annual cases, confirming the results of Bonaccorso and Aronica [121]; this outcome is particularly evident when using Euclidean metrics in the AP implementation. High-frequency data combined with Euclidean metrics highlights an increasing trend of extreme events over the years, while weekly averaged data does not provide the same evidence. In this context, 2021 clearly emerges as one of the most anomalous years.

A statistical validation confirms that three indicators—maximum per day (md), maximum daily variation (mv), and heavy rain percentage (h)—effectively describe anomalous clusters, showing that these are most often characterized by extreme events. The AP algorithm proves suitable for detecting anomalies, namely extreme stations, when applied to the full dataset: with Euclidean metrics, Augusta, Siracusa, and Pedara are identified as anomalous at the first iteration, while Palazzolo Acreide and Messina emerge at the second and third runs, respectively. The Euclidean metrics also shows sensitivity to micro-climatic differences, since geographically close stations may be assigned to different clusters. Conversely, the correlation metrics tends to identify more uniform clusters, as seen in the full case where the algorithm divides Sicily into eastern and western regions.

Overall, high-frequency data with Euclidean metrics emerges as the most effective setting for detecting extreme rainfall events through geographical clustering. At the

same time, reducing the dataset to weekly means proves useful to identify geographically uniform clusters, merging anomalies and territorial clusters in a balanced way and still capturing extreme clusters, particularly in eastern Sicily.

Limitations and future directions

The study nonetheless has some limitations, mainly due to the short observational period, which may be influenced by natural variability. Further research is needed to assess the most suitable dimensionality reduction methods for local analyses and to refine rainfall indicators. Extending the spatial and temporal coverage, and applying more robust aggregation strategies, would strengthen the detection of extreme rainfall trends and potential climate change signals.

3.3 Wearable Swarm Sensors for Air Quality Monitoring

This section summarizes and adapts the work presented in [131] and [38], which develops a wearable air quality monitoring tool to collect geo-localized measurements of pollutants and environmental parameters in Siena (Italy). The study integrates these novel spatio-temporal datasets with a neural network model, capable of predicting the geo-localization of an observation given the air quality monitoring information (RQ4). This work serves as an application of data-driven techniques for environmental monitoring, highlighting the potential of such datasets to support policy decisions, such as optimizing the placement of new fixed monitoring stations.

3.3.1 Introduction

Air quality monitoring is increasingly important for public health, given its link to respiratory, cardiovascular and other diseases [132], [133]. Traditional fixed stations provide valuable data but are limited in spatial coverage. Wearable and portable sensors represent a promising solution, enabling real-time, geo-localized monitoring of pollutants such as PM, NO_2, CO_2, and VOCs [133]. These devices can complement fixed stations by providing dense spatio-temporal measurements.

In this work we present WeAIR, a prototype wearable sensor node that integrates electrochemical and infrared gas sensors with on-board processing, storage, and wireless communication. Unlike most commercial devices, WeAIR is customizable, supports open communication protocols, and can be integrated into broader monitoring platforms.

Using WeAIR, we conduct a monitoring campaign in Siena (Italy), producing a novel geo-localized dataset that we publicly release. We further apply a neural network model to predict the geographical location of observations based on air quality parameters. This demonstrates how individual-level wearable data can support both citizens' awareness and institutional decision-making, particularly for validating fixed stations and planning their optimal distribution.

Compared with related wearable systems [134]–[136], our approach is distinctive in combining a data acquisition tool and an AI-based processing method. To our knowledge, this is among the first works proposing a complete framework for mobile air quality monitoring and geo-localization, showing the potential of pervasive, AI-enabled sensing for environmental management.

In this work, my contribution focuses on the data preprocessing phase, which significantly enhances my skills in data management and strengthens my ability to handle complex multivariate datasets.

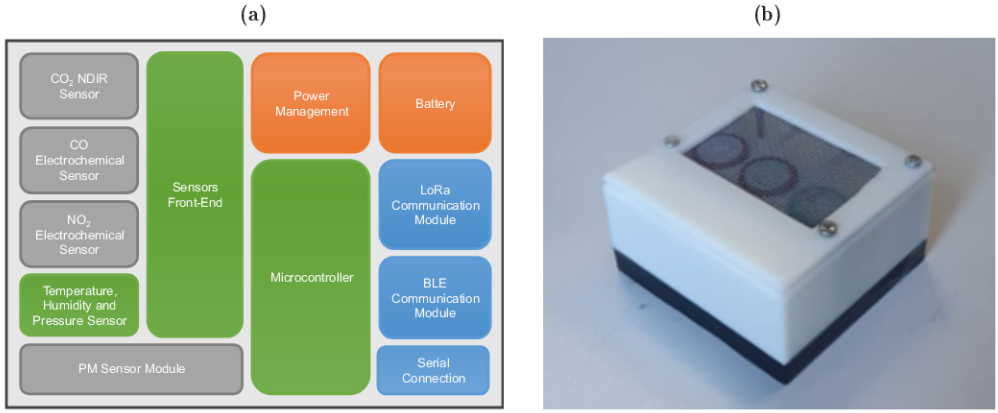

Figure 3.5: **(a)**: Sensor Node Architecture and **(b)**: Prototype.

3.3.2 Methods

Sensor Node Architecture Design

The WeAIR node is a wearable device integrating electrochemical and NDIR gas sensors together with modules for PM, temperature, humidity and barometric pressure. Data are transmitted via Bluetooth Low Energy (BLE) to a smartphone, enriched with GPS coordinates, and uploaded to a server. The architecture of the sensor node and the prototype of the sensor node with the plastic enclosure (dimensions: $80mm \times 80mm \times 45mm$, weight: $250g$) are shown in Figure 3.5.

The WeAIR node is wearable, battery-powered, and transmits data via BLE to a smartphone app. The app enriches measurements with GPS and user ID, then uploads them to a cloud server. Specifically, the app is developed using the Android Studio environment (Android SDK API 35) and tested on Android phones. This first version of the app is intended for system testing purposes only. The node architecture minimizes energy consumption, avoids additional infrastructure, and supports large-scale adoption. All data are stored with timestamps and geo-references, forming a continuous spatio-temporal dataset ready for analysis.

Data

Using the WeAIR prototype, we collect a novel geo-localized air quality dataset in Siena (Italy), publicly available at the GitHub Repository. Data are acquired at 1-second intervals and resampled every 5 seconds to synchronize with localization.

The monitored parameters include environmental temperature (AMBT, [°C]), relative humidity (AMBH, [%]), barometric pressure (AMBP, [Pa]), carbon monoxide (CO, [ppm]), nitrogen dioxide (NO_2, [ppm]), carbon dioxide (CO_2, [ppm]), and particulate matter with diameter smaller than 10 μm (PM10, $[\mu g/m^3]$).

These variables are selected for their relevance to urban air quality and for comparability with the only fixed monitoring station in Siena, used as reference for validation. CO and NO_2 are toxic gases typically produced by combustion processes (traffic, heating), while PM10 provides a robust index of urban and industrial pollution. Temperature, humidity and pressure are essential contextual variables for interpreting pollutant dynamics.

Each record in the dataset is associated with geographical coordinates, allowing for spatio-temporal analysis. Data are collected during everyday activities, both indoors and outdoors, by car and on foot. The campaign lasts from January 22 to February 18, 2024, producing 270,089 samples at a 5-second resolution. This dataset is, to our knowledge, the first large-scale geo-localized collection of air quality data in Siena.

Data Pre-processing

Raw data undergo several preprocessing steps to obtain a clean and consistent dataset. First, GPS traces obtained with the Sports-Tracker App[1] are merged with sensor observations using a 5-second threshold. In this way, we obtain a complete dataset for each campaign day.

We filter out cases where we have location data but no sensor data. We then synchronize missing positions within the same days by filling the gaps with the last recorded position to ensure no sensor data is lost. The same process is applied across datasets from different days and finally, we combine them into a unique dataset of about 300,000 records with a 5 seconds sampling rate.

Outliers from device initialization or anomalous events are removed, and a smoothed version of the dataset is created by averaging every 10 consecutive samples, removing therefore the natural oscillations of the time series.

Table 3.3: Summary statistics of the seven indicators under study: minimum, maximum, mean, and standard deviation.

Indicator	Min	Max	Mean	Std Dev	UoM
AMBT	10.17	32.30	23.20	2.94	°C
AMBH	10.97	73.66	33.07	6.78	%
AMBP	94248.28	101461.70	98495.18	1007.74	Pa
CO	∼0.00	7.46	0.78	0.63	ppm
NO_2	∼0.00	1.19	0.73	0.14	ppm
CO_2	50.00	240.00	87.90	28.28	ppm
MASS_PM10	0.00	330.42	4.28	7.64	$\mu g/m^3$

Table 3.3 summarizes the ranges, mean and standard deviation of the main air quality indicators after preprocessing.

Neural Network Model

To perform the prediction of latitude and longitude from air–monitored parameters collected with WeAIR, we consider a very simple neural network consisting of three layers. We perform hyperparameter tuning on the activation function, the number of hidden layers, and the number of neurons per hidden layer to identify the best configuration, shown in Figure 3.6. The architecture includes:

- Input layer: 7 neurons (humidity, pressure, CO, NO_2, CO_2, PM10, temperature); Each neuron utilizes the Rectified Linear Unit (ReLU) activation function to introduce non-linearity into the model.
- Dropout layer (rate 0.2), added to regularize the model by randomly dropping 20% of the neurons during training.
- Hidden layer: 40 neurons with ReLU activation, allowing the network to capture complex patterns in the data.
- Dropout layer (rate 0.2), added to further prevent overfitting.
- Output layer: 2 neurons (latitude and longitude coordinates), linear activation, enabling the model to predict continuous values, as latitude and longitude are.

[1] https://www.sports-tracker.com/dashboard

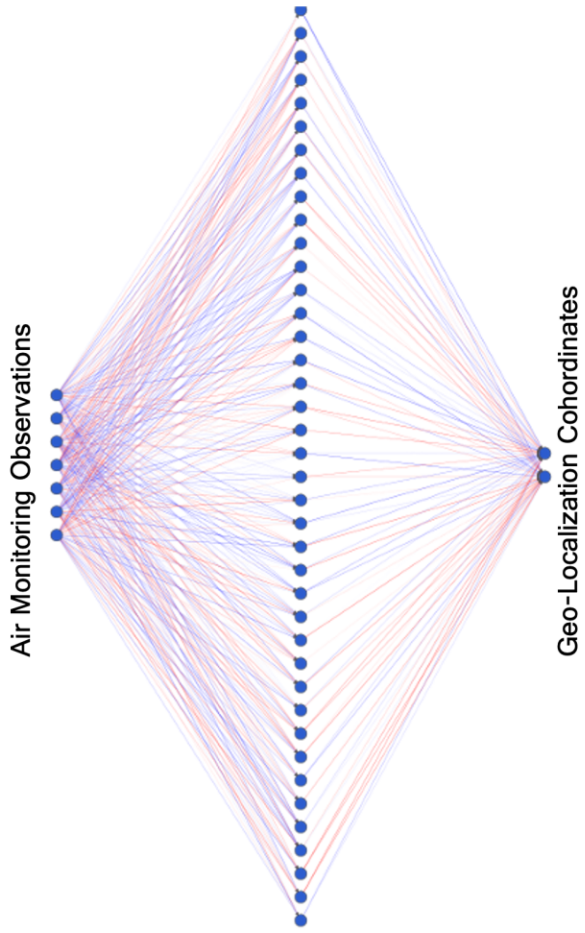

Figure 3.6: Neural network used in our experiments to predict latitude and longitude given air monitoring parameters. The hidden layer consists of 40 neurons, the input layer consists of 7 neurons for the humidity, pressure, CO, NO_2,CO_2, PM10 and temperature observations, while the output layer has 2 neurons to output the geographical coordinates.

3.3.3 Results

Exploratory Analysis

We perform temporal and spatial analyses of each pollutant. For example, Figures 3.7 and 3.8 illustrate the time series and the spatial heatmap mapped on Siena's street network using OSMnx of CO_2 concentrations, respectively.

To validate our prototype, we compared mobile measurements with the fixed ARPAT station at Viale Bracci. As shown in Figure 3.9, CO readings from WeAIR (in blue) closely follow the fixed station trend (in red), confirming calibration and consistency of the wearable device.

Specifically, our data are collected approximately every 1 second from 19:05:27 to 19:22:42, and then sampled every 5 seconds, while the ARPAT average corresponds to the data from 19:00 on 18/02/2024. The ARPAT sampling rate complies with Italian regulations, which require a sampling interval of approximately 0.6 seconds, followed by an hourly average. Occasionally, technical issues result in incomplete data collection for the full hour, but ARPAT ensures at least 75% data coverage.

Neural Network Experiments

We perform the following set of experiments. For each day of observation we train a model, able to predict the latitude and longitude of a sample, starting from the observations of

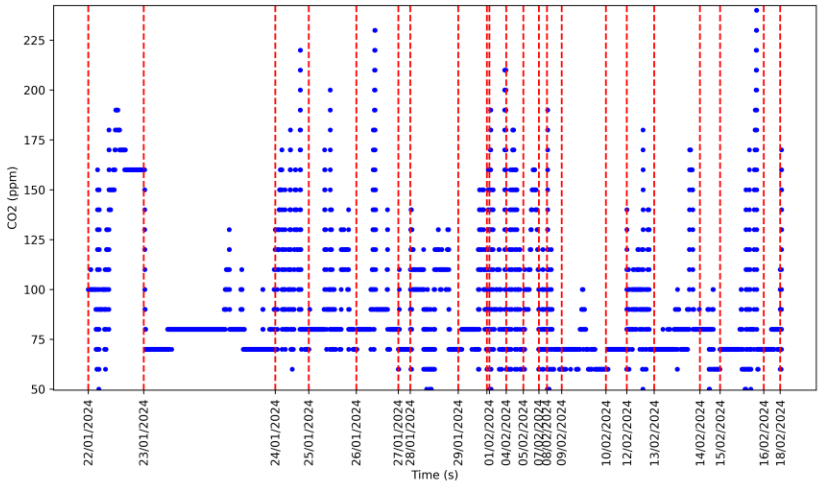

Figure 3.7: Temporal CO_2 data, measured in ppm and collected by the mobile sensor during the monitoring period. The discretization is determined by the resolution of the acquisition system.

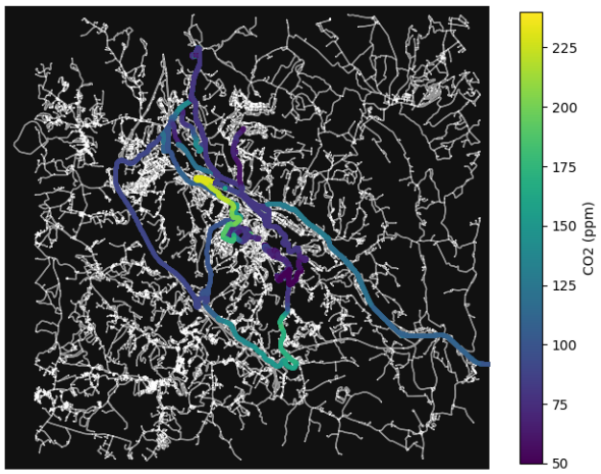

Figure 3.8: Spatial CO_2 data collected by the mobile sensor during the monitoring period. The data is represented using a heatmap over the range of measured values of ppm.

environmental humidity, pressure and temperature, CO, NO_2, CO_2 and PM10. Each daily observation dataset is divided into training and test, using hold-out method a random splitting (20%). The results of the test set performances in terms of Mean Square Error (MSE) and Mean Absolute Error (MAE) for each day are reported in Table 3.4.

The daily models achieved variable results depending on trajectory complexity, with MAE values ranging from 0.001 to 0.56. However, some days have an almost stable geo-localization, thus we consider a global model. In this case the training set is made up of all of the observations of the days in which a non-stable path is present. More specifically these are the days included in the final training set model: 22, 24, 25, 26, 28 and 29 of January, and for February we consider 1, 4, 5, 7, 8, 12, 13, 14 and 18. The model trained in this way obtains good performances in the test set, with a test MAE of 0.030229 and a test MSE of 0.005476, demonstrating robust predictive capabilities (see Table 3.4).

As a further experiment, we consider the median vector of all of the air monitoring observations of the test set. The rationale behind performing such experiments, is related to the fact that in this way we could have a summary input-vector, to then later predict where for instance optimal fixed station should have stayed. Performing this experiment, we obtain a predicted geo-localization of $(43.339325, 11.323781)$ (see Figure 3.10). Such

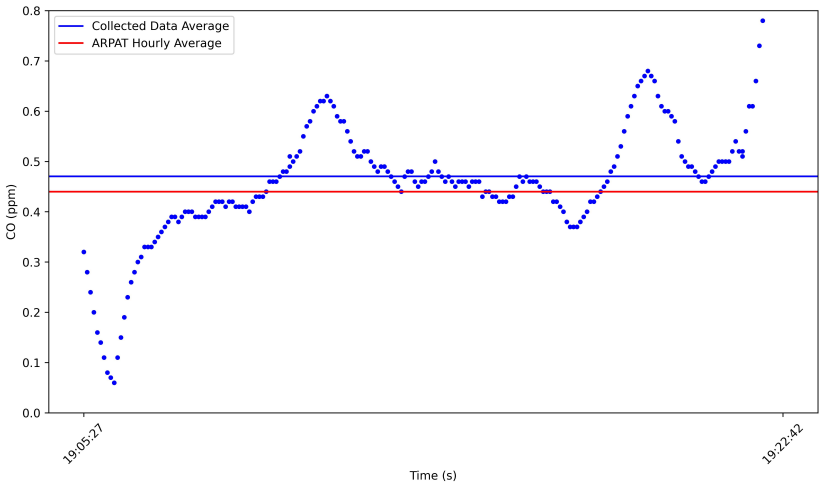

Figure 3.9: Visual representation of CO data measured in ppm on 18/02/2024. Blue points indicate readings collected by the mobile sensor, while the red line represents the hourly average derived from the fixed ARPAT station at Viale Bracci (Siena).

Table 3.4: Test set MAE and MSE for each day obtained with the daily models for the prediction of the GPS location given the air monitoring coordinates. Unit of measures reported for MSE and MAE are the squared errors with respect to the GPS coordinates.

Day	MAE	MSE	Day	MAE	MSE
22 Jan 2024	0.053	0.005	05 Feb 2024	0.352	0.245
23 Jan 2024	0.001	6.3e-07	07 Feb 2024	0.317	0.145
24 Jan 2024	0.217	0.086	08 Feb 2024	0.269	0.095
25 Jan 2024	0.020	0.0006	09 Feb 2024	0.269	0.135
26 Jan 2024	0.205	0.076	10 Feb 2024	0.030	0.001
27 Jan 2024	0.017	0.0008	12 Feb 2024	0.217	0.090
28 Jan 2024	0.150	0.034	13 Feb 2024	0.182	0.060
29 Jan 2024	0.229	0.097	14 Feb 2024	0.368	0.223
31 Jan 2024	0.563	0.508	15 Feb 2024	0.141	0.034
01 Feb 2024	0.113	0.024	16 Feb 2024	0.101	0.023
04 Feb 2024	0.023	0.001	18 Feb 2024	0.284	0.181
All days together: MAE = 0.027, MSE = 0.009					

latitude and longitude pair is located very close to where the fixed station of Siena is. This suggests the feasibility of using wearable data to guide optimal placement of new fixed stations. All trained models and visualization files are available in the public GitHub Repository.

3.3.4 Discussion

The use of wearable devices for air monitoring represents a promising approach to better understand air quality and its impact on health. In this work we introduce WeAIR, a prototype wearable sensor for pollutants and environmental parameters, and demonstrate its application in a monitoring campaign in Siena (Italy).

Our main contributions are: (i) the design and release of the WeAIR device; (ii) the collection and public release of a novel geo-localized dataset; (iii) the release of trained neural network models and spatial maps derived from the campaign.

Experimental results showed that a simple feedforward neural network can predict geo-localization from air quality observations with good accuracy. Notably, the median observation vector predict coordinates close to the existing fixed monitoring station, suggesting that such models could support decision-making on the placement of new stations. Furthermore, WeAIR can foster citizen engagement by providing real-time

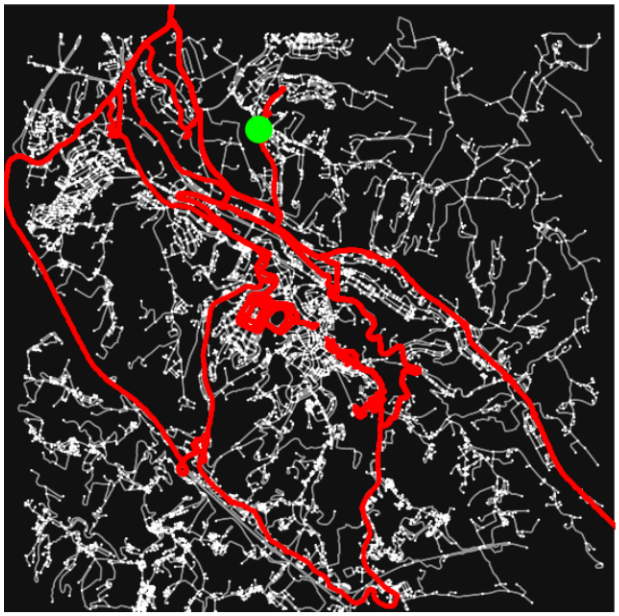

Figure 3.10: Neural network predictions of geo-localization in Siena, visualized with OSMnx. Predictions for the median observation vector, using the model trained on all monitored days. Training data are shown in red, predicted data in green. The center and edge of each map are adjusted ad hoc to enhance visualization (edge ∼6 km).

awareness of pollution exposure. This paradigm emphasizes active participation and education.

Limitations and future directions

Limitations remain, particularly the need for large-scale adoption to ensure representative coverage. As future work, we plan to extend the monitoring campaign, produce multiple devices, and explore user-friendly designs (e.g., 3D-printed cases) to encourage wider participation.

II Novel Methods for Psychology

Chapter 4

Egosyntonicity and Emotion Regulation: A Probabilistic Model of Valence Dynamics

Contents

This Chapter summarizes and adapts the work presented in [39], which introduces a novel Markovian model that describes the impact of egosyntonicity on emotion dynamics (RQ5-RQ6). We focus on the dominant current emotion, and describe the time evolution of its valence, modeled as a binary variable, where 0 and 1 correspond to negative and positive valences, respectively. In particular, the one-step transition probabilities will depend on the external events happening in daily life, the attention the individual devotes to such events, and the egosyntonicity, modeled as the agreement between the current valence and the internal mood of the individual. A steady-state analysis shows that, depending on the model parameters, four classes of individuals can be identified. Two classes are somewhat expected, corresponding to individuals spending more (less) time in egosyntonicity experiencing positive valences for longer (shorter) times. Surprisingly, two further classes emerge, *the self deluded* individuals, where egosyntonicity is associated to a prevalence of negative valences, and *the troubled happy* individuals, where egodystonicity is associated to positive valences. These findings are aligned with the literature showing that, even if egosyntonicity typically has a positive impact in the short term, it may not always be beneficial in the long run.

IV

4.1 Introduction

Emotional theories in psychology seek to understand how emotions are generated and experienced, focusing on the interplay between physiological, neurological and cognitive processes, and emotional responses [137]. Emotion dynamical patterns are the complex results of a large number of factors, that shape its evolution over time. We are interested in *process theories*, where emotions are assumed to be an adaptive element of a feedback loop that involves the situations we encounter, our perceptions of these situations, the emotions they trigger, and the actions we take to alter our circumstances [138], [139]. In this context, emotional regulation plays a crucial role in human behavior and well-being. In fact, not only how good or bad people feel on average, but also how their feelings fluctuate across time is crucial for psychological health [140]. Emotion regulation can be either deliberate or automatic, the latter being pervasive in everyday life, and having far-reaching consequences for individuals' emotions [141].

The study of emotion dynamics allowed researchers to make inferences about features of the emotion regulatory system [142]. Namely, the main principles describing emotion dynamics are:

- *Contingency*: emotions are typically contingent on internal or external events. Internal events include physiological states or cognitive processes (e.g., feeling

anxious due to personal worries), while external events involve interactions with the environment or social contexts (e.g., feeling happy upon receiving good news). For instance, both excessive and reduced emotional reactivity are believed to contribute to mood disorders like depression and bipolar disorder.

- *Inertia*: emotional states display an intrinsic resistance to change, as we tend to perceive and interpret the world around us in ways congruent with our current emotional state. For instance, high emotional variability and excessive emotional inertia are both linked to indicators of ill-being and psychopathologies like depression, bipolar disorder, and borderline personality disorder.
- *Regulation*: individuals manage their emotional experiences using various deliberate or automatic strategies. For instance, antecedent-focused regulation involves techniques like cognitive reappraisal, where a person reinterprets a situation to change its emotional impact, such as seeing a job interview as a learning opportunity instead of a threat. In contrast, response-focused regulation involves managing emotions after they are felt, such as expressive suppression, where one hides feelings of sadness.
- *Interaction*: the components of emotions (physiological, experiential, behavioral), or the emergent emotional states as they are experienced as a whole, continuously interact with, augment, and blunt one another, creating a system of interacting elements.

Based on these fundamental principles, several alternative theories on emotions have been developed [143]–[146]. However, such theoretical frameworks typically lack a clear connection with the substantial amount of empirical research on emotions [147], both within neuroscientific [148] and physiological research [149]. To bridge this gap, researchers have sought to use mathematical models that offer a formal language to capture both quantitative and qualitative aspects of concepts and theories [28], [150]–[154]. For instance, [25] underlines individual differences in affect dynamics through a model that effectively captures the dynamics observed in real data.

Recently, Markov models have emerged as a powerful mathematical tool for capturing the key features of emotion dynamics [36], [75]. As argued by [155], affects, as dynamic and evolving processes, can be effectively analyzed using Markov chain approaches to decipher how emotional states change over time. In [156], the authors have used Markov models to capture the mental models that individuals build to predicting the others' emotional dynamics. In [157], two Markov chains have been identified from data on healthy and schizophrenic individuals, respectively, revealing that schizophrenic individuals tend to remain in negative emotional states and show maladaptive transitions.

A recent work from [31] has first used a Markov chain as a generative model of emotions in daily life. In particular, their model, grounded in the *principle of contingency*, formalized the link between external situations and emotions. Transitions between situations are described by a Markov model, which is characterized by one parameter, that corresponds to the probability of transitioning to any of the other situations. In turn, being in a situation determines the mean of the Gaussian distribution that describes the emotions experienced by the individual. This simple, yet effective model is capable of reproducing several empirical phenomena that are observed in the literature, such as the skewed distribution exhibited by some emotion variables [158].

Following [144], also [31] suggest to extend their basic model to complete a feedback loop between situations, attention, emotion and action. The goal of our study is then to make a first step in this direction and model the dynamics of the valence, i.e. the pleasantness or unpleasantness associated with an emotion according to the Russell circumplex model [159], illustrating how the conflict between real and expected situations influences emotion regulation. Rather than studying the dynamics of an ensemble of emotions, we focus on the valence of a single generic emotion that represents the overall emergent emotional state at each time instant, and build a tractable model that simultaneously accounts for the principles of *contingency*, *inertia*, and *regulation* described above. Depending on

the model parameters, the valence evolution can be diversely affected by egosyntonicity, that is, the coherence between the experienced and expected emotions. Egosyntonicity and egodystonicity describe how certain emotions, ideas and beliefs align or conflict with an individual's self-perception [160]–[162]. For example, if a person feels happiness due to upcoming holidays, and such emotion was expected, the experience would be considered egosyntonic. Conversely, if the same person in the same situation expects to feel happiness but instead experiences a different emotion, like distress, it would be regarded as egodystonic.

A parametric study of the model allowed us to identify four key classes of individuals, corresponding to commonly observed healthy or pathological behaviors. Crucially, the four classes differ for the way they regulate the valence based on the time spent in egosyntonicity. Namely, we identify the *balanced happy*, who are healthy individuals that experience long-term positive emotions fostered by egosyntonicity; the *self-deluded*, who is primarily egosyntonic yet experiences negative emotions, as in individuals suffering from personality disorders [163]; the *chronically troubled*, who struggles with internal conflict and negative emotions, as in individuals with obsessive compulsive disorder [164]; and the *troubled happy*, who maintains a positive attitude despite ongoing internal conflicts, as is typical of self-aware egodystonic individuals that seek help e.g through therapy.

The Chapter proceeds as follows: in Section 4.2 we provide a detailed description of the proposed Markovian model, focusing on its defining features and theoretical foundations; in Section 4.3, we conduct both a general and a parametric analysis to uncover insights and identify emerging behaviors associated with the model's dynamics. Section 4.4 concludes the work.

4.2 Methods

Following [156] and [31], we employ a discrete-time Markov model to describe the time-evolution of the valence of the individual emotional state. We consider three binary state variables, associated to the internal mood M, the external events E, and the experienced valence V. In particular, a value of 1 (0) for M, E, or V represents a positive (negative) mood, external situations, and valence, respectively.

The model is grounded in the *principles of inertia, contingency, and regulation*[1]. Specifically, based on the *principle of inertia*, the individual will have a positive probability r of remaining in the same mood at the next time-step. Moreover, based on the *principle of contingency*, the valence dynamics will be influenced by those of internal mood and external events. Finally, according to the *principle of regulation*, the transitions between negative and positive valences will be affected by egosyntonicity, that is, the coincidence between the internal mood and the valence, $M = V$.

We further assume that the dynamics of the internal mood and external events are not affected by each other, and by the valence. The rationale behind this assumption is to preserve the tractability and interpretability of the model, at the same time retaining its ability to align with the principles of *contingency*, *inertia*, and *regulation*. In what follows, we start by describing the dynamics of M and E, to then clarify how they influence the valence dynamics.

Mood and External situations dynamics

The transitions between negative ($M = 0$) and positive ($M = 1$) moods are modeled as a Markov chain with a transition probability matrix:

$$P_M = \begin{pmatrix} r & 1-r \\ 1-r & r \end{pmatrix}, \tag{4.1}$$

where the parameter $r \in]0, 1[$ represents the probability of remaining in the same mood in the next time step. The higher r, the more the behavior of the individual is aligned with

[1]We do not consider the principle of interaction since we are focusing on the dominant emotion.

the *principle of inertia*, according to which they are inclined to remain in their habitual mood.

The transitions between negative ($E = 0$) or positive ($E = 1$) external situations are regulated by a Markov chain whose transition probability matrix is:

$$P_E = \begin{pmatrix} s & 1-s \\ 1-s & s \end{pmatrix}, \tag{4.2}$$

where the parameter $s \in]0, 1[$ denotes the probability of staying in the same external situation in the next time step.[2]

Valence dynamics

The valence of the emotion, representing the individual's overall emotional state, is formalized by $V(t) \in \{0, 1\}$, and its dynamics is modeled by the transition probability matrix

$$P_V(t) = \begin{pmatrix} p_{00}^V(t) & 1 - p_{00}^V(t) \\ 1 - p_{11}^V(t) & p_{11}^V(t) \end{pmatrix}, \tag{4.3}$$

where $p_{ii}^V(t) = P(V(t) = i | V(t-1) = i)$ is the probability of remaining in the same valence at the next time step. The transition probability will depend on whether the individual is egosyntonic or not, that is, whether its current valence $V(t)$ coincides with its internal mood $M(t)$. In particular:

- The probability of remaining in a negative valence in the next step is

$$\begin{aligned} p_{00}^V(t) &= \omega(1 - E(t-1)) + (1-\omega)\eta_0(t), \\ \eta_0(t) &= \begin{cases} 1-\alpha, & \text{if } V(t-1) = M(t-1), \\ 1, & \text{if } V(t-1) \neq M(t-1), \end{cases} \end{aligned} \tag{4.4}$$

  where $\omega \in]0, 1[$ represents the attention that magnifies the impact of external events on valence dynamics [165]; for instance, a higher ω implies that positive external events, for which $E(t-1) = 1$, will correspond to lower probabilities of remaining in a negative valence. The time-varying parameter η_0 takes two different values depending on whether the individual is egosyntonic in the previous time step, with $\alpha \in]0, 1[$ modulating how much egosyntonicity decreases the probability of remaining in a negative valence.

- The probability of remaining in a positive valence in the next step is

$$\begin{aligned} p_{11}^V(t) &= \omega E(t-1) + (1-\omega)\eta_1(t), \\ \eta_1(t) &= \begin{cases} 1, & \text{if } V(t-1) = M(t-1), \\ 1-\beta, & \text{if } V(t-1) \neq M(t-1), \end{cases} \end{aligned} \tag{4.5}$$

  where, as in (4.4), the attention parameter ω quantifies the impact of external events on valence dynamics, whereas η_1, similar to η_0 in (4.4), changes according to the presence or absence of egosyntonicity, with $\beta \in]0, 1[$ modulating how much egodystonicity decreases the probability of remaining in a positive valence.

We emphasize that we have modeled valence dynamics according to the principles of *contingency* and *regulation*. Indeed, the dependence of V on both M and E allows to distinguish between the impacts of internal and external situations on the emotion dynamics, in agreement with the *principle of contingency*.

[2] To exclude the case of a deterministic evolution of M and E, we have considered both r and s in the open interval $]0, 1[$.

In our model, regulation does not take place through deliberate strategies, but is mediated through egosyntonicity, which is known to promote acceptance of emotions, in contrast with egodystonic feelings with often result in avoidance or desire for change [142], [166]–[168]. Specifically, the second term at the right-end side of (4.4) and (4.5) changes depending on whether the individual is egosyntonic, thereby representing an implicit mechanism of adjustment that aligns with the *principle of regulation* [144]. Egosyntonic experiences are perceived as positive, thus increasing the probabilities of remaining or transitioning towards a positive valence. The opposite happens for egodystonic experiences, which are perceived as unpleasant [164]. Albeit egosyntonicity steers the transition probabilities towards a positive valence, its effect on the long-term, steady-state valence of the emotion is non-trivial and will depend upon the three parameters α, β, and ω in (4.4) and (4.5), and r in (4.1), as we will illustrate in Section 4.3. The state variables and the related parameters of the model are summarized in Table 4.1.

Table 4.1: State variables and associated parameters modulating their transition probabilities.

State variables	Short description	Related parameters
$M(t)$	Internal Mood	r
$E(t)$	External situations	s
$V(t)$	Valence of the emotion	α, β, ω

Overall Markov model

By combining equations (4.1)–(4.5), the overall dynamics of the valence, mood, and external events yield an 8-state Markov chain, which can be described as follows:

1. A state space $X = \{1, \dots, 8\}$, where $1 \equiv (V = 0, M = 0, E = 0)$, $2 \equiv (V = 0, M = 0, E = 1)$, $3 \equiv (V = 0, M = 1, E = 0)$, $4 \equiv (V = 0, M = 1, E = 1)$, $5 \equiv (V = 1, M = 0, E = 0)$, $6 \equiv (V = 1, M = 0, E = 1)$, $7 \equiv (V = 1, M = 1, E = 0)$, $8 \equiv (V = 1, M = 1, E = 1)$. Every possible state corresponds to being in a given valence, mood and subject to a given external situation, simultaneously.
2. An initial state probability vector $\pi_i(0) = P[X_0 = i]$, for all $i \in X$.
3. The transition probabilities $p_{ij} = P[X_{t+1} = j | X_t = i]$, where i is the current state and j is the next state, collected in the following 8×8 matrix P:

$$\begin{pmatrix}
(\omega+\overline{\alpha\omega})rs & (\omega+\overline{\alpha\omega})r\overline{s} & (\omega+\overline{\alpha\omega})\overline{r}s & (\omega+\overline{\alpha\omega})\overline{r}\,\overline{s} & \alpha\overline{\omega}rs & \alpha\overline{\omega}r\overline{s} & \alpha\overline{\omega}\overline{r}s & \alpha\overline{\omega}\overline{r}\,\overline{s} \\
\overline{\alpha\omega}r\overline{s} & \overline{\alpha\omega}rs & \overline{\alpha\omega}\overline{r}\,\overline{s} & \overline{\alpha\omega}\overline{r}s & (\omega+\alpha\overline{\omega})r\overline{s} & (\omega+\alpha\overline{\omega})rs & (\omega+\alpha\overline{\omega})\overline{r}\,\overline{s} & (\omega+\alpha\overline{\omega})\overline{r}s \\
\overline{r}s & \overline{r}\,\overline{s} & rs & r\overline{s} & 0 & 0 & 0 & 0 \\
\overline{\omega}r\overline{s} & \overline{\omega}rs & \overline{\omega}r\overline{s} & \overline{\omega}rs & \omega r\overline{s} & \omega\overline{r}s & \omega r\overline{s} & \omega rs \\
(\omega+\overline{\omega}\beta)rs & (\omega+\overline{\omega}\beta)r\overline{s} & (\omega+\overline{\omega}\beta)\overline{r}s & (\omega+\overline{\omega}\beta)\overline{r}\,\overline{s} & \overline{\omega}\overline{\beta}rs & \overline{\omega}\overline{\beta}r\overline{s} & \overline{\omega}\overline{\beta}\overline{r}s & \overline{\omega}\overline{\beta}\overline{r}\,\overline{s} \\
\overline{\omega}\beta r\overline{s} & \overline{\omega}\beta rs & \overline{\omega}\beta\overline{r}\,\overline{s} & \overline{\omega}\beta\overline{r}s & (\omega+\overline{\omega}\overline{\beta})r\overline{s} & (\omega+\overline{\omega}\overline{\beta})rs & (\omega+\overline{\omega}\overline{\beta})\overline{r}\,\overline{s} & (\omega+\overline{\omega}\overline{\beta})\overline{r}s \\
\omega\overline{r}s & \omega\overline{r}\,\overline{s} & \omega rs & \omega r\overline{s} & \overline{\omega r}\overline{s} & \overline{\omega r}s & \overline{\omega}rs & \overline{\omega}r\overline{s} \\
0 & 0 & 0 & 0 & \overline{r}\,\overline{s} & \overline{r}s & r\overline{s} & rs
\end{pmatrix}, \tag{4.6}$$

with $\overline{r} = 1 - r$, $\overline{s} = 1 - s$, $\overline{\alpha} = 1 - \alpha$, $\overline{\beta} = 1 - \beta$, and $\overline{\omega} = 1 - \omega$.

The transient dynamics of the model is described by the equation

$$\pi(t+1) = \pi(t)P, \tag{4.7}$$

where $\pi(t)$ is the (row) probability state vector at time t. Since all the parameters lie in the interval $]0, 1[$, the Markov chain is finite, irreducible, and aperiodic, thus guaranteeing the existence of a unique steady-state probability vector for any choice of the parameters [58]. Therefore, we can study the asymptotic steady-state probabilities $\overline{\pi} = [\overline{\pi}_1, \dots, \overline{\pi}_8]$ of being in any given state. The steady-state distribution $\overline{\pi}$ can be then obtained by solving

$$\overline{\pi} = \overline{\pi}P, \tag{4.8}$$

where the elements of $\overline{\pi}$ satisfy the constraints $\overline{\pi}_j \geq 0$ and $\sum_j \overline{\pi}_j = 1$. We remark that $\overline{\pi}_i$ can be interpreted as the asymptotic fraction of time spent in a given state. Therefore, in the next Section, we analytically and numerically investigate how $\bar{\pi}$ will depend on the model parameters, which are in turn related to behavioral characteristics of individuals.

4.3 Results

Steady-state probabilities

Here, we compute the steady-state probabilities of i) having a certain mood, ii) experiencing a positive/negative external event, and iii) experiencing an emotion with positive/negative valence.

We start by focusing on i) and ii), since the dynamics of M and E are independent from the valence. By solving the systems $\overline{\pi}_M = \overline{\pi}_M P_M$ and $\overline{\pi}_E = \overline{\pi}_E P_E$, we obtain $\overline{\pi}_M = \overline{\pi}_E = (0.5, 0.5)$, that is, in the long run the individuals will spend the same amount of time in positive or negative mood states, as well as will equally experience positive and negative external events.

We then turn our attention to iii) and, since the valence depend on both M and E, we solve (4.8) for computing the probability of experiencing a positive emotion. Namely, we compute $\pi_{V_1} := \sum_{i=5}^{8} \overline{\pi}_i$, thereby obtaining

$$\pi_{V_1} = \frac{\omega(3\alpha\omega + \beta\omega - \beta - 2\omega)(2r-1)/4 - \alpha\omega(5r/2 - 7/4) + (\alpha+\omega)(r-1)}{\omega^2(\alpha+\beta-1)(2r-1) - \omega(\alpha+\beta)(3r-2) + (\alpha+\beta+2\omega)(r-1)} \tag{4.9}$$

whereas $\pi_{V_0} := \sum_{i=1}^{4} \overline{\pi}_i = 1 - \pi_{V_1}$. This indicates that, in the long run, the steady-state valence probabilities are not influenced by the parameter s that modulates the variability of external events. The analysis of our model suggests that valence dynamics are affected by the attention that we give on external events, rather than by their variability. Indeed, the attention that the individual gives to external events and the mood variability matter, and are captured by ω and r, respectively. The impact of egosyntonicity on π_{V_1} is evidenced by its dependence on parameters α and β.

We notice that, when $r = 0.5$ or $\alpha = \beta$, equation (4.9) simplifies to

$$\pi_{V_1} = \frac{\omega - \alpha(\omega - 1)}{2\omega - (\alpha+\beta)(\omega-1)}. \tag{4.10}$$

In this case a positive valence is prevalent only if $\alpha > \beta$, indicating greater sensitivity to egosyntonicity. Furthermore, we note that, when $\alpha = \beta$, independent of the value of all other parameters, (4.9) further simplifies, and $\pi_{V_1} = 0.5$.

Parametric analysis

Here, we numerically investigate the dependence of the steady-state valence probability π_{V_1} (and, therefore, of the average time spent with a given valence in the long run) on the model parameters. In particular, we vary α, β, r and ω between 0.1 and 0.9 with step 0.1, and we also consider the extreme values 0.01 and 0.99. We fix $s = 0.1$, as external events tend to change rapidly over time, but the results that we are going to illustrate are not affected by the value of s. Specifically, for each of the 14641 parameter combinations, we have computed the steady-state valence probability π_{V_1} from (4.9), and performed a 500,000 steps long simulation of equation (4.7) to compute the difference δ_{ego} between the fraction of time steps spent in egosyntonicity and in egodystonicity.

First, we notice that regardless of the values of parameters r and ω, when $\alpha > \beta$, the steady-state positive valence probability π_{V_1} is larger than 0.5, and the opposite happens for $\alpha < \beta$, in agreement with the empirical evidence in [164], [169] showing that egosyntonic experiences tend to reinforce positive affective states, whereas egodystonic experiences are associated with increased negative affect.

This is illustrated for two sample pairs (r, ω) in Figure 4.1, which shows that, for a given value of α (β), π_{V_1} monotonically increases with the mismatch $\alpha - \beta$, which represents how much an individual is more sensitive to egosyntonicity versus egodystonicity, see the transition probabilities in (4.4) and (4.5). As we have just uncovered the fundamental role

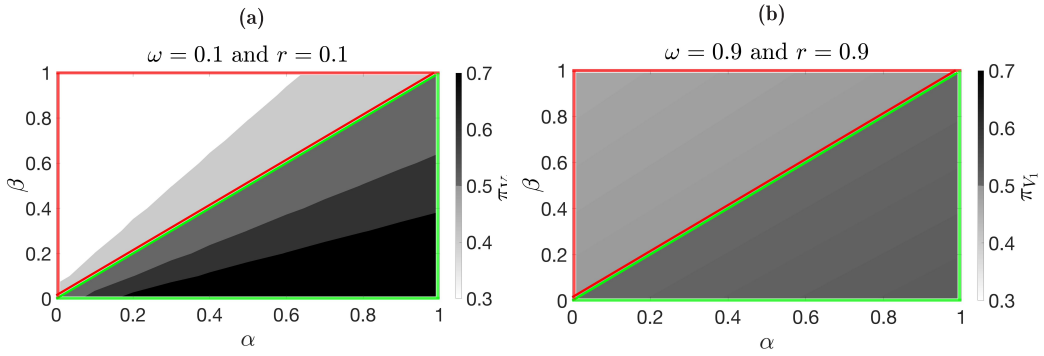

Figure 4.1: Colormap of the steady-state positive valence probability π_{V_1} as a function of α and β when (a) $\omega = 0.1$, $r = 0.1$ and (b) $\omega = 0.9$, $r = 0.9$.

played by the mismatch $\alpha - \beta$ on the asymptotic time spent in a positive valence, we then try to determine how this is related to the time spent in egosyntonicity/egodystonicity. To do this, among all pairs (α, β), we consider those such that $\alpha + \beta = 1$, so that $\alpha - \beta$ will range between -0.98 and 0.98. In Figure 4.2, for three representative values of the attention parameter ω, we report two colormaps of the steady-state probability of positive valence $\pi_{V_1}(\alpha - \beta, r)$ and the difference in frequency $\delta_{\text{ego}}(\alpha - \beta, r)$ between the time spent in egosyntonicity and egodystonicity, respectively. First, by comparing panels (a), (c), and (e), we notice that the effect of an increased mismatch $\alpha - \beta$ on π_{V_1}, is mitigated by an increase in either the attention to the external events ω or the inertia to mood change r. Moreover, when $\alpha = \beta$, $\pi_{V_1} = 0.5$, as expected from Section 4.3. Then, to decipher the relationship between the steady-state probability of positive valence and the time spent in egosyntonicity, we start by comparing $\pi_{V_1}(\alpha - \beta, r)$ and $\delta_{\text{ego}}(\alpha - \beta, r)$ when $\omega = 0.5$, see panels (c) and (d). We notice the emergence of four classes of individuals, characterized by qualitatively different behaviors:

1. The balanced happy (BH) are individuals who benefit from the larger share of time spent in egosyntonicity ($\delta_{\text{ego}} > 0$), and experience positive valences with a probability higher than chance ($\pi_{V_1} > 0.5$). In Figure 4.2, BH are encountered for parameter combinations corresponding to blue regions both in the left panels and in the corresponding right panels.
2. The self-deluded (SD) prevalently experiences negative emotions ($\pi_{V_1} < 0.5$) albeit being generally in sync with themselves ($\delta_{\text{ego}} > 0$). In Figure 4.2, SD are encountered for parameter combinations corresponding to coral regions in the left panels and blue regions in the corresponding right panels.
3. The chronically troubled (CT) are individuals who pay the price for being prevalently egodystonic ($\delta_{\text{ego}} < 0$) by experiencing negative emotions ($\pi_{V_1} < 0.5$). In Figure 4.2, CT are encountered for parameter combinations corresponding to coral regions both in the left panels and in the corresponding right panels.
4. The troubled happy (TH) prevalently experiences positive emotions ($\pi_{V_1} > 0.5$) despite spending more time in egodystonicity ($\delta_{\text{ego}} < 0$). In Figure 4.2, TH are encountered for parameter combinations corresponding to blue regions in the left panels and coral regions in the corresponding right panels.

Looking at panels (a), (b), (e) and (f), we notice that the above classification holds for all values of ω. The effect of variations in the attention parameter is that of mitigating or amplifying the difference between the classes.

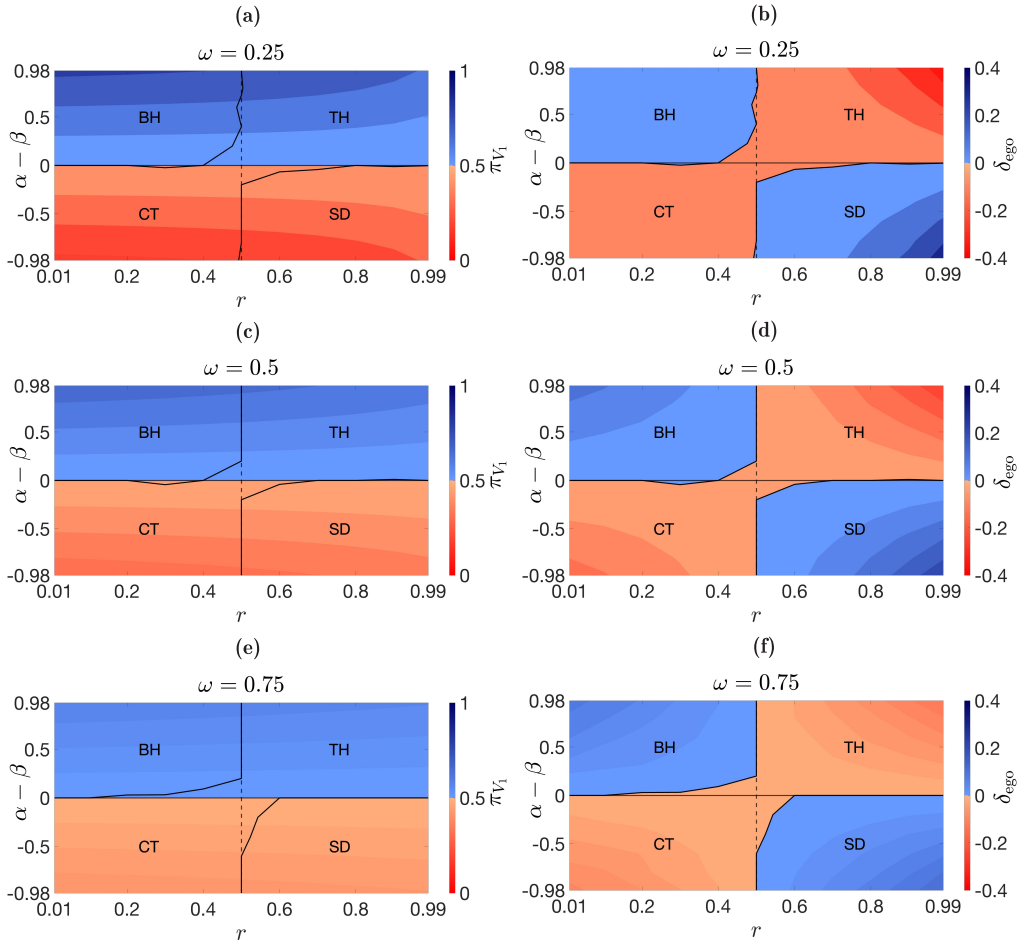

Figure 4.2: Colormap of the steady-state valence probability π_{V_1} and the difference δ_{ego} between egosyntonicity and egodystonicity frequencies as a function of $\alpha - \beta$ and r when the attention level is (a),(b) $\omega = 0.25$, (c), (d) $\omega = 0.5$, (e),(f) $\omega = 0.75$. Each plot is divided in four areas, each corresponding to a different class of individuals, where BH stands for balanced happy, TH for troubled happy, CT for chronically troubled, and SD for self-deluded. The differences between the four classes are more pronounced for extreme values of $\alpha - \beta$ and r.

4.4 Discussion

In this work, we introduced a novel Markovian model of emotion dynamics that is grounded on three fundamental principles of the branch of psychology that studies how emotions shape over time: *inertia*, *contingency* and *regulation*. In particular, the *principle of inertia* is captured by the internal mood dynamics, with a parameter that quantifies the reluctance to change mood. The *principle of contingency* is reflected in the valence dynamics, which depends on the complex interplay between the internal mood and the external events. Finally, the model also considers an implicit mechanism of *regulation*, whereby the individual behavior modifies depending on whether they are egosyntonic.

By performing a parametric analysis of the model, four classes of individuals have emerged based on the relationship between the time spent in egosyntonicity and the long-term emotional valence: the balanced happy, the self-deluded, the chronically troubled and the troubled happy. Interestingly, the four identified classes correspond to behaviors that are typically observed either in healthy individuals or in individuals with mental disorders. The class of balanced happy includes individuals that spend more time in egosyntonicity, thus living in harmony with their emotions. This healthy behavior enhances their mental health by increasing the experienced positive emotions. On the opposite end, the chronically troubled is often in internal conflict and experiences negative

emotions in the long term. Such a behavior is typical, for instance, of obsessive compulsive disorder (OCD) and eating disorder (ED). Indeed, obsessions in the OCD and intrusive thoughts in ED are generally egodystonic, as they are experienced as distressing and unwanted [164]. More generally, the experience of egodystonic thoughts or emotions is not uncommon. Most people will note strange, out-of-character thoughts at some point. But for someone, the fear, anxiety and self judgment associated with the experience of these egodystonic thoughts can negatively impact emotional well-being and may be associated with symptoms [161].

The remaining two classes, the self-deluded and troubled happy, are somewhat unexpected, yet very interesting. Indeed, from the valence dynamics in Section 4.2, one could inaccurately infer that egosyntonicity may only have a positive impact on the valence. However, the interplay with mood dynamics makes this relationship less obvious. For instance, the class of self-deluded includes individuals who are generally in sync with themselves but experience negative emotions in the long term. They can be viewed as individuals who ignore signs of distress, living with a false sense of well-being that does not materialize into lasting happiness. Such behavior is typical of personality disorders. For instance, grandiosity is an egosyntonic symptom of the narcissistic personality disorder [163], which strongly challenges the treatment of the disorder, as the individual may be reluctant to change their behavior. On the other hand, the troubled happy, despite often being in internal conflict (egodystonic), manages to maintain a positive emotional valence in the long term. Their discomfort seems to drive growth, leading to unexpected emotional resilience. This is the paradigmatic behavior observed in a successful therapy, where individuals might deliberately engage in egodystonic behaviors for a period of time with the goal of feeling better in the long term. In such individuals, therapy helps them navigate internal conflicts and fosters personal growth. The behavioral repertoire showcased by our minimalistic model is surprisingly rich, and yet grounded on fundamental psychological principles.

Limitations and future directions

The promising results of this work are not free of limitations, and could pave the way for future investigations. First, the binary modeling of mood, valence, and external events could be replaced by a multi-level discretization that would enable a more nuanced description of their dynamics. Second, the model deliberately focuses on a single emotion, which can be considered as the prevalent one that the individual is experiencing. This allows to elucidate the relationship between egosyntonicity and behavioral regulation, however future, richer models should consider the effect of interacting emotions. Indeed, in its current form, the model captures the dynamics of the dominant emotion, and simply assumes mood dynamics to be independent from other variables. To represent moods that arise from the combination of different emotions, mood dynamics should then be changed, considering transition probabilities that are a function of the different emotions experienced by an individual at each time step. Third, albeit the model reproduces four well-known interplays between egosyntonicity and emotional well-being, its present formulation does not allow individuals to learn and evolve from past experiences. Future works could consider the presence of adaptive mechanisms, whereby the individual learns from past experiences and modifies their behavioral parameters. This would turn the model parameters into manipulable variables that can be adjusted, for instance, through psychological therapy. Finally, although our model is founded on psychological principles and is capable of reproducing commonly observed behaviors, future empirical works could collect longitudinal data on emotion dynamics with the goal of further refine the model and the underlying hypotheses on which it is based. For instance, the possible dependencies between internal mood and external events could be incorporated in the model, including also feedback mechanisms from valence to internal and external states.

Chapter 5

Complex Dynamics in Psychological Data: Mapping Individual Symptom Trajectories to Group-Level Patterns

Contents

This Chapter summarizes and adapts the work presented in [40], which integrates causal inference, graph analysis, temporal complexity measures, and machine learning to examine whether individual symptom trajectories can reveal meaningful diagnostic patterns (RQ7-RQ9). Testing on a longitudinal dataset of $N = 45$ individuals affected by General Anxiety Disorder (GAD) and/or Major Depressive Disorder (MDD) derived from Fisher, Reeves, Lawyer, *et al.* [29], we propose a novel pipeline for the analysis of the temporal dynamics of psychopathological symptoms. First, we employ the PCMCI+ algorithm with a nonparametric independence test to determine the causal network of nonlinear dependencies between symptoms in individuals with different mental disorders. We found that the PCMCI+ effectively highlights the individual peculiarities of each symptom network, which could be leveraged towards personalized therapies. At the same time, aggregating the networks by diagnosis sheds light to disorder-specific causal mechanisms, in agreement with previous psychopathological literature. Then, we enrich the dataset by computing complexity-based measures (e.g. entropy, fractal dimension, recurrence) from the symptom time series, and feed it to a suitably selected machine learning algorithm to aid the diagnosis of each individual. The new dataset yields 91% accuracy in the classification of the symptom dynamics, proving to be an effective diagnostic support tool. Overall, these findings highlight how integrating causal modeling and temporal complexity can enhance diagnostic differentiation, offering a principled, data-driven foundation for both personalized assessment in clinical psychology and structural advances in psychological research. This Chapter also has an associated Appendix C with additional details.

5.1 Introduction

The conventional approach to the study of mental disorder is to seek for a common underlying cause of all symptoms, in analogy with medical work where the presence of a symptom is typically associated to the presence of a disease [170]. Such an approach to mental disorder is typically labelled latent variable, to recall the search for an invisible root cause of the disorder. Although latent variable models allowed to explain the effects of dynamic latent internalizing and externalizing factors in the development of comorbidity among common mental disorders [171], they failed to capture the dynamic and interactive nature of symptom evolution [172]. As pointed out in recent literature, this is due to the absence of a central disease mechanism or pathogenic pathway in mental disorders [173]–[175].

In response to these limitations, network analysis has gained traction as a promising alternative for studying the complexity of psychopathology [28], [176]. Unlike traditional

approaches that treat symptoms as independent entities, network-based methods conceptualize mental disorders as systems of interacting symptoms that cause each other. Disentangling the causal mechanisms that underlie symptom activation allows for a more granular exploration of their dynamics [177]–[179].

Network analysis provides several advantages over classical statistical models. First, it enables researchers to identify key symptoms—so-called "bridge symptoms"—that link different disorder networks and contribute to comorbidity [180]–[182]. Second, it allows for the investigation of stable symptom structures, capturing how symptoms relate to each other within groups of individuals at a given point or over short time frames [183], [184]. Third, by leveraging intensive longitudinal data, network analysis can uncover temporal trajectories and dynamic interactions among symptoms, offering insight into how psychopathology evolves over time and supporting the development of adaptive, personalized interventions [185]–[189].

However, these approaches often rely on the assumption of linear relationships between symptoms, thereby neglecting the intricate nonlinear relationships between them [190], [191]. Under the assumption of linearity, many approaches rely on correlation-based techniques, such as Structural Equation Modeling (SEM) [29] or Vector Autoregression (VAR) [192], which may only capture linear temporal dependencies [98], [99]. This limitation is particularly problematic for understanding the complex feedback loops underlying psychopathologies, where symptom interactions may be strongly nonlinear [193].

Moreover, network approaches typically focus on group-level analyses and overlook individual variability [194], [195]. Additionally, current studies face challenges in generalizing individual-level findings to broader populations [196], [197]. Heterogeneity in symptom expression raises concerns about whether individual symptom networks can meaningfully inform group-level patterns [198]. Addressing this challenge requires methodological innovations that can balance personalized symptom structures with generalizable insights applicable to clinical practice [199].

Given these limitations in both latent variable and network approaches, our study offers an innovative approach that combines causal inference and machine learning techniques to provide a deeper understanding of symptom dynamics in psychopathology. While previous studies have explored idiographic symptom networks [29] or group-level linear dependencies [192], to the best of our knowledge no method has yet fully uncovered nonlinear dependencies in individual and group-level analysis in psychopathology.

This study addresses three main questions: (1) How can we reconstruct individual-level, possibly nonlinear, causal interactions among symptoms? (2) Do group-level patterns emerge despite individual heterogeneity, and can they help distinguish diagnostic groups? (3) Can dynamic symptom features be used to classify diagnosis at the individual level?

We outline two complementary methodological pipelines (see Figure 5.1), designed to answer such distinct yet interrelated open questions. The first pipeline addresses the first two questions. Specifically, we elect the PCMCI+ algorithm to reconstruct causal interactions between symptoms. We first show its superiority in recovering nonlinear interactions on a toy model for which ground truth is available to then illustrate its effectiveness on real data. Then, we bridge individual-level analyses and group-level generalizations through aggregated fusion networks, which capture shared causal patterns across diagnostic groups. This step allows to distinguish different diagnostic groups.

The second pipeline builds on the use of complexity-based measures extracted from temporal symptom dynamics. The use of these metrics boosts the performance of the supervised classification algorithm that we use to classify diagnosis at the individual level.

While these pipelines serve distinct analytical purposes, their outcomes are interdependent: causal patterns derived from idiographic networks can guide the interpretation of classification results, whereas diagnostic outcomes may, in turn, inform the refinement of causal models by highlighting symptom dynamics of clinical relevance.

To illustrate the viability of our analysis pipelines, we test them on a longitudinal dataset on idiographic symptom networks for Generalized Anxiety Disorder (GAD) and Major Depressive Disorder (MDD) [29]. GAD and MDD are among the most

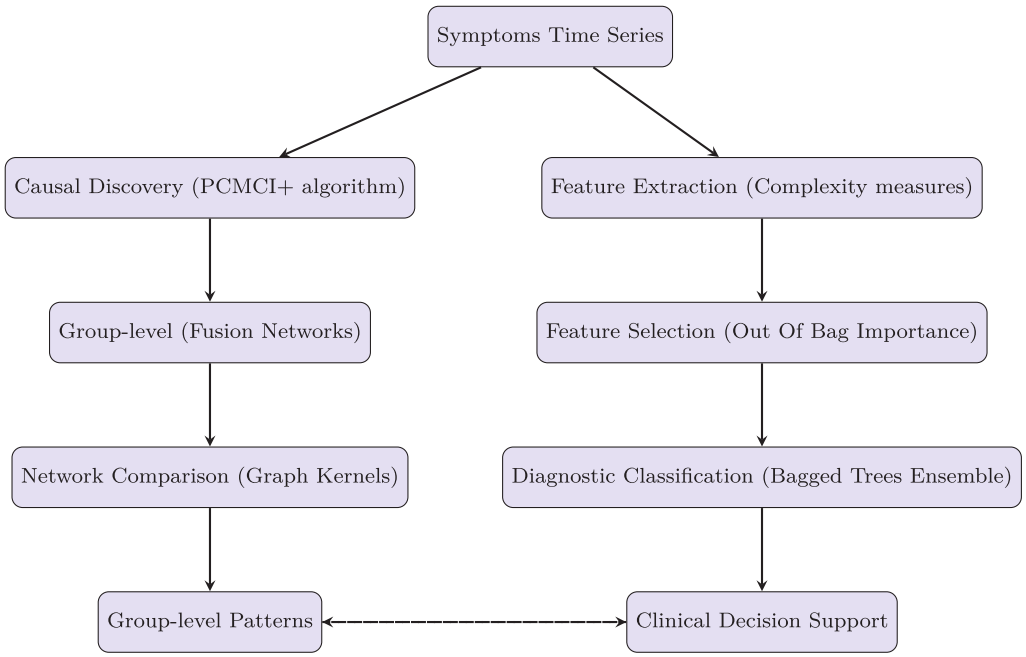

Figure 5.1: Dual analysis pipeline for idiographic multivariate time series: the left branch performs causal discovery using PCMCI+ and group-level network aggregation, leading to pattern identification; the right branch extracts complexity measures, selects predictive features, and performs diagnostic classification for clinical decision support. Dashed bidirectional arrows indicate the complementary nature of the two analyses: causal insights support diagnostic interpretation, while diagnostic outcomes inform and refine causal understanding.

prevalent and debilitating mental health conditions [200], often co-occurring and sharing underlying mechanisms [201]–[203]. While GAD is primarily characterized by excessive and uncontrollable worry, heightened physiological arousal, and cognitive hypervigilance, MDD manifests through persistent low mood, anhedonia, and dysregulation in reward-processing circuits [202], [204].

The frequent comorbidity between these disorders suggests shared vulnerability factors; however, their distinct clinical presentations necessitate precise differentiation for accurate diagnosis and effective treatment [205], [206], making them an ideal test for our analysis pipelines. Indeed, the application to longitudinal data from subjects with GAD, MDD, or both disorders in comorbidity enables us to identify distinct patterns that differentiate the three groups. Specifically, our approach reveals the underlying causal relationships among symptoms while preserving individual heterogeneity, and addresses the challenging task of differential diagnosis among these closely related clinical presentations.

The remainder of the Chapter is structured as follows: Section 5.2 outlines the dataset and the methodological approaches used to address our research objectives; Section 5.3 presents the primary findings of the work; and Section 5.4 describes the implications, limitations, and future directions of the study.

5.2 Methods

In this Section, we describe the data and the methodological framework employed in our study. First, in Section 5.2.1 we present the dataset provided by [29], which includes idiographic symptom time series from individuals diagnosed with GAD, MDD, or both. Second, we outline the two complementary methodological pipelines of Figure 5.1. Specifically, in Section 5.2.2 we describe the application of PCMCI+ to our dataset.

We also introduce the extension of PCMCI+ individual results to group-level analysis, enabling the comparison of symptom dynamics across diagnostic groups.

In Section 5.2.3 we describe the graph comparison techniques employed to analyze symptom dynamics and diagnostic group differences. Lastly, in Section 5.2.4 we present the Bagged Tree algorithm used to classify individuals among diagnostic groups, including the feature extraction and selection procedures that support this analysis.

5.2.1 Data

The dataset used in this study was derived from the work of [29], which describes a longitudinal study in which participants with a primary diagnosis of mainly Generalized Anxiety Disorder (GAD), Major Depressive Disorder (MDD), or comorbid GAD and MDD completed intensive repeated measures assessments – four per day for at least 30 days – prior to therapy. This rich and detailed dataset offers unique opportunities for dynamic and person-specific analyses. In the original dataset (see https://osf.io/8yadb/), the primary diagnosis was the main focus, while other comorbidities were recorded but not central to the analysis. This approach was based on the assumption that the primary diagnosis would be the most relevant for studying the specific mechanisms underlying anxiety and depressive disorders [29].

For our study, we followed a similar approach but, at Fisher's recommendation, expanded the sample by including five additional participants from a more comprehensive dataset provided directly by him, reaching 45 individuals. This expansion allowed for a more detailed exploration of symptom dynamics and increased the robustness of our findings. To remain consistent with the original framework, we focused our analyses on the primary diagnosis only. Furthermore, we focused specifically on distinguishing between GAD, MDD, and their comorbidity, as these represent the core diagnostic categories of interest. Therefore, participants with a primary diagnosis that included GAD, MDD, or both were assigned to one of these three categories, disregarding any additional comorbidity. For example, a participant diagnosed with GAD and agoraphobia was considered solely within the GAD group.

In Table 5.1 there is a summary of participants' characteristics and diagnostic information. Diagnoses were established through structured clinical interviews using the Anxiety and Related Disorders Interview Schedule for DSM-5, administered by trained graduate students under the supervision of a licensed clinical psychologist. The table also reports symptom severity scores based on the Hamilton Rating Scale for Anxiety (HAM-A) and the Hamilton Rating Scale for Depression (HAM-D). The HAM-A consists of 14 items rated from 0 to 4, yielding a total score range of 0–56, while the HAM-D includes 13 similarly rated items, with a total score range of 0–52. We refer to [29] for more details about the assessment procedure.

Each participant completed an experience sampling protocol in which they responded to surveys delivered via mobile phone four times per day over a period of approximately 30 days. At each time point, participants rated their current experience of 22 mood and anxiety-related symptoms using a 0–100 visual analog slider with the anchors 'not at all' (0) and 'as much as possible' (100). The symptom list included both core DSM-5 symptoms of GAD and MDD (e.g., felt worried, felt down or depressed, loss of interest or pleasure) and a broader set of affective, cognitive, and behavioral dimensions (e.g., felt energetic, felt hopeless, felt angry, avoided activities, felt accepted or supported; see Table 5.2 for the full list). As a result, each participant's data can be represented as a time series with 22 variables (columns) capturing symptom dynamics over time. We further normalized the data column-wise by subtracting the mean and dividing by the standard deviation. Each individual completed an average of 112.8 responses (SD = 12.87), with a maximum of 151 and a minimum of 90. For each individual, entries with missing symptom values were excluded from the analysis. Aggregating data across individuals yielded 5076×22 observations, corresponding to 5076 time points and 22 symptom variables. For each observation, we also included the participant ID and their primary diagnosis (GAD, MDD, or comorbid GAD and MDD), replicated across time

Table 5.1: Participants' characteristics: ID, sex, age, ethnicity, primary diagnosis, other comorbidities, Hamilton Rating Scale for Depression score (HAM-D), Hamilton Rating Scale for Anxiety score (HAM-A).

ID	Sex	Age	Ethnicity	Primary Diagnosis	Other Comorbidities	HAM-D	HAM-A
P001	Female	28	Latin	MDD,GAD	Panic	23	27
P003	Male	29	White	MDD,GAD	NA	16	15
P004	Female	32	Latina	GAD	NA	16	33
P006	Male	26	White	MDD,GAD	SAD	13	13
P007	Female	33	Black	MDD,GAD	Agor,SAD,SpecPhob	11	17
P008	Female	23	AsianAmerican	MDD,GAD	PTSD,BodyDys	19	15
P009	Female	25	Other	GAD,SAD	SpecPhob	17	9
P010	Male	33	AsianAmerican	MDD,GAD	SAD	22	22
P012	Female	36	Latin	GAD,Agor	NA	9	13
P013	Male	26	White	MDD,GAD	SAD	14	19
P014	Male	22	Latin	MDD	NA	10	12
P019	Female	30	AsianAmerican	MDD	SAD	10	10
P021	Male	59	Other	GAD	SAD	15	16
P023	Female	64	White	GAD	NA	8	7
P025	Male	31	White	GAD,SAD	NA	15	14
P033	Female	28	White	GAD	Agor,SAD,OCD	8	14
P037	Female	28	Latin	GAD,SAD	IllnessAnxiety,SpecPhob	21	41
P040	Female	29	White	GAD	Agor,SAD,MDD,SpecPhob	21	41
P048	Male	57	AsianAmerican	MDD,GAD	SAD,SpecPhob	14	17
P068	Female	42	White	GAD	NA	11	14
P072	Female	38	AsianAmerican	MDD	GAD	15	13
P074	Female	56	White	MDD	NA	12	10
P075	Female	27	AsianAmerican	GAD	NA	18	23
P100	Male	31	White	GAD	PTSD	7	14
P111	Female	23	AsianAmerican	GAD	Panic,SAD,PTSD	18	15
P113	Female	46	Black	GAD	SAD,SpecPhob	4	15
P115	Female	42	White	MDD,GAD	SAD	18	19
P117	Male	59	White	MDD,GAD	NA	12	18
P127	Male	29	Latin	GAD	SAD	9	13
P137	Male	45	AsianAmerican	MDD	NA	16	15
P139	Female	62	White	MDD	GAD	14	12
P145	Female	47	Other	GAD	SAD,PTSD	21	30
P160	Male	50	White	GAD	PDD	13	11
P163	Female	58	AsianAmerican	MDD	GAD,PDD	16	16
P169	Male	29	White	MDD	NA	13	15
P202	Female	34	White	GAD	PDD	10	11
P203	Female	21	AsianAmerican	MDD,GAD	SAD	18	20
P204	Female	57	White	GAD	NA	12	16
P206	Female	39	Other	GAD,SAD	NA	11	16
P215	Female	31	Black	GAD	NA	17	23
P217	Female	31	White	GAD	MDD	17	14
P219	Female	23	AsianAmerican	GAD	MDD	21	27
P220	Male	64	White	MDD	GAD	14	13
P223	Male	56	White	MDD	GAD	21	12
P244	Female	21	AsianAmerican	MDD	NA	12	8

Note. GAD = generalized anxiety disorder; MDD = major depressive disorder; Panic = panic disorder; Spec Phob = specific phobia; Agor = agoraphobia; PTSD = posttraumatic stress disorder; Body = body dysmorphia; AUD = alcohol use disorder; PDD = persistent depressive disorder.

points, resulting in a final dataset with 5076×24 entries, where each row corresponds to one survey response.

Although the diagnostic groups were unbalanced (GAD = 23, MDD = 11, comorbid = 11, see Table 5.3 for complete group-level statistics), analyses were designed to be robust to class size differences. No resampling or weighting techniques were applied unless otherwise specified. Treating comorbid GAD and MDD as a distinct group acknowledges growing evidence that symptom co-occurrence reflects unique dynamic patterns rather than additive effects of single disorders.

Based on the primary diagnosis reported in Table 5.1, all 45 participants were included in the analysis, comprising 29 females and 16 males, with ages ranging from 21 to 64 years (mean age = 37.8). The sample was ethnically diverse, including participants identifying as White (n = 20), Asian American (n = 12), Latin/Latina (n = 6), Black (n = 3), and Other (n = 4).

5.2.2 Applying the PCMCI+ to our dataset

Importantly, we applied PCMCI+ at the level of each individual participant i. Each analysis was based on a time series of shape $T_i \times 22$, where T_i denotes the number of observations associated to individual i. This individual-level approach allows for the construction of personalized causal graphs that reflect the intra-individual variability of symptom dynamics. The analysis was configured with a maximum lag of one time step,

Table 5.2: List of the 22 symptoms assessed in the experience sampling protocol. Each item refers to how the participant felt or behaved during the time interval between the previous beep and the current one.

Symptoms	
Felt energetic	Felt hopeless
Felt enthusiastic	Felt down or depressed
Felt content	Felt positive overall
Felt irritable	Felt fatigued or low energy
Felt restless	Experienced muscle tension
Felt worried	Had difficulty concentrating
Felt worthless or guilty	Felt accepted or supported
Felt frightened or afraid	Felt threatened, judged, or intimidated
Loss of interest or pleasure	Dwelled on the past
Felt angry	Avoided activities
Procrastinated	Avoided people

Table 5.3: Descriptive statistics by diagnostic group: number of individuals (N), mean (M) and standard deviation (SD) of Hamilton Rating Scale for Depression score (HAM-D), Hamilton Rating Scale for Anxiety score (HAM-A), age and responses to the experience sampling protocol.

Variable	**GAD**	**MDD**	**Comorbid GAD and MDD**
N	23	11	11
HAM-D (M ± SD)	13.87 ± 5.09	13.90 ± 3.14	16.36 ± 3.98
HAM-A (M ± SD)	18.70 ± 9.55	12.36 ± 2.42	18.36 ± 3.82
Age (M ± SD)	36.61 ± 11.86	43.72 ± 16.37	34.27 ± 13.03
Responses (M ± SD)	112.13 ± 13.74	109.09 ± 8.22	117.90 ± 14.17

Note. GAD = generalized anxiety disorder; MDD = major depressive disorder.

as our primary interest lays in short-term rather than long-term trajectories, and with a significance level of $\alpha = 0.01$. We set $k = 4$ for the CMIknn estimator, as recommended for small sample sizes in previous studies [108]. This choice ensures a good balance between sensitivity and robustness. All analyses were implemented using the Tigramite Python package (version 5.2.7.0), which provides a comprehensive framework for time series causal discovery, including full support for CMIknn. To ensure transparency and reproducibility, all code and data will be made available upon publication.

While causal discovery via PCMCI+ was conducted at the individual level—resulting in one causal graph per participant— we also constructed group-level fusion networks by aggregating individual adjacency matrices within each diagnostic category (GAD, MDD, or comorbid). Specifically, we computed the element-wise sum of the binary causal graphs inferred by PCMCI+, yielding weighted matrices where each entry reflected the frequency of a specific edge within a group.

This aggregating approach, while methodologically distinct, aligns with prior work in network neuroscience [207], where individual-level connectivity patterns were combined to identify common structural features across subjects. In our case, it enables the extraction of robust structural patterns that characterize each diagnostic profile, while preserving the idiographic nature of the analysis.

5.2.3 Graph comparison

To quantify the role of symptoms within each causal network, we first employed classical network measures from graph theory that capture both local and global aspects of node importance [208]. These metrics — whose details are available in Appendix C— provide a multi-faceted view of symptoms importance to capture both local connectivity and global flow properties.

Secondly, to compare the graphs—both at the individual level and between fusion

networks—we also employed graph kernels, a family of methods designed to quantify similarity between networks [209]. A graph kernel $K(G, G')$ is a positive semi-definite function that computes the similarity between two graphs G and G', with the key property that there exists a map ϕ from G to a high-dimensional feature space such that $K(G, G') = \langle \phi(G), \phi(G') \rangle$ [210].

We considered two graph kernels differing in expressive power and computational complexity. For sparse graphs—such as the individual-level PCMCI+ outputs—we employed the *degree distribution kernel*, which compares graphs by evaluating similarities in their node degree histograms [211], [212]. In sparse networks, where variability in node connectivity is more pronounced, this kernel provides a computationally efficient and informative summary of the overall graph structure. Conversely, in denser graphs—where most nodes tend to exhibit uniformly high degrees—the degree kernel becomes less effective in distinguishing topological differences, as it captures less structural variability. Thus, for comparing group-level networks, which are substantially denser than individual ones, we employed the *Weisfeiler-Lehman (WL) kernel* [213].

The WL kernel is a state-of-the-art method that assigns an initial color to each node and iteratively refines node colors by combining each node's current color with those of its neighbors. After a fixed number of iterations— e.g. when the kernel matrix converges—each graph is represented by a histogram of node color counts, and similarity is computed as the dot product between these histograms. The WL kernel is particularly well suited for detecting structural differences in dense graphs, where local subgraph configurations carry greater discriminative power. While more computationally intensive, it provides higher expressiveness when structural complexity increases.

Importantly, in our case all the causal networks included the same set of nodes, ensuring that kernel comparisons were not affected by topological mismatches. We computed kernel matrices both at the individual level (comparing all pairwise causal graphs) and at the group level (comparing fusion networks), enabling a multi-scale analysis of symptom dynamics. This allowed us to formally assess individual-level heterogeneity within and across diagnoses, as well as structural differences in the fusion networks.

5.2.4 Classification through Bagged Tree

While the network-based analysis aimed at providing valuable insights into the structural patterns of symptom interactions at both individual and group levels, a complementary objective of our study was to explore whether temporal symptom dynamics could also support diagnostic classification. To this end, we implemented a supervised machine learning approach designed to leverage time series features for improving the accuracy and interpretability of diagnostic predictions in clinical psychology.

In this phase of analysis, we moved from an idiographic perspective to a global one, combining data from all individuals into a unified dataset. Data from individuals with comorbid GAD and MDD diagnoses were excluded from the training set and reserved for out-of-sample evaluation to assess model generalizability. The final column of the dataset contained the diagnosis label (GAD or MDD), which served as the target variable for classification.

We employed a Bagged Tree classifier—implemented in MATLAB using the `TreeBagger` function—as our predictive model [96]. Bagging, or bootstrap aggregation, is an ensemble learning method that improves predictive performance by reducing variance through model averaging [94], [95].

The model works in three steps: (1) random sampling with replacement creates diverse training sets, (2) individual decision trees are trained independently on these samples, and (3) predictions are aggregated via majority voting. In order to account for diagnosis imbalance in the training set, we introduced class weights inversely proportional to class frequencies.

Our implementation consisted of 300 decision trees, each trained on a bootstrapped subset of the training data. All available predictors were considered at each split.

Although predictions were computed for each observation, individual-level classification was performed by averaging the predicted class probabilities across all time windows per participant. We first assessed generalization using a leave-one-out cross-validation strategy, training the model on all individuals except one, who was used for testing. This simulates a real-world diagnostic setting in which a previously unseen participant is classified based on learned patterns from others. The final classification was based on an optimal decision threshold, determined by minimizing the Euclidean distance from the ideal point (0,1) in the ROC (Receiver Operating Characteristic) space—thereby balancing sensitivity and specificity.

To further enrich the analysis, we computed a comprehensive set of complexity features for each individual, designed to quantify different aspects of signal regularity, unpredictability, fractal geometry, and recurrence. Although they have not been widely applied in clinical psychology, prior studies in physiology and complex systems have shown that entropy, fractal dimension, and recurrence-based metrics can capture meaningful dynamic patterns in biological and behavioral data [8], [214]–[216]. The full list of complexity measures is available in Table 5.4, while detailed descriptions can be found in Appendix C.

Thus, we obtained a high-dimensional dataset of approximately 3000 features. Each individual is represented by multiple rows in the dataset, corresponding to different configurations of parameters used to compute the complexity measures. Each column corresponds to a specific feature. We then trained the Bagged Tree classifier described above on this new enriched dataset.

Nonetheless, feature selection was performed post hoc leveraging out-of-bag (OOB) variable importance scores, specifically the Permuted Predictor Delta Error [217], [218]. Variable importance scores were averaged across all iterations of the leave-one-out cross-validation to obtain a stable ranking of features contributing to diagnostic classification. Features were then ranked in descending order of importance. Notably, some variables received negative importance values, indicating a detrimental effect on classification performance. To refine the feature set, we iteratively retrained the model, each time retaining only variables with positive importance. This Boruta-type process was repeated until only positively contributing variables remained and model performance reached a stable plateau [219].

Table 5.4: Complexity metrics extracted from each time series or pairwise combination.

Complexity metrics	
Number of Zero Crossings	Permutation Entropy
Approximate Entropy	Sample Entropy
Hurst Exponent	Detrended Fluctuation Analysis (DFA)
Correlation Dimension	Higuchi Fractal Dimension
Petrosian Fractal Dimension	Recurrence Rate
Determinism	Laminarity
Trapping Time	Maximum diagonal line length (L_{max})
Maximum vertical line length (V_{max})	Divergence
Entropy of Diagonal Line Lengths	Average Diagonal Length
Average Vertical Length	Cross Recurrence Rate
Cross Determinism	Cross Laminarity
Cross Trapping Time	Cross L_{max}
Cross V_{max}	Cross Divergence
Cross Entropy of Diagonal Line Lengths	Cross Average Diagonal Length
Cross Average Vertical Length	

5.3 Results

5.3.1 PCMCI+ outperformes classical approaches to inference from psychological data.

To determine the most appropriate method for causal inference in longitudinal psychological data, we generated synthetic datasets designed to compare the ability of the PCMCI+ to reconstruct both linear and nonlinear dependencies, and compared it with Vector Autoregression (VAR) [99], commonly used in the psychopathological literature [192], [220], and transfer entropy (TE), a popular inference method from information theory [100]. Each dataset included three variables, X_1, X_2, and X_3, observed over 100 time points, with known ground-truth causal structures. The choice of relatively small number of datapoints aims to replicate a common limitation in idiographic psychological data, typically described by short time series. Specifically, $X_{1,t}$ and $X_{2,t}$ were sampled independently from a standard normal distribution, $X_{i,t} \sim \mathcal{N}(0,1)$. The variable $X_{3,t}$ was generated according to three different causal scenarios, capturing either linear or nonlinear dependencies:

- Scenario 1 (Linear): $X_{3,t} = 3X_{2,t-1} + \varepsilon_{3,t}, \quad \varepsilon_{3,t} \sim \mathcal{N}(0,1)$;
- Scenario 2 (Interaction): $X_{3,t} = 3X_{1,t-1}X_{2,t-1} + \varepsilon_{3,t}, \quad \varepsilon_{3,t} \sim \mathcal{N}(0,1)$;
- Scenario 3 (Quadratic): $X_{3,t} = 3X_{2,t-1}^2 + \varepsilon_{3,t}, \quad \varepsilon_{3,t} \sim \mathcal{N}(0,1)$.

The results of this comparison highlight the superior performance of the PCMCI+ algorithm—particularly when combined with the CMIknn independence test—in identifying both linear and nonlinear causal relationships, see Table 5.5. Indeed, VAR and TE were restricted to detecting only linear dependencies. Interestingly, PCMCI+ with partial correlation also failed to recover nonlinear effects, emphasizing the value of nonparametric conditional independence testing in complex scenarios.

The superior performance compared with the VAR model can be explained by the underlying linearity assumption. The case of transfer entropy is instead different, whereby it is a nonlinear method that quantifies how much knowing the past of a source variable reduces uncertainty about the future of a target variable. However, its main limitation lies in its data hungriness. Indeed, the computation of transfer entropy requires the discretization of the time series and the computation of empirical joint distributions. The accuracy of such estimation is critically limited for short time series [105], as it is often the case for idiographic psychological datasets.

Table 5.5: Detection of linear and nonlinear causal relationships in synthetic datasets with three variables, evaluated across four methods: Vector Autoregression (VAR), Transfer Entropy (TE), PCMCI+ with partial correlation (parcorr), and PCMCI+ with the CMIknn independence test.

Causal relation	VAR	TE	PCMCI+ (parcorr)	PCMCI+ (CMIknn)
$X_2 \to X_3$	✓	✓	✓	✓
$X_1 \cdot X_2 \to X_3$	✗	✗	✗	✓
$X_2^2 \to X_3$	✗	✗	✗	✓

5.3.2 Group-level patterns in GAD, MDD, and comorbid participants emerge despite individual heterogeneity.

Following our first pipeline (see Figure 5.1, left branch), we started the analysis of the extended dataset on GAD and MDD from [29] by applying the PCMCI+ algorithm to each individual's time series, yielding 45 mixed causal graphs that incorporate both contemporaneous (lag-0) and lagged (lag-1) relationships, see the GitHub Repository. Then, we quantified pairwise similarities between them using the degree distribution

kernel to evaluate the extent of heterogeneity within each diagnostic category. Figures 5.2, 5.3 and 5.4 display the three similarity matrices (one per each diagnostic group), showing a substantial variability in the graph structure even among individuals sharing the same diagnosis. These findings support prior literature, highlighting within-diagnosis heterogeneity in symptom expression and network topology [197], [198].

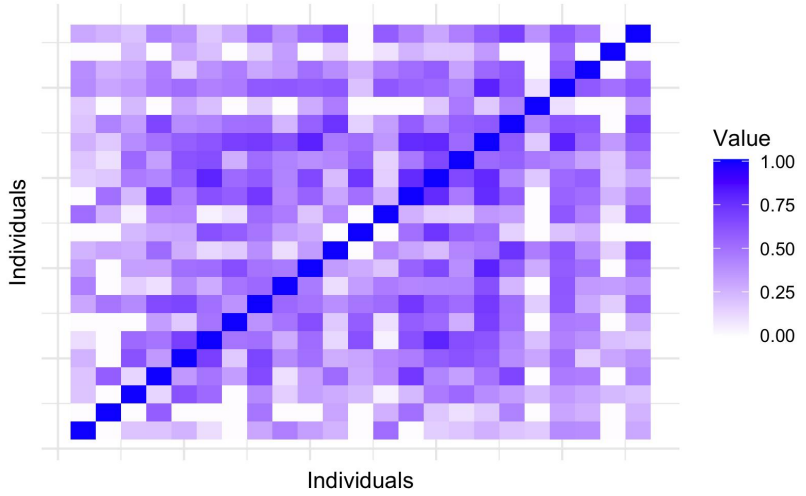

Figure 5.2: Degree kernel across individuals with Generalized Anxiety Disorder (GAD). The matrix shows the pairwise kernel similarity value among individual networks.

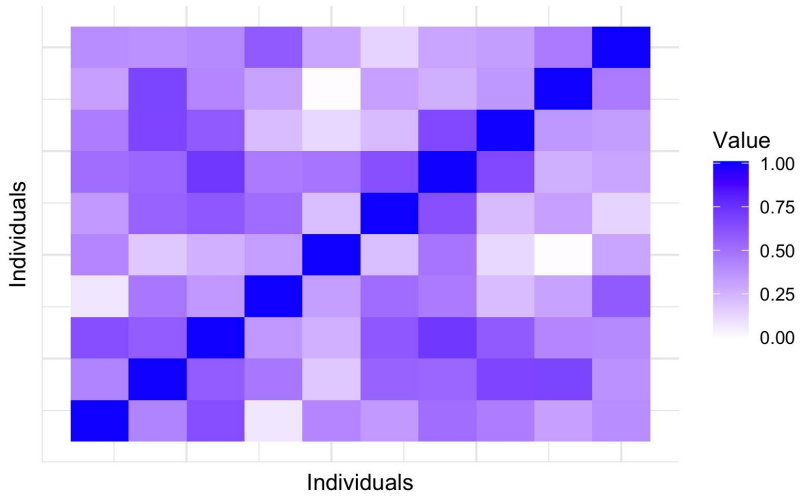

Figure 5.3: Degree kernel across individuals with Major Depressive Disorder (MDD). The matrix shows the pairwise kernel similarity value among individual networks.

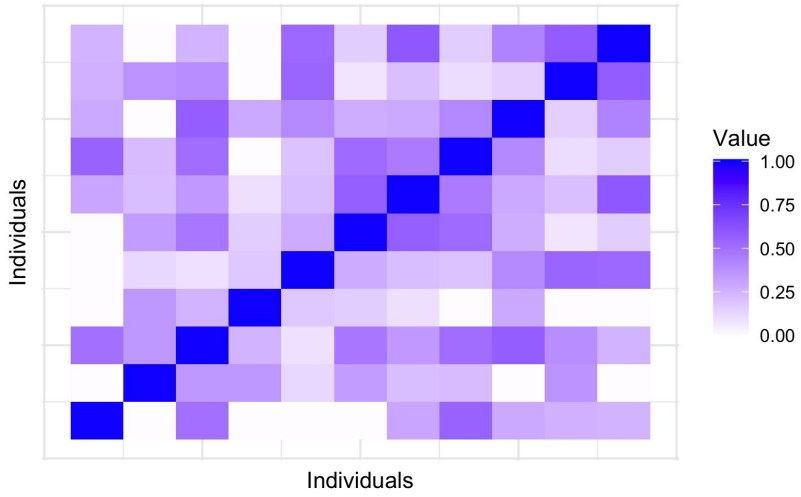

Figure 5.4: Degree kernel across individuals with comorbidity (both GAD and MDD). The matrix shows the pairwise kernel similarity value among individual networks.

To identify broader diagnostic patterns while preserving individual complexity, we considered the fusion causal networks, obtained by summing the individual adjacency matrices within each diagnostic group. This procedure yielded one group-level network for GAD, one for MDD, and one for comorbid GAD and MDD. Figures 5.5, 5.6 and 5.7 display these full aggregated graphs.

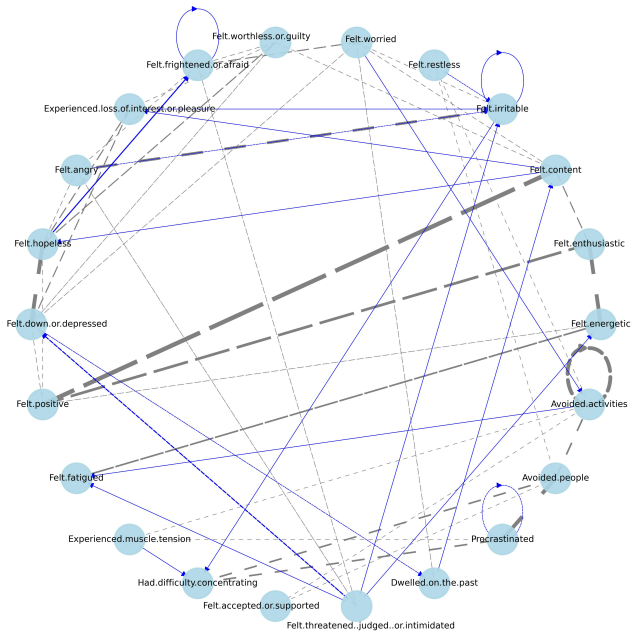

Figure 5.5: Fusion causal network for Generalized Anxiety Disorder (GAD). The graph represents the group-level symptom dynamics derived from individual causal networks. Grey and blue arrows indicate statistically significant undirected and directed causal relationships, respectively. Dashed and solid lines indicate lag-0 and lag-1 causal relationships, respectively.

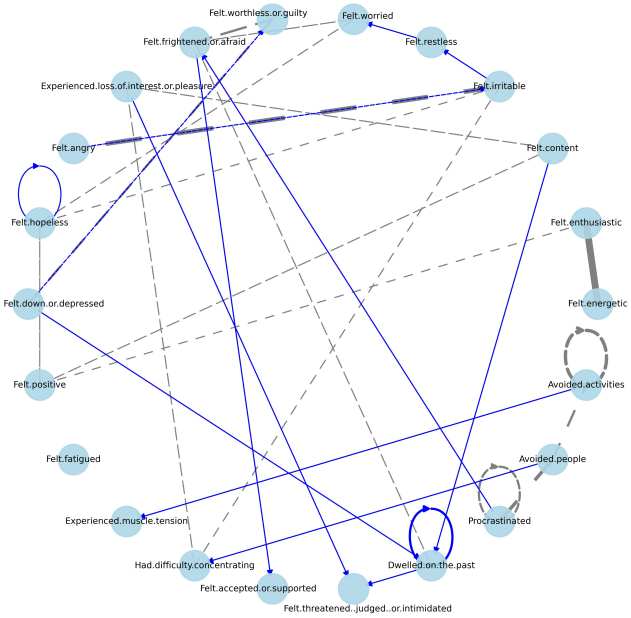

Figure 5.6: Fusion causal network for Major Depressive Disorder (MDD). The graph represents the group-level symptom dynamics derived from individual causal networks. Grey and blue arrows indicate statistically significant undirected and directed causal relationships, respectively. Dashed and solid lines indicate lag-0 and lag-1 causal relationships, respectively.

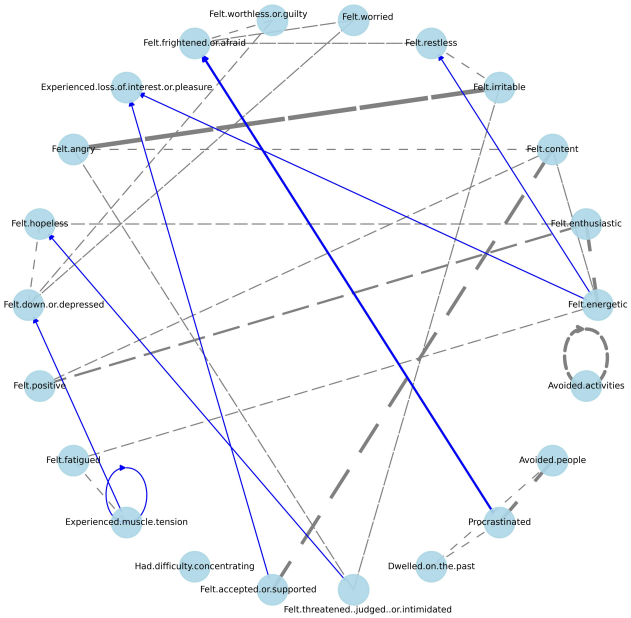

Figure 5.7: Fusion causal network for comorbidity (both GAD and MDD). The graph represents the group-level symptom dynamics derived from individual causal networks. Grey and blue arrows indicate statistically significant undirected and directed causal relationships, respectively. Dashed and solid lines indicate lag-0 and lag-1 causal relationships, respectively.

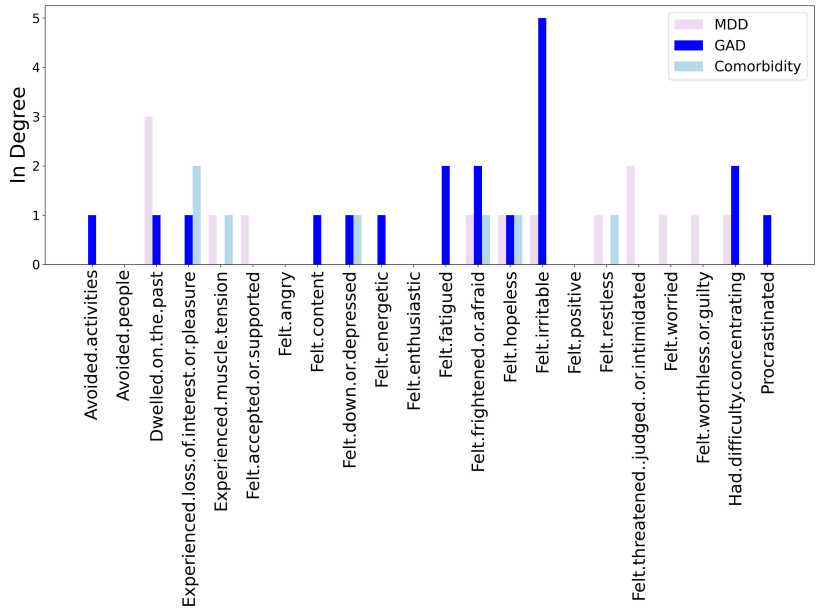

Figure 5.8: Comparison of in-degree values across symptoms for General Anxiety Disorder (GAD), Major Depressive Disorder (MDD) and comorbidity fusion networks. Each bar represents the number of incoming connections for a given symptom in the directed network.

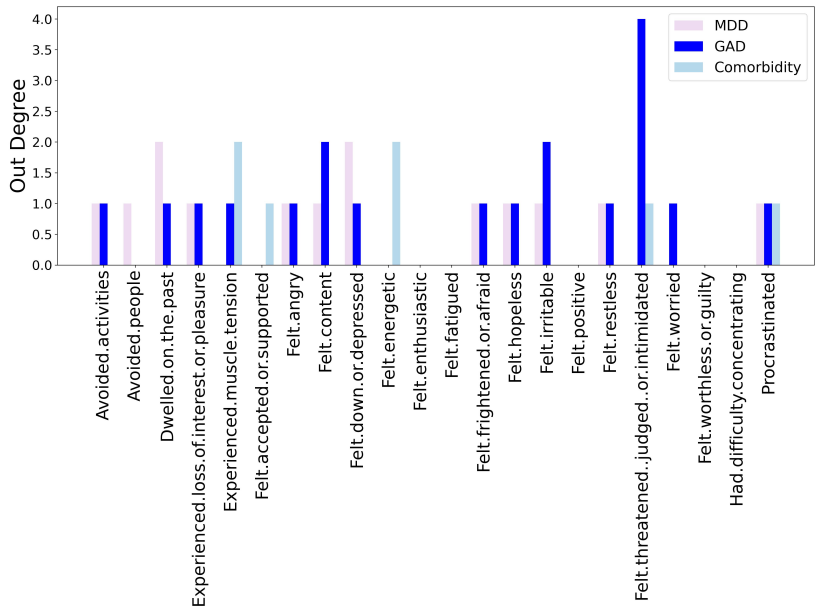

Figure 5.9: Comparison of out-degree values across symptoms for General Anxiety Disorder (GAD), Major Depressive Disorder (MDD) and comorbidity fusion networks. Each bar represents the number of outgoing connections for a given symptom in the directed network.

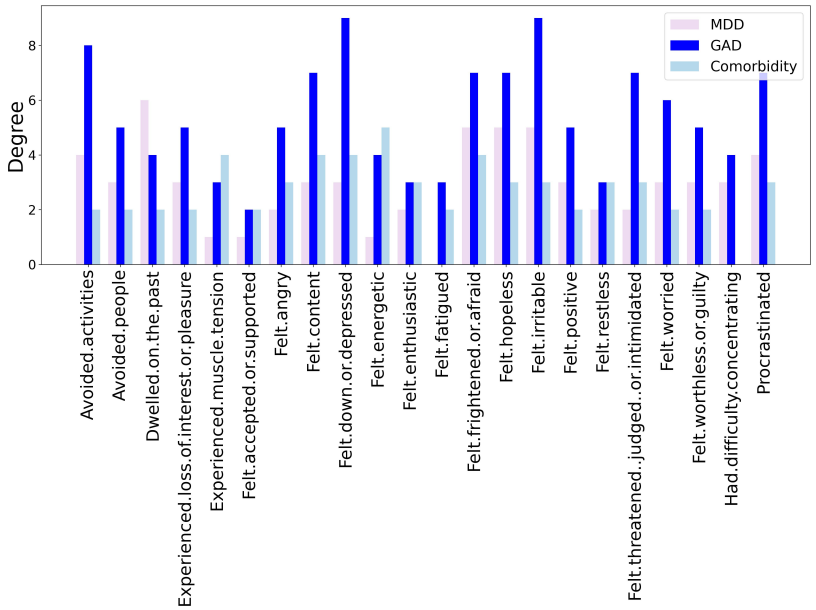

Figure 5.10: Comparison of degree values across symptoms for General Anxiety Disorder (GAD), Major Depressive Disorder (MDD) and comorbidity fusion networks. Each bar represents the number of connections for a given symptom in the mixed network.

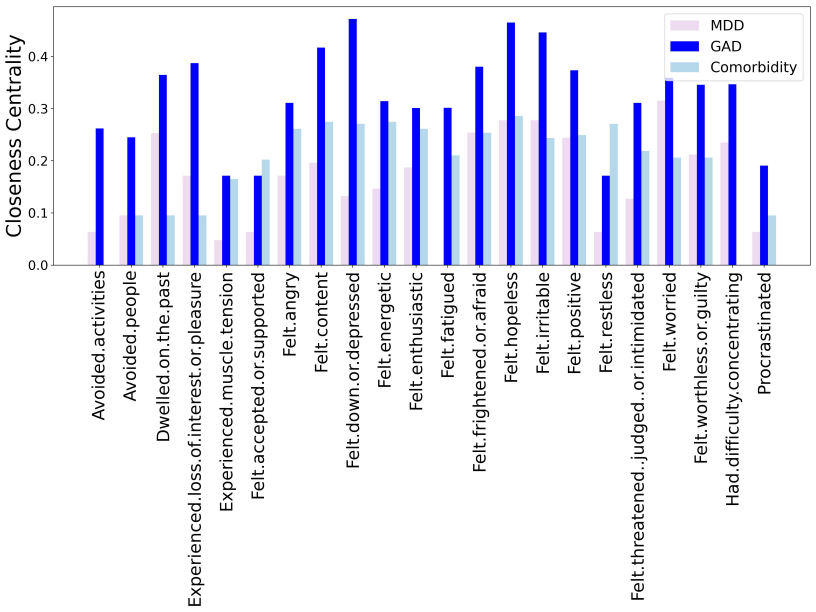

Figure 5.11: Comparison of closeness centrality values across symptoms for General Anxiety Disorder (GAD), Major Depressive Disorder (MDD) and comorbidity fusion networks.

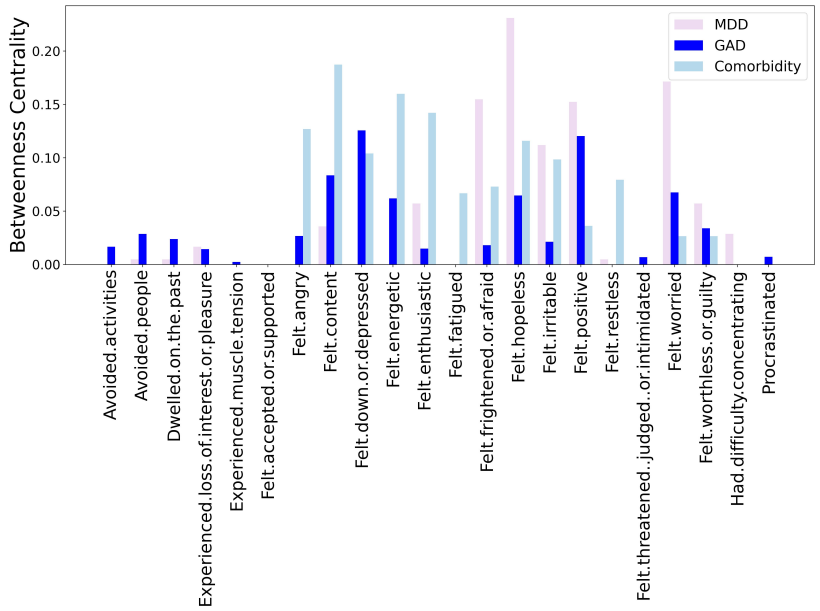

Figure 5.12: Comparison of betweenness centrality values across symptoms for General Anxiety Disorder (GAD), Major Depressive Disorder (MDD) and comorbidity fusion networks.

A visual inspection of the graphs—supported by quantitative network measures—highlights significant differences in causal interactions between diagnostic groups, especially between GAD and MDD (see Figures 5.8—5.12).

Notably, MDD and comorbid networks show higher values of betweenness centrality, while GAD is characterized by higher degrees and closeness centrality. This pattern aligns with the literature that conceptualize GAD as characterized by physiological hyperarousal and pervasive cognitive worry, leading to highly interconnected and rapidly interacting symptoms [221]. In contrast, the more compartmentalized network structures observed in MDD and comorbid cases—with central symptoms acting as mediators—are consistent with the literature emphasizing reduced behavioral engagement, narrowed affective experience, and distinct symptom clusters [222], [223].

We also observe several symptom-specific differences among diagnostic groups. For instance, in the GAD network, the symptom "dwelled on the past" functions as a driver, influencing "felt content". In contrast, in MDD, it acts more as an endpoint, often reinforced by self-loops: indeed, it has the highest in-degree value for MDD (Figure 5.8). Similarly, "felt irritable" plays a central role in GAD, strongly influencing several other symptoms and having the highest in-degree in that network, while its role is more marginal in MDD.

The symptoms "felt hopeless" and "felt down or depressed" exhibit the highest closeness centrality in GAD, see Figure 5.11, and are also connected by the second strongest undirected link. This is not true for MDD, where the two symptoms are even disconnected. "Felt threatened, judged, or intimidated" further exemplifies differential dynamics in the two disorders, whereby it is a cascade initiator in GAD, showing the highest out-degree (Figure 5.9), whereas in MDD, it emerge as a consequence of other symptoms and has the second-highest in-degree. More generally, we can identify a few instances, where initiating symptoms in MDD become terminal symptoms in GAD or viceversa.

The comorbid GAD and MDD network, while sharing elements with both GAD and MDD, also reveals unique patterns. For instance, "dwelled on the past" is linked to "procrastinated" and "avoided people," suggesting a pattern of avoidance and disengagement not as clearly observed in the other groups. Additionally, "experienced muscle tension" appears to precede "felt down or depressed," potentially indicating a stronger somatic contribution to mood in the comorbid profile. Interestingly, "experienced

loss of interest or pleasure" serves as an arrival point in this network, in contrast to its trigger role in GAD and MDD (Figure 5.8).

Notably, in the comorbid GAD and MDD network, "felt content" exhibits the highest betweenness centrality across all groups, acting as a key bridge in the flow of symptom activation. Overall, these patterns suggest that comorbidity does not simply reflect an additive overlap of GAD and MDD symptoms but rather reveals unique and potentially more complex causal interactions.

Our findings highlight how symptom interactions—not just symptom presence—may differ between disorders. This qualitative observation is further backed by the Weisfeiler-Lehman (WL) graph kernel used to assess the similarity between the aggregated causal networks for GAD, MDD, and comorbid cases. Indeed, the resulting similarity matrix revealed a strong and clear separation across groups, see Figure 5.13. This suggests that diagnostically meaningful structure can be recovered when individual networks are aggregated, despite substantial intra-group variability.

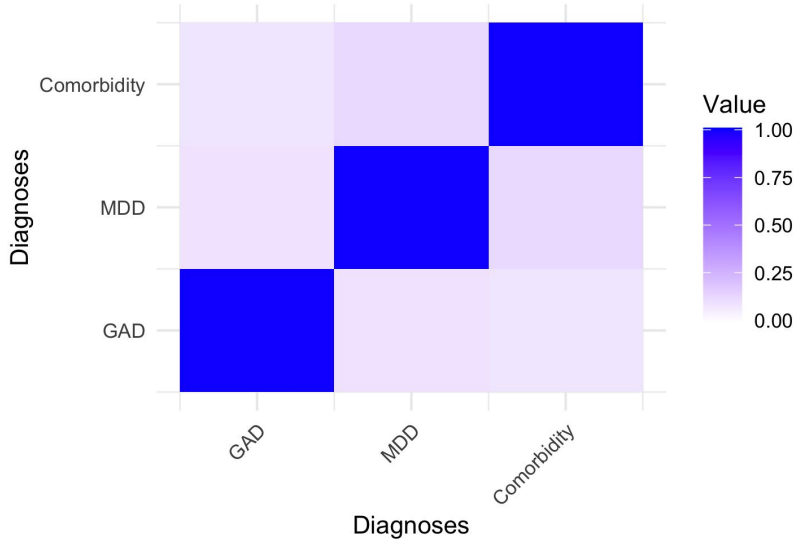

Figure 5.13: Weisfeiler-Lehman (WL) graph kernel similarity matrix comparing the fusion causal networks for Generalized Anxiety Disorder (GAD), Major Depressive Disorder (MDD), and comorbid cases (GAD and MDD). The matrix shows the pairwise kernel similarity value among diagnostic groups.

5.3.3 Complexity Measures are Key towards an Accurate Diagnostic Classification.

The application of the PCMCI+ algorithm revealed structural differences in the causal networks describing the three diagnostic groups. Our second pipeline (see Figure 5.1, right branch) now aims at predicting diagnosis based on symptom dynamics, which is a critical goal for clinical purposes. Following our pipeline, we enriched the dataset by computing a set of complexity-based features extracted from each individual's symptom time series (see Table 5.4 and Appendix C for their definitions), which helped extract the salient dynamical aspects of symptom expression.

Next, starting from this enriched dataset, we performed feature selection using Boruta-type out-of-bag (OOB) variable importance scores to improve interpretability and filter out noise [219]. The trained classifier obtained by involving only the 10 top-ranked features shown in Figure 5.14, selected through the iterative procedure described in Section 5.2 yields excellent performance: AUC = 0.92, sensitivity = 0.91, specificity = 0.91, accuracy = 0.91. We emphasize that performance is substantially higher compared to that of the Bagged Tree ensemble model trained on the raw symptom time series (AUC = 0.23, sensitivity = 0.09, specificity = 0.91, accuracy = 0.65), see Figure 5.15 for a

detailed comparison through ROC curves. The substantial performance improvement is likely due to the nature of the selected features, which include entropy and fractal-based descriptors of key symptoms, thereby reflecting the multidimensional and dynamic nature of symptoms across diagnoses.

Finally, we assessed the generalizability of the classificator by applying the model to the 11 participants with comorbid GAD and MDD, who were excluded from training. Interestingly, the classifier produced predictions that aligned with each participant's dominant clinical profile. In particular, when HAM-A scores exceeded HAM-D scores, the predicted diagnosis was typically GAD, and vice versa. A summary of these predictions is presented in Table 5.6.

Table 5.6: Model predictions for comorbid participants, not included in training. The model assigns diagnosis based on a probability threshold of 0.77 for classifying MDD, as determined by the leave-one-out cross-validation.

ID	Predicted Class	Pr(MDD)	HAM-D	HAM-A
P001	GAD	0.663	23	27
P003	GAD	0.560	16	15
P006	GAD	0.473	13	13
P007	GAD	0.043	11	17
P008	GAD	0.153	19	15
P010	MDD	0.866	22	22
P013	GAD	0.273	14	19
P048	GAD	0.570	14	17
P115	GAD	0.713	18	19
P117	GAD	0.463	12	18
P203	GAD	0.253	18	20

Note. HAM-D = Hamilton Rating Scale for Depression score; HAM-A = Hamilton Rating Scale for Anxiety score; MDD = major depressive disorder; GAD = generalized anxiety disorder.

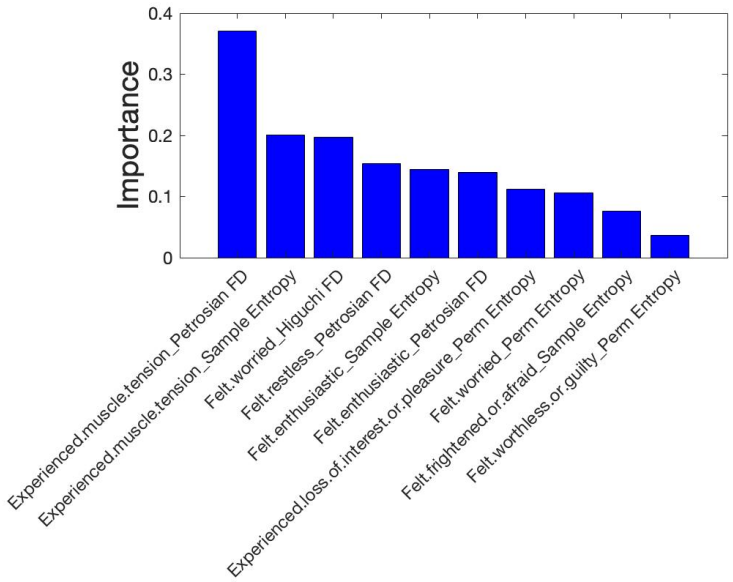

Figure 5.14: Most important features identified as crucial in distinguishing between General Anxiety Disorder (GAD) and Major Depressive Disorder (MDD) based on feature importance scores from the Bagged Tree classifier.

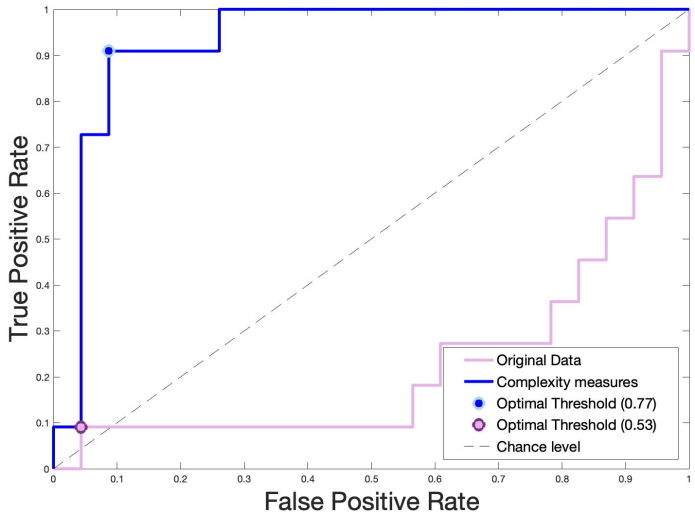

Figure 5.15: Receiver Operating Characteristic (ROC) curve for the classification between General Anxiety Disorder (GAD) and Major Depressive Disorder (MDD). The blue (violet) curve includes the selected complexity-based features (the original data). Each curve illustrates the model's performance across classification thresholds, with an Area Under the Curve (AUC) of 0.92 (0.23). The blue (violet) circle marks the optimal classification threshold of 0.77 (0.53), above which cases are classified as MDD. These thresholds were selected to maximize both sensitivity and specificity. The diagonal dashed line represents chance-level performance.

5.4 Discussion

This study aimed to enhance our understanding of symptom dynamics in clinical psychology, integrating advanced causal inference techniques, network-based methods, and machine learning tools. Our novel, integrated approach has been demonstrated on a case study where we attempt at deciphering the specificities of Generalized Anxiety Disorder (GAD), Major Depressive Disorder (MDD), and their comorbidity. Addressing a critical gap in previous literature—specifically, the tension between individual-level complexity and group-level diagnostic generalization—we implemented a structured analytical pipeline with three core methodological innovations.

Firstly, applying the PCMCI+ causal discovery algorithm to our case study on GAD and MDD participants revealed meaningful causal structures within individual symptom trajectories. Unlike traditional models (e.g., VAR and Transfer Entropy), PCMCI+ is capable of effectively identifying both linear and nonlinear causal relationships from short time series.

Secondly, by employing fusion networks combined with graph kernel methods to the PCMCI+ results, we successfully demonstrated that meaningful group-level patterns could emerge despite significant individual heterogeneity. The Weisfeiler-Lehman kernel highlighted clear structural differences between diagnostic groups, validating the potential of aggregating individual causal graphs into coherent, group-level representations. This methodological step provides a robust view of diagnostic differences at a structural level.

Importantly, our findings align well with previous theoretical and clinical conceptualizations [204], [221], demonstrating that GAD and MDD indeed differ at the causal level, particularly concerning central symptoms such as rumination, avoidance, and emotional reactivity.

Thirdly, incorporating complexity measures within a machine learning framework—specifically, a Bagged Tree classifier—substantially enhanced diagnostic classification accuracy compared to models relying only on raw symptom data. Notably, entropy, fractal dimensions, and recurrence-based metrics proved crucial in distinguishing between GAD and MDD, and to inform on the prevalent diagnosis in comorbidity cases. The final

classification model, trained on selected complexity-based features, achieved an impressive accuracy (≥ 0.9), underscoring the clinical relevance of dynamic complexity in symptom expression. To the best of our knowledge, the use of complexity measures represents a novel extension in clinical psychology aimed at exploring whether complex temporal features can help differentiate diagnostic categories based on symptom dynamics.

The findings of this study pave the way for fundamental advances in our understanding of mental disorders, whereby they represent a solid step towards discriminating disorders by means of their symptom dynamics. Indeed, the first pipeline, grounded on the PCMCI+ algorithm, allows to discriminate the main group-level differences in symptom dynamics across mental disorders, filtering out the unavoidable individual heterogeneities. The second pipeline then allows the identification of the complexity measures that best capture the differential symptom dynamics across psychopathologies.

In addition, our results seem promising also towards personalized diagnostics and therapeutic interventions. Indeed, the outcome of the two pipelines may prove to be a valid support for practitioners. The classification coming from the second pipeline can represent a first, automatic screening supporting the diagnosis. In a prudent approach, the automatic diagnosis can represent an alert flag for the practitioner. Once a diagnosis has been finalized, the individual causal graphs from the first pipeline can be then used to support personalized therapy, whereby it allows to identify central and source nodes, which may prove critical for the persistence of the disorder.

Limitations and future directions

Our study is not free of limitations, which should be addressed in future work. First, our pipelines should be tested on other datasets, to further stress the ability of our approach to deal with short time series and relatively small sample sizes. Second, towards the application of the pipelines to support practitioners in diagnosis, datasets including control groups should also be tested. Moreover, from a methodological standpoint, one should consider that the PCMCI+ algorithm—despite its strengths—relies on several key assumptions. In particular, it assumes causal sufficiency, meaning that all relevant variables influencing the system have been measured. This implies that if hidden confounders are present, the inferred causal relations may be biased or spurious. Moreover, while PCMCI+ can capture both linear and nonlinear dependencies, it may still be sensitive to violations of temporal stationarity and to the quality of the time series data, and therefore suitable data preprocessing might be required [224]. Finally, an underlying assumption in graph representations is that symptom interactions are pairwise. However, recent work has pointed out that higher-order multibody interactions between symptoms may play a role in explaining their dynamics. Alternative metrics that also account for higher-order interaction, such as the O-information, could be considered [225].

Conclusions

Chapter 6

Conclusions and Future Perspectives

This thesis focused on model-based and data-driven approaches to the study of complex systems, spanning from established domains of application to the novel and sensitive field of psychology.

In Part I of the thesis, these approaches have been used to address 4 research questions (RQ1-RQ4) related to sustainability and climate change, fields where complexity methods have been widely employed. Collectively, the four case studies established a solid methodological foundation and suggested that affective components play a crucial role in decision making even in socio-ecological contexts – thereby motivating the transition to the psychological domain in the second part of the thesis, a field where the application of complexity science tools is less ripe. Specifically, Part II focused on applying complex-systems frameworks to individual psychological processes, building upon the methodologies developed in Part I and addressing research questions RQ5-RQ9.

In what follows, I first summarize the answer to each of the nine research questions, to then provide a broader perspective on the strengths and limitations of the complexity-based approach, with reference to their potential impact on the study of human behavior and psychology.

Answer to RQ1: the urban topology of Siena constrains the diffusion of sustainable behavior. The first study employed an agent-based model to explore how citizens' awareness, opinions, and behaviors interact on social networks over time and influence sustainable actions, showing that the coexistence of activists, deniers, and indifferent agents –whose behavior follows game-theoretic rules– can generate complex, collective outcomes. Surprisingly, we found that the diffusion of sustainable behavior is influenced by the specific topological structure of the system.

Specifically, we surveyed 324 residents of Siena's historical center to both map climate awareness and parameterize our geo-referenced ABM. Education emerged as the strongest predictor of awareness while women reported higher concern than men (eco-gender gap). The survey informed five behavioral types mapped to evolutionary games; the ABM was then developed in two different settings (regular lattice vs Siena) to study dynamics not inferable from cross-sectional data. Two main findings follow: first, adding small-world ties fosters cooperation relative to purely geographic neighborhoods; second, the real topology of Siena promotes cooperation less than an ideal regular lattice. Taken together, these findings indicated that the diffusion of cooperative behavior is more difficult in Siena's historical center than in an idealized regular city, raising important questions about how urban topology shapes the sustainability practices of its residents.

The main limitation of the study is that individual features (age, gender, educational level) as well as climate awareness scores from the survey were only used as labels and did not affect agents' decision making. Next steps include modeling awareness as an actual driver of individual choices, exploring richer agent sets (e.g., tourists), incorporating multilayer ties (e.g., work, hobbies), scaling the simulation from 324 to the full resident population, and replicating the study in other urban contexts. Another promising direction is to evaluate targeted interventions by embedding "special" influence nodes (e.g., activists or bots) in the social network; preliminary results suggested that increasing a specific type of agents enlarges the cooperation regime.

Answer to RQ2: intuitive and analytical reasoning styles differently shape the perception of extreme rainfall events over time. In the second study, a Markov decision process was used to model how individuals perceive and respond to climate

risks under uncertainty over time. We identified two different attitudes: Climate Aware (CA) and Climate Susceptible (CS) individuals, depending on a specific model parameter capturing reasoning propensity (analytic vs intuitive).

Results identified a critical transition from (CA) to (CS) individuals, which is more evident in locations of Sicily clustered as extreme in Vitanza, Dimitri, and Mocenni [37]. Thus, (CS) individuals showed more sensitivity to extreme rainfall events, indicating that policy efforts should focus on reducing their responses below the critical transition threshold. The determination of factors changing the reasoning propensity parameter can be supported by attitude surveys on the local population, considering both specific and universal factors such as the individual's basic education and the climate literacy, as suggested by the literature. Preliminary results suggested that individual perception depends on the time horizon considered, with age and life expectancy influencing local dynamics.

The model was intentionally simple: transitions and rewards were stylized, the discount term was specified ad hoc, and the parameter tuning was minimal. Validation was limited and potential confounders were not taken into account. On the data side, the focus on a single region, time period, and extreme rainfall events restricted generalization. These limitations highlighted directions for future research, particularly to enhance model reliability and external validity. Nevertheless, the exploratory nature of this application allowed to gain familiarity with Markov models and to assess their potential in decision-making contexts under uncertainty.

Answer to RQ3: Eastern Sicily emerges as the most extreme rainfall zone of the island. In the third study, a multimodal machine-learning framework was developed to detect areas affected by extreme rainfall, by clustering high-frequency spatio-temporal rainfall data from Sicily (2009–2021) using Affinity Propagation. Results showed that Eastern Sicily is increasingly affected by extreme rainfall events.

From a temporal perspective, using high-frequency data with Euclidean metric highlighted an increasing trend of extreme events over the years, whereas weekly averaged data did not provide the same evidence. In this context, 2021 clearly emerged as one of the most anomalous years. A statistical validation confirmed that three indicators regarding heavy rain percentages effectively describe anomalous clusters, proving that these are most often characterized by extreme events. From a spatial perspective, high-frequency data with the use of Euclidean metric emerged as the most effective setting for detecting extreme rainfall events through geographical clustering. At the same time, reducing the dataset to weekly means proved useful to identify geographically uniform clusters, merging anomalies and territorial clusters in a balanced way.

Limitations appeared mainly due to the short observational period, which may be influenced by natural variability. Further research is needed to assess the most suitable dimensionality reduction methods for local analyses and to refine rainfall indicators. Extending the spatial and temporal coverage, and applying more robust aggregation strategies, would strengthen the detection of extreme rainfall trends and potential climate change signals.

Answer to RQ4: spatio-temporal air quality data enable informed policy decision-making. In the fourth study, a wearable-sensor network for pollutants and environmental parameters was integrated with neural networks to predict geo-location from air quality observations.

The main contributions of the work were: (i) the design and release of the WeAIR device; (ii) the collection and public dissemination of a novel geo-localized dataset in Siena (Italy); and (iii) the release of trained neural network models and spatial maps derived from the campaign. Experimental results showed that a simple feedforward neural network can predict geo-location from air quality observations with good accuracy. Notably, the median observation vector predicts coordinates close to the existing fixed monitoring station, suggesting that such models could support decision-making on the

placement of new stations. Furthermore, this framework can foster citizen engagement by providing real-time awareness of pollution exposure.

The study presents limitations, particularly the need for large-scale adoption to ensure representative coverage. Future work should extend the monitoring campaign, produce multiple devices, and explore user-friendly designs (e.g., 3D-printed cases) to encourage wider participation of the population.

Answer to RQ5-RQ6: egosyntonicity, while adaptive in the short term, can entail long-run maladaptive costs. In part II, a Markov model of emotion dynamics was developed to formalize how individuals regulate affective states over time, revealing that maintaining internal coherence between expected and current emotions (egosyntonicity) –while adaptive in the short term– can sometimes entail long-run maladaptive costs.

In more detail, the model is grounded on three fundamental principles of emotion dynamics: inertia, contingency, and regulation. Inertia is captured by internal mood dynamics, with a parameter quantifying the reluctance to change mood. Contingency is reflected in the valence dynamics, which depend on the complex interplay between mood, external events, and attention. Finally, regulation is modeled implicitly through the concept of egosyntonicity.

A parametric analysis of the model revealed four classes of individuals, based on the time spent in egosyntonicity and the resulting long-term emotional valence. Balanced happy individuals spend more time in egosyntonicity, thus living in harmony with their emotions. At the opposite end, chronically troubled individuals are often in internal conflict and experience negative emotions in the long term (e.g., in obsessive compulsive or eating disorders). The remaining two classes are somewhat unexpected yet theoretically interesting: self-deluded, generally in sync with themselves but experiences negative emotions in the long term (typical of personality disorders); troubled happy, often in internal conflict but manages to maintain a positive emotional valence in the long term (e.g., in successful therapies). Despite its minimalism, the model generates a surprisingly rich behavioral repertoire grounded in fundamental psychological principles, suggesting that simple and parsimonious models can capture psychologically plausible dynamics without requiring over-detailed representations.

Limitations remain: first, the binary modeling of mood, valence, and events should be replaced by multi-level states, allowing a more nuanced depiction of emotional dynamics. Second, future works should consider the effect of interacting emotions, since in its current form the model captures the dynamics of the dominant emotion, and simply assumes mood dynamics to be independent from other variables. Mood dynamics should then be changed, considering transition probabilities that are a function of the different emotions experienced by an individual at each time step. Third, albeit the model reproduces four well-known interplays between egosyntonicity and emotional well-being, its present formulation does not allow individuals to learn and evolve from past experiences. Future works could consider the presence of adaptive mechanisms, whereby the individual learns from past experiences and modifies their behavioral parameters. Finally, although the model is founded on psychological principles and is capable of reproducing commonly observed behaviors, future empirical works could collect longitudinal data on emotion dynamics to further refine the model and the underlying hypotheses on which it is based.

Answer to RQ7-RQ9: causal inference, group-level structure, and complexity measures jointly advance psychological understanding. As final study, a dual analysis pipeline was proposed to study mental disorders: causal inference, machine learning and complexity measures were combined to investigate longitudinal symptom data. The framework was validated on a case study of individuals with a primary diagnosis of either Generalized Anxiety Disorder (GAD), Major Depressive Disorder (MDD), or their comorbidity.

The first pipeline, based on the PCMCI+ algorithm, recovered causal relations among symptoms at the idiographic level and aggregated them into fusion networks.

Unlike traditional models, PCMCI+ revealed capable of effectively identifying both linear and nonlinear causal relationships from short time series. Moreover, employing fusion networks combined with graph kernel methods to the PCMCI+ results allowed to identify meaningful group-level patterns despite significant individual heterogeneity. Importantly, findings demonstrated and confirmed that GAD and MDD indeed differ at the causal level, particularly concerning central symptoms such as rumination, avoidance, and emotional reactivity.

The second pipeline leveraged complexity metrics, feature selection and machine learning to distinguish diagnostic categories based on the dynamic features of symptom trajectories. Incorporating complexity measures within a machine learning framework represented a novel extension in clinical psychology and substantially enhanced diagnostic classification accuracy ($\approx 91\%$) compared to models relying only on raw symptom data, underscoring the clinical relevance of dynamic complexity in symptom expression. Notably, entropy, fractal dimensions, and recurrence-based metrics proved crucial in distinguishing between GAD and MDD.

Beyond their theoretical contribution, the proposed pipelines highlight a potential complementarity between data-driven and clinical practice. Complexity-based and machine-learning analyses may support practitioners as an initial screening layer, while preserving the possibility of descending into individual-level causal symptom dynamics for personalized clinical interpretation. At the same time, the same framework enables research-oriented investigations of similarities, differences, and causal structures across disorders at the group level.

Our pipelines should be tested on other datasets, to further stress the ability of our approach to deal with short time series and relatively small sample sizes; datasets including control groups should also be tested. Moreover, the PCMCI+ algorithm –despite its strengths– relies on several key assumptions. In particular, it assumes causal sufficiency, meaning that all relevant variables influencing the system have been measured. This implies that if hidden confounders are present, the inferred causal relations may be biased or spurious. Moreover, while PCMCI+ can capture both linear and nonlinear dependencies, it may still be sensitive to violations of temporal stationarity and to the quality of the time series data, and therefore suitable data preprocessing might be required. Finally, recent work has pointed out that higher-order multibody interactions between symptoms may play a role in explaining their dynamics. Alternative metrics that also account for higher-order interaction could be considered.

6.1 Broader impact and future outlook

Rather than constituting a collection of domain-specific applications, this thesis provides a reusable methodological template whose conceptual structure can be transferred across domains, scales, and datasets. Taken together, the presented results demonstrate that complex-systems methodologies can bridge idiographic and nomothetic perspectives, providing a complex-based framework for understanding psychological mechanisms in their dynamical nature. Across both parts, the thesis contributes to a growing convergence between complexity science, data analysis, and psychology, offering conceptual and computational tools for understanding human systems at multiple scales. Moreover, this thesis illustrates how methods from complexity science can extend psychological inquiry beyond static or reductionist views, paving the way for a truly dynamical understanding of human behavior.

Here we provide a broad overview of the current limitations of the complexity-based approaches adopted in this thesis, illustrate their potential in applications to human behavior, and discuss possible avenues for future research.

Model-based frameworks often rely on strong simplifying assumptions –such as rational behavior, fixed transition structures, or linear dynamics– that, while offering interpretability and formal clarity, are difficult to validate empirically. Conversely, data-driven methods excel in predictive accuracy and flexibility but frequently lack

interpretability, particularly when applied to human-related domains where cognitive, emotional, and contextual factors interact in complex, nonstationary ways. Future research should aim to leverage hybrid frameworks in psychological applications, where model-based and data-driven components complement each other: theoretical models can constrain data exploration, while data-driven methods can refine parameters, uncover nonlinearities, and adapt to temporal changes. Such integration would combine explanatory power with empirical robustness.

Building on the shift in this thesis from climate-related studies (Part I) to individual-level complexity (Part II), a promising research direction is to connect individual affective dynamics and proenvironmental behavior. As highlighted by recent work, the interplay between personal emotional complexity and collective climate actions remains largely unexplored [226]. Integrating individual and group levels would allow a bottom-up study of how affective states scale up to social patterns of engagement or inaction, contributing to a more comprehensive framework for sustainability research. Such work calls for an interdisciplinary approach with psychology and complexity science at its core.

Given the centrality of time in the phenomena analyzed throughout this thesis, future work should aim to move beyond cross-sectional designs and adopt longitudinal approaches to climate-related behavioral research. Dynamical modeling would allow for a deeper understanding of how emotions, beliefs, and behaviors evolve and influence each other over time.

Recent empirical work further illustrates how emotional and cognitive factors shape climate-related behavior. For instance, Doell, Conte, and Brosch [227] showed that interindividual differences in environmentally relevant positive trait affect impacts sustainable behavior in everyday life, leveraging longitudinal ecological experience sampling to capture within-person temporal dynamics.

In contrast, studies such as Vlasceanu, Doell, Bak-Coleman, *et al.* [228] and Ogunbode, Doran, Hanss, *et al.* [229] have relied on cross-sectional designs to examine climate-related beliefs and emotions at the population level. The former tested eleven expert-designed behavioral interventions across 63 countries, revealing small, audience-dependent effects; the latter analyzed data from 32 countries, showing that climate anxiety is positively associated with exposure to climate information, perceived social norms, and pro-environmental behavior, but negatively associated with mental well-being. Future research could build on these contributions by adopting dynamical frameworks to investigate how such psychological and behavioral relationships evolve over time.

Overall, capturing temporal dependencies appears essential for understanding how individual processes co-evolve, reinforcing the view highlighted in this thesis that time is a fundamental dimension of complexity.

Appendices

Appendix A

Supplementary Information for Model-based Approaches to Complex Systems

A.1 Supplementary Information for Agent-based Models

This section provides additional information supporting Section 2.1, along with further details on the data collection and modeling procedures underlying the study described in Section 2.2 and presented in [35].

A.1.1 Game Theory essentials

Definition A.1.1 (*Nash equilibrium*)

Consider a two–player normal–form game with strategy sets S_1, S_2 and payoff functions u_1, u_2. A (pure–strategy) profile $(s_1^*, s_2^*) \in S_1 \times S_2$ is a Nash equilibrium if each player's action is a best response to the other's:

$$u_1(s_1^*, s_2^*) \geq u_1(s_1, s_2^*) \quad \forall s_1 \in S_1, \qquad u_2(s_1^*, s_2^*) \geq u_2(s_1^*, s_2) \quad \forall s_2 \in S_2.$$

A (mixed–strategy) Nash equilibrium is a pair of probability distributions (π_1, π_2) over (S_1, S_2) such that each player's support contains only best responses to the opponent's mixture [51]. □

Prisoner's Dilemma (PD) The Prisoner's Dilemma (PD) refers to two suspects, accused of committing a crime, arrested by the police and locked in two different cells preventing them from communicating [230], [231]. Both are given two choices: confess or remain silent. If both confess, the total number of years in jail will be higher than when both choose to remain silent. If one confesses and the other remains silent, the confessor gains a personal benefit by being freed from all charges, while the other will receive a more severe sentence than if both would have chosen to stay quiet. The two pure strategies "confess" and "remain silent" of the game can be renamed as "defection" and "cooperation", respectively. The "confession" is often interpreted as an action of defection, in which one prisoner betrays the other by collaborating with the prosecution, gaining a personal benefit at the expense of the other. On the other hand, "remaining silent" can be interpreted as a cooperative action in which one prisoner chooses not to betray the other, forgoing a personal advantage and preserving a better outcome for both. Paradoxically, rational logic drives both suspects to confess (defection), being the more individually convenient option, even if this choice leads to a more socially disadvantageous outcome than if both had remained silent. In this non-iterated version of the PD game, the two criminals never have to work together again.

Stag-Hunt (SH) The Stag-Hunt (SH) game focuses on the concept of social cooperation and the dilemma between self-interest and collective ones [51]. The game can be described imagining two hunters facing a dilemma: they go hunting and must decide whether to hunt a stag or a hare. Their decision has to be made without knowing the decision of others, and keeping in mind that to hunt a stag successfully both of them must cooperate,

while for the hare the efforts of a single person are sufficient. Therefore, each player can choose between two pure strategies: "Stag" and "Hare", which can be renamed as "cooperation" and "defection", respectively. Each player will choose the Stag strategy when also the other will choose the same and likewise for the Hare strategy, depicting a herding mechanism.

Hawk-Dove (HD) The Hawk-Dove (HD) captures a basic feature of animal conflict and can be used to analyze strategic behaviors between individuals in situations of conflict and cooperation, as in the previous two cases [232]. The game is defined by imagining two animals fighting for a limited resource of food and having two possible strategies: "Hawk" and "Dove". The Hawk strategy is more aggressive and violent and can be interpreted as "defection", while the Dove one is more passive and docile and can be seen as "cooperation". If both players choose the Hawk strategy, they will fight until one is defeated and the other wins the resource, while if both players choose the Dove strategy, they will avoid the fight and will share the resource. Finally, if one player chooses the Hawk strategy and the other the Dove one, then the former will get the entire food resource for himself, while the latter will flee. In this context, each player will prefer to have an aggressive strategy when the other is more docile and vice versa, representing an anti-herding mechanism.

Payoff Matrices For the three games we get the payoff matrices shown in Table A.1, where (x, y) = (score of player 1, score of player 2).

Table A.1: Payoff matrices of PD, SH, and HD games.

PD game		
P1/P2	**C**	**D**
C	$(1, 1)$	$(0, \alpha)$
D	$(\alpha, 0)$	$(0, 0)$

SH game		
P1/P2	**C**	**D**
C	$(1, 1)$	$(0, 0)$
D	$(0, 0)$	$(1, 1)$

HD game		
P1/P2	**C**	**D**
C	$(0, 0)$	$(1, 1)$
D	$(1, 1)$	$(0, 0)$

In the three classic 2-player games the structure of the payoff matrices determines the existence and type of Nash equilibria. In the PD game, if $\alpha \in (1, 3)$, defection strictly dominates cooperation for both players, leading to a unique pure-strategy Nash equilibrium at (D,D), even though mutual cooperation (C,C) would yield higher joint payoffs. In the SH game, two pure-strategy Nash equilibria exist: (C,C) and (D,D). In contrast, the HD game admits two asymmetric pure-strategy equilibria—(C,D) and (D,C). Both SH and HD have a symmetric mixed-strategy equilibrium in which both players randomize between C and D with equal probability. From normalized 2-player matrices, we move to an iterated network model where each player plays with neighbors. In PD, payoffs scale with the number of cooperators; in SH, players follow the majority; in HD, they tend to oppose it.

A.1.2 Survey and Dataset

The dataset used in this study has been obtained by spreading a survey among citizens living in the historic center of Siena from the mid of May to the end of July 2023, obtaining 324 responses. The survey is organized in two sections, which are reported in Table A.2 together with the corresponding questions.

Section S.A Section S.A is composed of five questions in which we ask the interviewees their age, gender, educational level, address (without house number) and the area of the historic centre of Siena in which they live. Specifically, the city of Siena has been historically subdivided into three neighbourhood, hereafter called "Terzi": "Terzo di Città" (C), "Terzo di Camollia" (CM) and "Terzo di San Martino" (SM). The percentages of respondents belonging to each category are shown in Figure A.1.

Table A.2: Survey on environmental behaviors for the inhabitants of the historical centre of Siena. F = Female, M = Male, NS = Not specified, MS = Middle School, HS = High School, D = Degree, C = Terzo di Città, CM = Terzo di Camollia, SM = Terzo di San Martino, POS = Most of the times/Always, IND = Sometimes, NEG = Never.

	Question	**Possible answers**
S.A	**Q.1** Age	14-25 / 25-40 / 40-60 / Over 60
	Q.2 Gender	F / M / Other / NS
	Q.3 Educational level	MS / HS / D / NS
	Q.4 "Terzo" of Siena where you live	C / CM / SM
	Q.5 Address where you live	Open question
S.B	**Q.6** In your opinion, how much can your daily choices influence the global impact on the environment?	Range 1-10
	Q.7 How often do you try to reduce energy and water consumption?	POS / IND / NEG
	Q.8 Do you participate in the waste sorting organised by your municipality correctly?	POS / IND / NEG
	Q.9 How often do you recycle products (paper and cardboard, organic, plastic, glass, etc.) at home?	POS / IND / NEG
	Q.10 How often do you correctly dispose of special dangerous waste (batteries, expired medicines, etc.)?	POS / IND / NEG
	Q.11 When dealing with waste sorting, what is your main approach?	I actively participate independently of others / I am interested in the approach of the community I live in, besides my own attitude / I do not take part regardless of the others
	Q.12 Have you ever participated in cleaning public places such as beaches, seafronts, parks, squares?	Yes, once or more / No but I may decide to do so if the opportunity arises / No, I don't think it is useful
	Q.13 How careful are you about the environmental impact of your purchases (food, cars, clothings, etc.)?	A lot / Enough / Not at all
	Q.14 What is your approach towards waste sorting in relation to the behaviour of others?	I follow the recycling practices adopted by the majority of my neighbours / I behave differently from the majority of my neighbours / In general, I follow the guidelines of the administrators

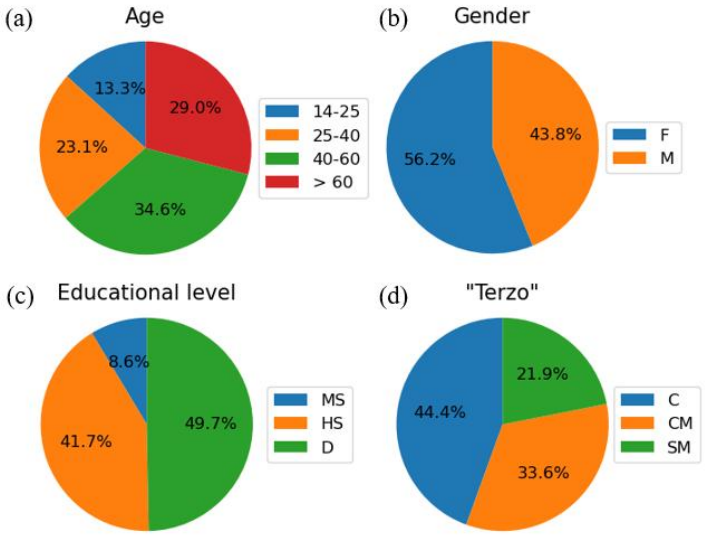

Figure A.1: Percentages of the (a) age categories 14-25, 25-40, 40-60 and Over 60. (b) gender categories F and M. (c) educational level categories: Middle School (MS), High School (HS) and Degree (D). (d) three "Terzi": "Terzo di Città" (C), "Terzo di Camollia" (CM) and "Terzo di San Martino" (SM).

The two largest age classes are the 40-60 and Over 60 ones, representing 34.6% and 29% of the sample, respectively. The 25-40 age category accounts for 23.1% of the sample, and the 14-25 category, which is the smallest, accounts for 13.3% of the sample. Citizens who participated in the survey were predominantly women (F), accounting for 56.2% compared to 43.8% of men (M). The largest educational category is composed of citizens owning a degree (D), followed by people with a high school (HS) and a middle school (MS) diploma, representing the 49.7%, 41.7%, and 8.6% of the sample, respectively. Finally, 44.4% of the respondents live in the "Terzo" (C), 33.6% in the "Terzo" (CM), and 21.9% in the "Terzo" (SM). This distribution in the three "Terzi" along with the address allows us to give a position to each of the respondent on the map of Siena, enabling to geographically visualize the answers. To this aim we have first built the map of the city by means of the python OSMnx library which transforms the OpenStreetMap into a graph. The map has been generated by setting as central point the geographical coordinates of Piazza Salimbeni and a radius of 1200 m. Key elements of the historic city centre of Siena are clearly visible, see Figure A.2. Furthermore, the 324 respondents of the survey (red dots in the figure) approximately cover the entire historic center.

Section S.B Section (S.B) contains nine questions on citizens' environmental habits, allowing to both estimate their climate awareness level and identify several types of agents according to their attitudes towards sustainable practices:

- *Activists*: people strongly involved in environmental issues.
- *Deniers*: people not involved in sustainable behaviors, potentially taking actions damaging the environment or believing that there is not a real and urgent problem.
- *Indifferents*: people characterized by indifference towards environmental problems. Among them, we have identified three different types, specifically *(i)* the *indifferent imitators of the majority of neighbors*, *(ii)* the *indifferent opponents of the majority of neighbors* and *(iii)* the *indifferent imitators of the best neighbor*.

This classification will be used to define the different games embedded in the agent-based model.

The climate awareness level of each respondent is estimated using question Q.6 of the survey, asking each citizen how much he thinks his daily choices can influence the global impact on the environment. Respondents can choose a numerical option from 1 to 10,

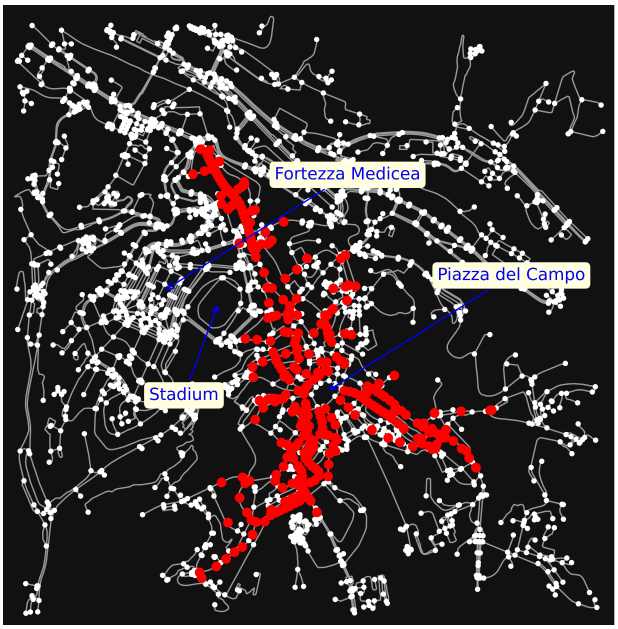

Figure A.2: Geo-referencing agents on the map of Siena. Red dots represent respondents of the survey. White dots represent the intersections between roads.

where 1 means a total lack of awareness and vice versa for 10. Figure A.3 reports the bar diagrams related to the climate awareness level for each of the age, gender, educational level and "Terzo" categories considered in the survey, where data have been normalized.

Figure A.3a shows that the 40-60 age category is the most aware about climate change, presenting a bell-like pattern with a very high peak on level 8. Next we have the 25-40 age group, showing a bell-like pattern with a peak on level 7. The youngest age category 14-25 shows a lower awareness than the previous two, with its highest peak on level 5. Finally, we have the over 60 age class which is the least aware. Figure A.3b shows how the female category is slightly more aware than the male one. The women's class exhibits much higher peaks than men on the largest numerical choices 8, 9 and 10 and much lower peaks than men on the smaller numerical choices 1, 2, 3 and 4. Figure A.3c shows how the category owning a degree (D) is definitely the most aware, presenting much higher peaks on the greater numerical options 8, 9 and 10. The category possessing a high school (HS) diploma still presents a fairly high level of awareness. Finally, the category with a middle school (MS) diploma is clearly the least aware, showing very high peaks on the smallest numerical options 1 and 2. Finally, the bar diagrams in Figure A.3d show that there are also slight differences between the three "Terzi" (C), (CM) and (SM). Indeed, we can notice that (C) and (CM) present a better trend compared to the (SM) one.

This analysis shows that age, education and gender are important predictors of climate change awareness, consistently with recent findings [60]–[65], [74], [233]–[236]. Regarding the age predictor, the least aware age group is the Over 60 one, in agreement with many other studies showing that the older age categories are the least concerned about climate change [237], [238]. Nevertheless, the youngest age group 14-25 emerge as less aware than the 25-40 and 40-60 age classes.

We can classify respondents into five types of agents (A), (D), (PD), (SH) and (HD), according to their answers to Section S.B. All questions Q.7-Q.13 have three qualitative answer options, which are categorized as positive, indifferent and negative, and are used together with question Q.6 to identify whether a respondent is an activist, a denier or an indifferent agent. The approach used to determine the agent type is described in Figure A.4.

The prerequisite of an agent to be considered activist is that he has a high climate awareness level: score(Q.6) ≥ 7. The second necessary condition is that at least one

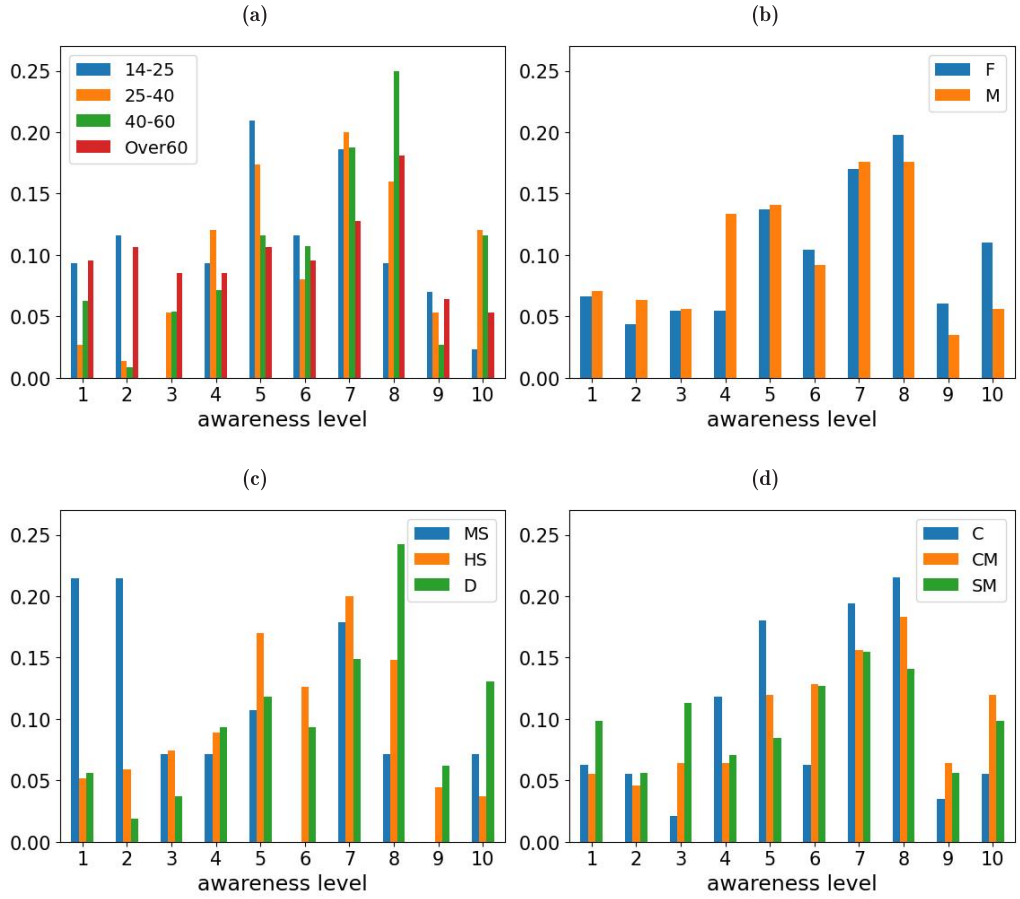

Figure A.3: Bar diagrams illustrating the awareness level for (a) age , (b) gender, (c) educational level, (d) "Terzo".

of the two following statements is fulfilled: (i) the agent responds positively to both questions Q.12 and Q.13, (ii) the agent answers positively to six out of the seven questions Q.7-Q.13. We have identified questions Q.12 and Q.13 as essential in the determination of an activist, since cleaning public places or paying attention to environmental impact in purchases are deliberate actions and not dictated by rules or laws as is the case for waste sorting, recycling materials or water and energy consumption. The requirement for activists to answer positively to at least six out of the seven questions Q.7 to Q.13 reflects the fact that being an activist requires a constant and widespread engagement in multiple aspects of sustainable practices. Moreover, in this way we can ensure that activists answered positively to at least Q.12 or Q.13, which are, in our opinion, essential in determining pro-environmental behavior.

A specular reasoning has been applied to identify the deniers. The prerequisite of an agent to be considered denier is that he has a low climate awareness level: score(Q.6) ≤ 4. The second necessary condition is that at least one of the two following statements is fulfilled: (i) the agent responds negatively to at least one of questions Q.8 and Q.11 (ii) the agent answers negatively to at least two out of the seven questions Q.7-Q.13. We have identified Q.8 and Q.11 as essential in the determination of a denier as they are both related to separate waste sorting, which is a consolidated sustainable practice. Giving a negative answer to at least two of the seven questions Q.7 to Q.13 indicates significant resistance to sustainable practices, as these questions cover a range of key sustainability-related behaviors.

Respondents who fulfill neither the condition for being activists nor the one for being deniers are classified as indifferent. Among them, an agent is defined as (i) imitator of the

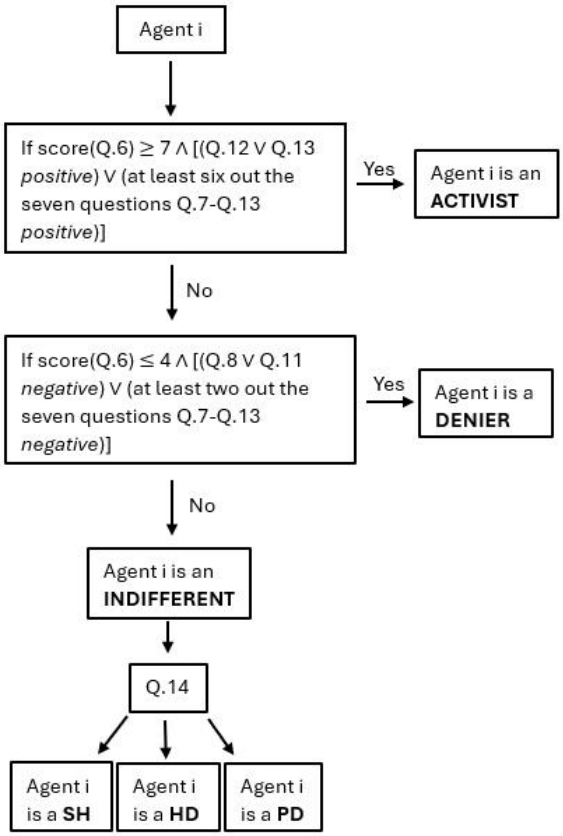

Figure A.4: Agents' classification rule.

majority of neighbors, (ii) imitator of the best neighbor, (iii) opponent of the majority of neighbors, depending on the answer to question Q.14. The criterion just described has been applied to our sample of 324 agents, giving rise to five classes of agents, each of them is associated to a different game:

1. 33 Activists (A)
2. 15 Deniers (D)
3. 276 Indifferent, subdivided as follows:
   - **(a)** 45 Indifferent imitators of the majority of neighbors (SH)
   - **(b)** 34 Indifferent opponents of the majority of neighbors (HD)
   - **(c)** 197 Indifferent imitators of the best neighbor (PD)

The robustness of the chosen classification criterion has been tested using a twofold approach. Firstly, our results show that the sample of 324 agents contains 10% activists and 4.6% deniers, consistently with the results found in [239], [240]. Secondly, by applying small variations to the thresholds used in the selection criteria, such as for example by defining an activist for score(Q.6) ≥ 6 and a denier for score(Q.6) ≤ 3, we obtained slight changes in the agent distribution: 22 (A), 12 (D), 47 (SH), 35 (HD) and 208 (PD).

A.1.3 ODD Protocol

Notation and symbols

Purpose To simulate how individual decisions (cooperate/defect with respect to environmental practices) evolve on social/spatial networks, and to identify conditions

Table A.3: Main symbols used in the model.

Symbols	Meaning
C, D	Cooperation / Defection (pure strategies)
$\alpha \in [0, 3]$	Defection-award
α_1	Critical threshold separating cooperation from defection
$ic \in [0, 100]\%$	Initial share of cooperating indifferent agents
$SWrp \in [0, 1]$	Rewiring probability (small-world construction)
tc	Total cooperating neighbors of a given agent
$score(i)$	Agent score (Eq. 2.7 in Section 2.1.1)
A/D/PD/SH/HD	Agent types: activists, deniers, indifferent PD/SH/HD

under which cooperation emerges and persists. We focus on the effect of (i) network topology and (ii) the defection-award α on the diffusion of pro-environmental behavior.

Entities, state variables, and scales **Entities.** $N = 324$ non-mobile agents (residents). Behavioral types: **A** (Activist, always C), **D** (Denier, always D), **PD**/**SH**/**HD** (indifferent). **Agent state variables.** *age* $\in$ {14–25, 25–40, 40–60, 60+}, *gender* $\in$ {F, M}, *education* $\in$ {MS, HS, D}, *awareness* $\in [1, 10]$, *type* $\in$ {A, D, PD, SH, HD}, *cooperate?* $\in \{0, 1\}$, *old-cooperate?* $\in \{0, 1\}$, *score* $\in \mathbb{R}_{\geq 0}$. In the Siena model, additional attributes: *terzo*, *location*, *lat*, *long*. **Global variables.** Counts by type/demography; parameters α (defection-award), ic (initial cooperation), $SWrp$ (rewiring probability). **Temporal scale.** Discrete time steps (ticks). **Spatial/topological scale.** *Basic:* 2D 18×18 lattice (Moore neighborhood, $k = 8$) or small-world via rewiring. *Siena:* geographic graph (edge if distance ≤ 120 m) or its small-world variant.

Process overview and scheduling **Setup.**

1. Build network: lattice (Basic) or geographic graph from GIS/coordinates (Siena); optionally apply Watts–Strogatz rewiring with $SWrp$.
2. Assign agent attributes and behavioral types to match survey marginals (type counts: A=33, D=15, PD=197, SH=45, HD=34).
3. Initialize *cooperate?* for indifferent types according to ic; set *score*= 0.

Go (per tick).

1. *Interaction & scoring:* for agent i, let $tc(i)$ be the number of cooperating neighbors; update
$$score(i) = \begin{cases} tc(i) & \text{if } i \text{ cooperates,} \\ \alpha \cdot tc(i) & \text{if } i \text{ defects.} \end{cases}$$
2. *Strategy update:* PD imitates the best neighbor (max *score*); SH follows the local majority; HD plays the opposite of the local majority; A always C; D always D.
3. *Recording:* update time series (share of cooperators/defectors), snapshots, summary statistics.

Nodes encode current and previous actions to make transients visible: *blue* = cooperates now and cooperated previously; *red* = defects now and defected previously; *green* = defects now, cooperated previously; *yellow* = cooperates now, defected previously. Fixed–strategy agents are shown as *white* nodes with a central dot: blue for Activists (always C) and red for Deniers (always D).

Design concepts *Basic principles.* Local decision rules based on evolutionary game-theoretic payoffs and neighborhood information. *Emergence.* Global regimes of cooperation vs. defection; thresholds in α separating regimes. *Sensing.* SH/HD sense neighbors' actions; PD observes neighbors' *score*. *Interaction.* Pairwise interactions along network edges. *Stochasticity.* Basic: random assignment of attributes respecting survey marginals and random initial C/D for indifferent types; Siena: attributes from data (deterministic import), random initial C/D for indifferent types; rewiring is stochastic when $SWrp > 0$. *Observation.* Global cooperation fraction, trajectories over time, and final spatial patterns.

Initialization $N = 324$; type counts fixed to survey-based proportions (A=33, D=15, PD=197, SH=45, HD=34). Demographic variables initialized to observed marginals. *score*= 0. Indifferent types' initial *cooperate?* set by $ic \in [0, 100]\%$. Experimental parameters $(\alpha, ic, SWrp)$ are specified before each run.

Input data *Basic:* survey marginals/type proportions only. *Siena:* (i) GIS map/road network and geocoded addresses to place agents; (ii) CSV with agent attributes (*terzo*, location, coordinates, type, awareness). The geographic network links agents within $\approx 120m$.

Implementation and platform The model is implemented in NetLogo (version 6.3.0), a programming environment for simulating complex systems. All experiments were executed with this pinned version to ensure reproducibility. A multi–run design is used for every parameter configuration to obtain robust results.

Submodels *Network construction:* lattice builder (Basic) or `create-graph` from geo-coordinates (Siena); optional Watts–Strogatz `rewiring` with parameter $SWrp$. *Attribute & type setup:* random assignment with constraints (Basic) or CSV import (Siena). *Interaction & update:* procedures for SH/HD/PD choice rules and *score* update, followed by state update of *cooperate?*.

Parameters *Defection-award* $\alpha \in [0, 3]$ (controls relative gain from defection); *initial cooperation* $ic \in [0, 100]\%$ (share of initial cooperators among indifferent types); *rewiring probability* $SWrp \in [0, 1]$ (0 = pure lattice/geographic; ~ 0.05 = small-world; $\to 1$ = random). In our experiments, outcomes are governed primarily by α; ic only affects transients.

Differences: Siena vs. Basic (1) Extra attributes in Siena (district and coordinates) and geo-coded placement; (2) Base topology is geographic (radius ≈ 120 m) instead of a lattice; (3) Less stochasticity in setup (attributes imported rather than randomized); (4) Same rewiring mechanism for small-world variants in both models.

A.1.4 Further details

Small-worldness

For any considered graph we evaluated the ω coefficient, which quantifies the small-worldness properties of networks. A SW graph is defined by high clustering, like regular lattices, and small characteristic path length, like random graphs [69]. Therefore, ω is computed by comparing the clustering and characteristic path length of the network with those of an equivalent lattice and an equivalent random graph, respectively. The parameter ω takes values in the range [-1,1] and indicates the transition from regular lattices to random graphs, with intermediate values (≈ 0) characterizing SW networks. The ω coefficients for the two graphs of the Basic model have values approximately equal to -0.63 and -0.21, respectively, confirming that the former has a more regular lattice

structure while the latter has characteristics very close to a SW network. Similarly, the ω coefficients for the two networks of the Siena model take values approximately equal to -0.61 and -0.19, respectively, confirming that the geographic graph has a structure similar to a regular network, while the second one has characteristics very close to a SW network.

Consistency check

A consistency check with the BES/ISTAT series on recycled urban waste (Fig. A.5) shows Siena trailing the national trajectory for much of the period, aligning with our findings.

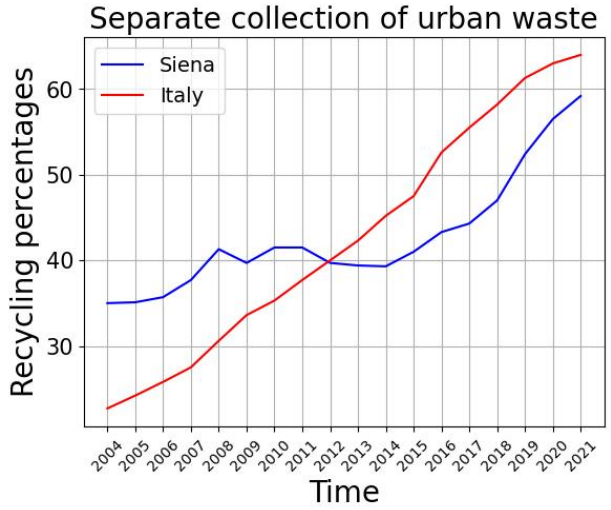

Figure A.5: Time series of recycled urban waste percentages out of the total collected. Data source: Istat - Elaboration on ISPRA data.

To see the complete agent-based model and the related analysis see the original paper [35] and the GitHub Repository.

A.2 Supplementary Information for Markov Models

In Markov chains, we will only be concerned with the total probability $p(x', x)$ of making a transition from x to x', regardless of which event actually causes the transition. Thus, we apply the rule of total probability to get $p(x', x) = \sum_{i \in \Gamma(x)} p(x' \mid x, i) \cdot p(i, x)$, where $i \in \Gamma(x)$ is the triggering event, $\Gamma(x)$ is the feasible event set at state x and $p(i, x)$ is the probability that event i occurs at state x. In the following useful definitions and information regarding irreducible and aperiodic Markov chains are provided.

Definition A.2.1 (*Irreducible state space*)

A closed set of states S is said to be irreducible if state j is reachable from state i for any $i, j \in S$. □

Definition A.2.2 (*Irreducible Markov chain*)

A Markov chain is said to be irreducible if its state space X is irreducible. □

Definition A.2.3 (*Hitting time*)

The hitting time T_{ij} represents the first time the chain enters state j given that it starts out at state i:

$$T_{ij} \equiv min\{t > 0 : X_0 = i, X_t = j\} \tag{A.1}$$

□

Definition A.2.4 (*Recurrence time*)

We refer to the random variable T_{ii} as the recurrence time of state i. □

Definition A.2.5

We define ρ_i^t to be the probability that the recurrence time of state i is t: $\rho_i^k \equiv P[T_{ii} = k]$. Then, let ρ_i be the probability of the event [ever return to i | current state is i, which is given by: $\rho_i = \sum_{k=1}^{\infty} \rho_i^k$. □

Definition A.2.6 (*Recurrent state*)

A state i is said to be recurrent if $\rho_i = 1$. If $\rho_i < 1$, state i is said to be transient. □

Definition A.2.7 (*Men recurrence time*)

Let i be a recurrent state. We denote by M_i the mean recurrence time of state i, given by: $M_i \equiv \mathbb{E}[T_{ii}] = \sum_{t=1}^{\infty} t\rho_i^t$. □

Definition A.2.8 (*Positive or null recurrent state*)

A recurrent state i is said to be positive (or non-null) recurrent if $M_i < \infty$. If $M_i = \infty$, state i is said to be null recurrent. □

Definition A.2.9 (*Periodic and aperiodic state*)

A state i is said to be periodic if the greatest common divisor d of the set $\{n > 0 : p_{ii}^n > 0\}$ is $d \geq 2$.If $d = 1$,state i is said to be aperiodic. □

Theorem A.2.1

If a Markov chain is irreducible, then all its states have the same period d. □

Definition A.2.10 (*Aperiodic Markov chain*)

An irreducible Markov chain is said to be aperiodic if $d = 1$ for any state. □

Appendix B

Supplementary Information for Data-driven Approaches to Complex Systems

VIII

B.1 Supplementary Information for Machine Learning

This section provides additional information supporting Section 3.1, along with further details on the data collection and modeling procedures underlying the study described in Section 3.2 and presented in [37].

Data preprocessing

On the basis of preliminary analysis, we select the most extreme stations among the 96 available ones. A station is considered *extreme* if it is possible to observe a high amount of rain in a relatively short time interval. We implement this concept of "extremeness" using the following strategy. First, we consider the following data for all the 96 available stations in Sicily and for all the years:

- The total annual precipitation in mm (tot).
- The percentage of rainy days over the year (rd), measured as number of days with more than 1 mm of rain.
- The mm of rain during the rainiest day in the year ($dmax$).

Afterwards, a selection strategy is applied. Extreme rainfall events are generally characterized by the increasing of either drought and/or excessive wetness [117]. The logical rule below highlights precisely such characteristics:

1) Fix a station.
2) Compute μ_1: the mean over years of the rd annual indicator.
3) Compute μ_2: the mean over years of the $dmax$ annual indicator.
4) Fix a year y.
5) If the rd value in the year y is less than μ_1 and the $dmax$ value in the year y is grater than μ_2, then the year y is considered as *extreme*. Otherwise no.

Since the procedure works year by year, we select the stations satisfying the *extreme events* detection rule for at least 3 years. In this way, we obtain 32 stations out of the 96 rain gauges. Furthermore, we decide to include all of the provincial capitals in the region, thus obtaining the 34 stations reported in Figure 3.1 of Chapter 3. After the selection, we observe rainfall data time series, by fixing a station and using full, annual, and monthly data plots, as well as mean data graphics. This preliminary analysis lead to different reasoning. The full plots prove the necessity of quantifying and understanding variation in the stations time series behavior. In contrast, the annual plots show a typical seasonality pattern. Moreover, the graphics observation lead to the idea of comparing annual time series. Finally, a similar reasoning is done with regard to the monthly view.

All of the above considerations suggest us to highlight the differences and the similarities both among stations and years, in order to identify multi-modal (geographical

and historical) rainfall changes. Instead of performing classical time series analysis, we proceed by applying the suitable clustering algorithms described in Section 3.1.

The dataset together with the code is available at the following GitHub Repository. The Affinity Propagation algorithm is implemented in Python programming language (version 3), making use of with the Scikit-learn library (V. 1.0.2), which is a free software machine learning library for Python, designed to inter-operate with the Python numerical and scientific libraries NumPy (V. 1.21.4), SciPy (V. 1.8.0) and Pandas (V. 1.3.5).

Comparison between Affinity Propagation and K-Means

To further validate our methodology, we carry out a detailed report comparing the AP and the K-Means algorithms. The comparison is conducted on the collections C.C and C.D of Table 3.1. Initial experiments are made by fixing both the number of clusters and the initial centroids in the K-Means algorithm, basing our choice on the AP results. A sensitivity analysis is then performed by varying the initial centroids, based again on the results achieved with the AP algorithm. The Jaccard score between each new experiment and the reference AP results is computed [241]. The Jaccard score is a statistical index used to compare the similarity and diversity of sample sets [241]. We use it to quantify the differences between two experiments A and B, by analyzing the composition of the corresponding clusters in the two cases. The Jaccard score is defined as the size of the intersection divided by the size of the union of the sample sets and it ranges in the interval $[0, 1]$:

$$J(A, B) = \frac{|A \cap B|}{|A \cup B|} \tag{B.1}$$

Furthermore, for each of those experiments, the cluster validation procedure is carried out, computing the p-values and finding the characterizing indicators for the clusters, among those in table 3.2. A second set of 200 K-Means experiments per collection is conducted fixing the number of clusters and randomly varying the initial centroids. Using the C.C collection we find that, by setting the five AP case anomalies as initial centroids and varying the sixth centroid, we obtain three cases: in almost the 80% of experiments (22 over 29) the K-Means and AP Cluster perfectly coincide (Jaccard score = 1 for all of the clusters). Among the remaining seven experiments, four of them differ from the reference case by one or at most two stations in eastern Sicily, (Jaccard score ≤ 0.5 at most one cluster; then, for only three experiments the difference is more significant (Jaccard score ≤ 0.5 for at least two clusters). For all the experiments, statistical validation is carried out with the Kruskal-Wallis test, as reported in figure B.1a. In the first case, no difference in the p-values respect to the AP case is detected; in the second case, the characterising indicators coincide with the reference ones, i.e. md maximum (per day), h heavy rain (%) and mv max daily variation; in the third case, almost all the indicators are characterising and thus are not related to extreme events detection, differently from the AP results.

The same analysis is done for the C.D collection of the weekly mean data. By fixing the centroids on the basis of the AP case, we get the same clustering. This is not as expected as in the C.C case, since this time we have more uniform clusters. Also in this case we do a sensitivity analysis with respect to the centroids of all clusters, finding that the 93% of experiments (27 out of 29) are coincident or similar (JS = 1 and JS > 0.5) to our baseline result. The remaining two experiments (JS $JS \leq 0.5$), however, turn out to be different. Unlike the C.C case, the statistical validity analysis shows homogeneous distributions among the characterizing indicators, as reported in figure B.1b. In fact, even in our result, most of the indicators are found to be characterizing for the clusters. This confirms the goodness of our results on finding extreme events using the C.C collection with respect to collection C.D, where, as expected, the weekly averaging masks the presence of extreme events, obtaining a more uniform clusters distribution.

Finally, we do an inter-cluster frequency analysis on 200 K-Means runs with random initial centroids for both C.C and C.D collections, reported in figures B.2a and B.2b, respectively. In the former case, we obtain that the most frequent clusters are precisely

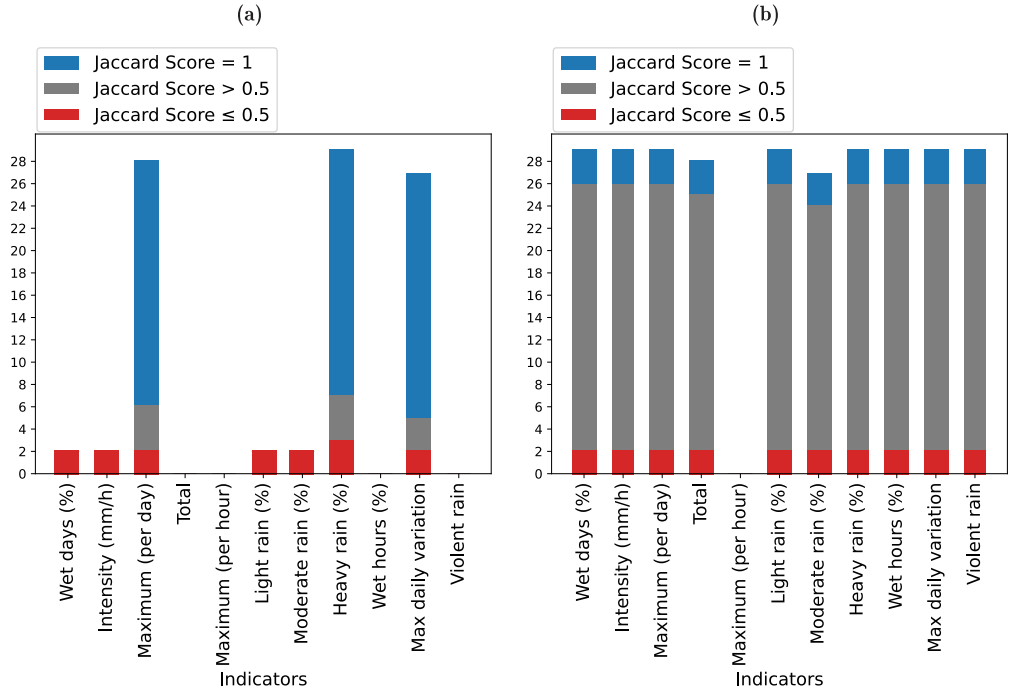

Figure B.1: Characterizing indicators in the K-Means initial centroids-based experiments. The histograms count over the experiments how many times the indicators result as characterizing for the clusters (p value < 0.05), grouped by the categories defined by the Jaccard score. **(a)**: C.*C* collection. Those experiments different from the AP case (in red) have many characterizing indicators, whereas those experiments similar or coinciding to the AP case (in blue and grey) have the same three characterizing indicator representing *extremeness*. **(b)**: C.*D* collection. Almost every indicator is characterizing for each type of experiment.

the five anomalies of the AP result. This confirms the robustness of our findings. In the second case, on the other hand, the only anomaly that is always present and corresponds to the most prevalent cluster, is Pedara, while for the remaining clusters there is not such a clear spread, as reported in table B.1.

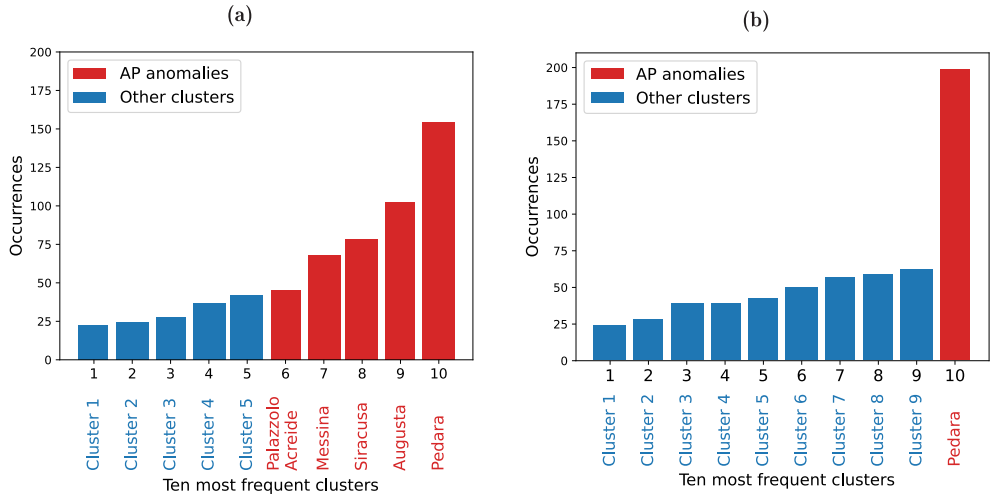

Figure B.2: K-Means - Clusters Frequency Analysis over 200 runs. **(a)**: C.*C* Collection (High frequency data). The five most frequent clusters are the five anomalies of the AP case. The other five are clusters composed by different stations, as reported in table B.1. **(b)**: C.*D* Collection (Weekly mean data). Except for *Pedara*, the most frequent clusters are different from the AP case. Those clusters are listed in table B.1.

Table B.1: 10 most frequent clusters (increasing order) obtained with K-Means clustering over the 200 runs.

Cluster	C.C Collection	C.D Collection
1	Bivona, Contessa Entellina, Monreale Bifarera, Monreale Vigna Api, Palermo	Agrigento Mandrascava, Alia, Bivona, Calascibetta, Caltanissetta, Canicattì, Contessa Entellina, Enna, Marsala, Mussomeli, Riesi, Trapani Fontanasalsa
2	Monreale Bifarera, Monreale Vigna Api, Palermo	Agrigento Mandrascava, Alia, Bivona, Calascibetta, Caltagirone, Caltanissetta, Canicattì, Contessa Entellina, Enna, Marsala, Mussomeli, Riesi, Trapani Fontanasalsa
3	Monreale Vigna Api, Palermo	Leni, Messina
4	Catania	Monreale Vigna Api
5	Marsala, Trapani Fontanasalsa	Catania, Francofonte, Mineo, Paternò, Ramacca Giumarra
6	Palazzolo Acreide	Modica, Palazzolo Acreide, Ragusa, Scicli
7	Messina	Augusta, Catania, Siracusa
8	Siracusa	Cesarò Vignazza, Lascari, Leni, Messina, Monreale Bifarera, Monreale Vigna Api, Palermo, Pettineo, Polizzi Generosa
9	Augusta	Augusta, Siracusa
10	Pedara	Pedara

Kruskal-Wallis test

It is a non parametric statistical test that assesses the differences among three or more independently sampled groups [242]. Kruskal-Wallis test is used to determine whether or not there is a statistically significant difference between the medians of three or more independent groups. It does not assume normality in the data and is much less sensitive to outliers than the standard analysis of variance (ANOVA) [243]. The test is based on the null hypothesis H_0 [244], which allows one to state whether the considered samples are realizations of identical populations. The application of the test returns a p-value which confirms or rejects the null hypothesis. If $p < 0.05$, then the null hypothesis is rejected, on the contrary, if $p \geq 0.05$, then the null hypothesis is confirmed [243]. The related p-value for the test is computed using the assumption that H has a χ^2 distribution.

Annual results

Here I report the annual clustering results for the year 2021 in all the considered settings. Figure B.3 shows the exceptional rainfall events occurred in East Sicily in 2021. In fact, among the characterizing indicators obtained with the procedure explained in the main document, *md* (maximum per day) is found to be particularly relevant. Figure B.3a shows the presence of a principal cluster and some anomalies, for instance *Catania*, *Augusta* and *Siracusa*. Differently, Figure B.3b presents several principal clusters distributed in the North, in the center, in the North-East, in the South-East and in the eastern center; in this case only *Augusta* and *Siracusa* are clustered as anomalous by the algorithm. Figures B.3c and B.3d represent the *md* indicator geographically referenced and value-based, respectively. Comparing independently Figures B.3a and B.3b, with Figure B.3c, we observe a coincidence between the maximum values and the anomalies in the clusters. In

particular, most of the anomalies in Figure B.3a represent the highest values of the *md* indicator in Figure B.3c or in Figure B.3d. The same happens with Figure B.3b for the two anomalies of *Augusta* and *Siracusa* and for the locations in the *light blue* cluster in Figure B.3b, which show the second highest values of the *md* indicator, with the only exception of *Contessa Entellina*. The same statement, not reported here, has been found also for the *mv* (maximum daily variation) indicator. Therefore, in 2021 the anomalous clusters consist of the stations with the highest *md* values. Moreover, East Sicily emerges as the most *extreme* zone of the island. On the other hand Figure B.4 shows that using the Correlation metrics, no coincidences between characterizing indicators and clusters are found for the year 2021. Actually, this happens in all of the other annual cases and in the full cases as well, in agreement with the fact that Correlation metric is less sensitive to outliers than the Euclidean one.

In general, these are phenomena happening in all of the annual cases (see Figures in GitHub Repository). Specifically, in the case of Euclidean metrics and C.A, results consist of a principal cluster and some exceptions, mainly in the East side of the island. This suggests the vulnerability to extreme events of the East side of Sicily respect to the West. In the case of C.B, there are many principal clusters and some exceptions, again mostly in the East side. Differently, in the cases of Correlation metrics with both C.A and C.B, most of the time results consist of two clusters splitting Sicily in half. It follows that Euclidean metrics let to better detect outliers respect to the Correlation metrics. Consequently, the Euclidean metrics seems to be more suitable and precise than the Correlation metrics for our purpose.

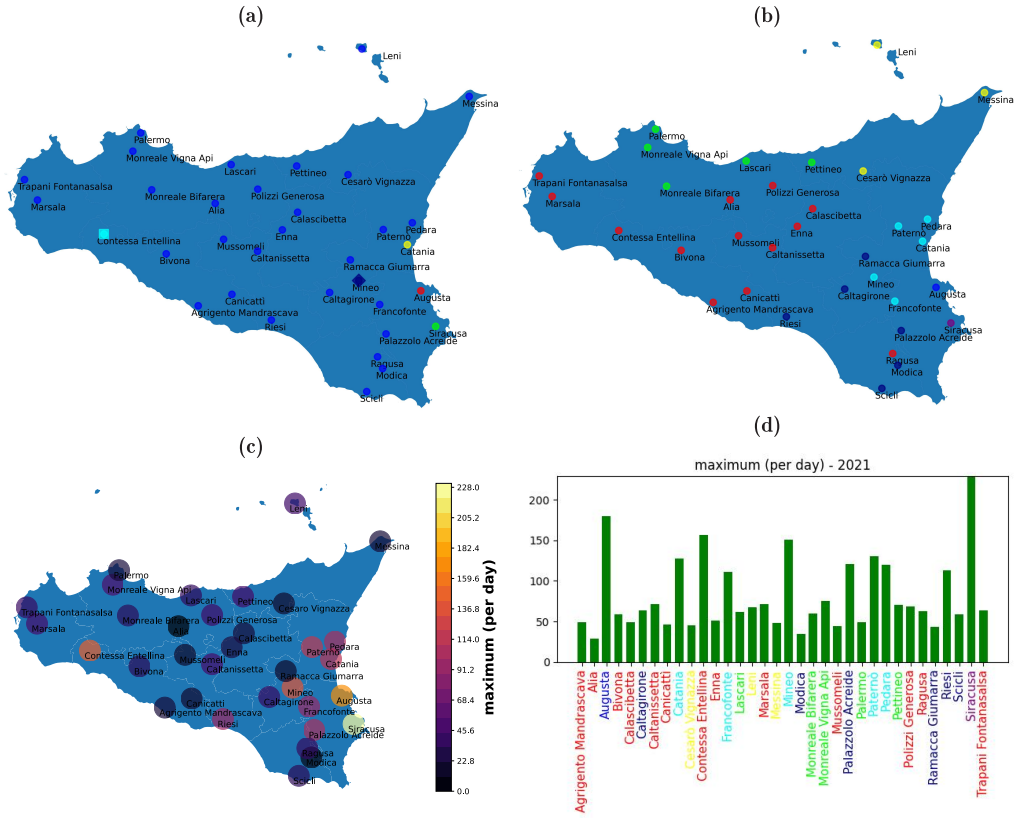

Figure B.3: Annual case for 2021 - Euclidean metrics. Different colors represent different clusters, both in the maps and in the histogram. **(a)**: C.A. The principal cluster is coloured blue. Square and diamond points indicate clusters obtained by the second and the third iteration of the algorithm, respectively. **(b)**: C.B. The five principal clusters are coloured red, green, blue, light blue and yellow. **(c)**: Heat-map of the *md* indicator for both C.A and C.B. **(d)**: Histogram of the *md* indicator with labels coloured as the C.B clustering.

Figure B.4: Annual case for 2021 - Correlation metrics. **(a)**: C.A. The colours of the four clusters are blue, red, yellow and green. **(b)**: C.B. The three clusters are coloured red, blue and yellow.

B.2 Supplementary Information for Causal Inference

Definition B.2.1 (*Partially Directed Acyclic Graph (PDAG)*)

A partially directed acyclic graph (PDAG) is a mixed graph $G = (V, E_{\mathrm{u}}, E_{\mathrm{d}})$ on a finite vertex set V with two types of edges: undirected edges $\{i, j\} \in E_{\mathrm{u}}$ (written $i - j$) and directed edges $(i, j) \in E_{\mathrm{d}}$ (written $i \to j$). It is acyclic in the sense that its directed part contains no directed cycle; that is, there do not exist $k \geq 2$ and vertices $v_1, \ldots, v_k \in V$ such that $v_1 \to v_2 \to \cdots \to v_k \to v_1$. Undirected edges indicate adjacencies whose orientation is not fixed. □

Appendix C

Supplementary Information for Complex Dynamics in Psychological Data

This Appendix provides additional details and definitions supporting Chapter 5 [40]. For any other information see the GitHub Repository.

C.1 Network measures

To quantify the role of symptoms within each causal network, we employed classical network measures from graph theory that capture both local and global aspects of node importance [208]. In particular, we computed:

- *In-degree* — the number of directed edges coming into a node v:

$$\deg^{\text{in}}(v) = |\{u \in V : (u \to v) \in E\}|$$

  Nodes with high in-degree may reflect symptoms that are highly reactive to others.

- *Out-degree* — the number of directed edges going out of a node v:

$$\deg^{\text{out}}(v) = |\{u \in V : (v \to u) \in E\}|$$

  A high out-degree suggests that the symptom may act as a driver, exerting influence over many others.

- *Degree*— the total number of direct or undirected connections of node v:

$$\deg(v) = \deg^{\text{in}}(v) + \deg^{\text{out}}(v) + \deg^{\text{undirected}}(v)$$

- *Closeness centrality*— quantifies how quickly a node can reach the rest of the network via shortest paths:

$$C_{\text{closeness}}(v) = \frac{1}{\sum_{u \in V \setminus \{v\}} d(v,u)},$$

  where $d(v,u)$ is the shortest path distance from v to u. Nodes with high closeness centrality can rapidly propagate changes or exert influence across the system.

- *Betweenness centrality,* capturing how often a node lies on the shortest paths between other pairs of nodes:

$$C_{\text{betweenness}}(v) = \sum_{s \neq v \neq t} \frac{\sigma_{st}(v)}{\sigma_{st}},$$

  where σ_{st} is the total number of shortest paths from node s to node t, and $\sigma_{st}(v)$ is the number of those paths that pass through v. Nodes with high-betweenness centrality may act as bridges or mediators between symptom clusters.

Closeness and betweenness centrality were computed on the mixed graph, meaning that both directed and undirected edges were taken into account in the path-based computations. These metrics provide a multi-faceted view of symptoms importance to capture both local connectivity and global flow properties.

C.2 Complexity measures

We computed a broad range of complexity measures for each symptom time series, designed to quantify different aspects of signal regularity, unpredictability, fractal geometry, and recurrence, offering a complete characterization of the underlying dynamics. Although they have not been widely applied in clinical psychology, prior studies in physiology and complex systems have shown that entropy, fractal dimension, and recurrence-based metrics can capture meaningful dynamic patterns in biological and behavioral data [8], [214]–[216]. More in details, for a generic time series x we first computed permutation entropy, approximate entropy and sample entropy measures [245]–[247]:

- *Permutation Entropy*, quantifying the degree of unpredictability in the ordering of values within local segments of the signal. Formally:

$$H = -\sum p(\pi) \log_2 p(\pi),$$

  where the sum is over all possible permutations π of order n. The probability $p(\pi)$ denotes the frequency of each permutation across the embedded vectors:

$$y(i) = [x_i, x_{i+\text{delay}}, \ldots, x_{i+(n-1)\cdot\text{delay}}].$$

  It ranges from 0 (fully predictable) to $\log_2(n!)$ (maximal randomness) and captures the unpredictability and information content of the time series.

- *Approximate Entropy*, the logarithmic likelihood that patterns of length m that are similar within a tolerance r remain similar at the next point. Formally:

$$H = \phi_m(r) - \phi_{m+1}(r),$$

  where

$$\phi_m(r) = \frac{1}{N-m+1} \sum_{i=1}^{N-m+1} \log C_i^m(r)$$

  and $C_i^m(r)$ is the fraction of vectors of length m that are within a Chebyshev distance r of the vector starting at time i. Approximate Entropy is biased toward lower values in short time series and includes self-matches, which makes it less robust than its successor, sample entropy.

- *Sample Entropy*, a modification of approximate entropy that reduces bias and removes data length dependence:

$$H(x, m, r) = -\log \frac{C(m+1, r)}{C(m, r)},$$

  where m is the embedding dimension, r is the similarity tolerance radius (commonly $r = 0.2 \cdot \text{std}(x)$), and $C(m, r)$ is the number of pairs of vectors of length m within distance r (typically using the Chebyshev metric). Higher values indicate greater signal complexity and vice versa.

Next, we computed Recurrence Quantification Analysis (RQA) indices, which capture the non linear patterns of the time series [216], [248], [249]:

- *Recurrence Rate (RR)*, a measure of the density of recurrent states in a system's phase space, defined as the percentage of recurrent points in a recurrence plot

$$\text{RR} = \frac{1}{N^2} \sum_{i=1}^{N} \sum_{j=1}^{N} R_{i,j},$$

where $R_{i,j}$ is the recurrence matrix given by:

$$R_{i,j} = \Theta(\varepsilon - \|\mathbf{x}_i - \mathbf{x}_j\|),$$

with $\mathbf{x}_i$ and $\mathbf{x}_j$ being state vectors reconstructed via time-delay embedding, $\|\cdot\|$ a norm (typically Euclidean), ε a fixed threshold, and Θ the Heaviside step function. Higher RR values indicate frequent returns to previous states, while lower values suggest more irregular or complex dynamics.

- *Determinism (DET)*, quantifying the predictability of a system by measuring the proportion of recurrence points that form diagonal lines in the recurrence plot:

$$\mathrm{DET} = \frac{\sum_{l=l_{\min}}^{l_{\max}} l \cdot P(l)}{\sum_{l=1}^{l_{\max}} l \cdot P(l)},$$

where $P(l)$ is the frequency distribution of diagonal line lengths l, and $l_{\min}$ is the minimum length of diagonal lines considered (usually $l_{\min} = 2$). Diagonal lines correspond to segments of the trajectory that evolve similarly for some time, so higher DET values indicate more deterministic, structured dynamics, while lower values suggest randomness or chaos.

- *Laminarity (LAM)*, measuring the fraction of recurrence points forming vertical lines in the recurrence plot. It reflects the presence of laminar (intermittent or trapping) states in the system. Formally:

$$\mathrm{LAM} = \frac{\sum_{v=v_{\min}}^{v_{\max}} v \cdot P(v)}{\sum_{v=1}^{v_{\max}} v \cdot P(v)},$$

where $P(v)$ is the frequency distribution of vertical line lengths v, and $v_{\min}$ is the minimal vertical line length considered (typically $v_{\min} = 2$). High LAM values indicate that the system spends extended periods in the same region of phase space, suggesting intermittency or laminar phases.

- *Trapping Time (TT)*, the average length of vertical lines in a recurrence plot, and quantifies the mean duration for which the system remains in a laminar (quasi-stationary) state. Formally:

$$\mathrm{TT} = \frac{\sum_{v=v_{\min}}^{v_{\max}} v \cdot P(v)}{\sum_{v=v_{\min}}^{v_{\max}} P(v)},$$

where $P(v)$ is the histogram of vertical line lengths v, and $v_{\min}$ is the minimal length considered (typically $v_{\min} = 2$). Higher TT values indicate longer periods during which the system exhibits little change, reflecting low dynamical activity or intermittent behavior.

- *Maximum diagonal line length L_{max}*, the longest period during which the system exhibits similar evolution in phase space:

$$L_{\max} = \max\{l_i\},$$

where l_i are the lengths of all diagonal lines (with $l_i \geq l_{\min}$). Longer diagonal lines indicate stronger temporal determinism and lower divergence in the system's dynamics.

- *Divergence (DIV)*, defined as the inverse of the longest diagonal line in a recurrence plot (excluding the main diagonal):

$$\mathrm{DIV} = \frac{1}{L_{\max}}.$$

  Higher DIV values indicate faster divergence of nearby trajectories in phase space, often associated with increased chaos or instability in the system.

- *Maximum vertical line length* V_{max}, the longest period during which the system remains in the same (or similar) state:

$$V_{\max} = \max\{v_i\},$$

  where v_i denotes the lengths of all vertical lines with $v_i \geq v_{\min}$. Higher $V_{\max}$ values indicate extended laminar or quasi-stationary phases in the system's dynamics.

- *Entropy of diagonal line lengths* L_{entr}, quantifying the complexity of the recurrence structure by measuring the Shannon entropy of the distribution of diagonal line lengths:

$$L_{\mathrm{entr}} = -\sum_{l=l_{\min}}^{l_{\max}} p(l) \log p(l),$$

  where $p(l)$ is the probability distribution of diagonal line lengths l in the recurrence plot. Higher values indicate greater variability in diagonal line lengths, reflecting increased dynamical complexity.

- *Average Diagonal Length* L, quantifying the mean time during which two segments of the system's trajectory evolve in a similar way. It is defined as:

$$L = \frac{\sum_{l=l_{\min}}^{l_{\max}} l \cdot P(l)}{\sum_{l=l_{\min}}^{l_{\max}} P(l)},$$

  where $P(l)$ is the number of diagonal lines of length l, and $l_{\min}$ is the minimum line length considered (usually $l_{\min} = 2$). Higher values of L indicate more extended periods of predictable, deterministic dynamics.

- *Average White Vertical Length* W, measuring the average duration of non-recurrence (i.e., white vertical gaps) in a recurrence plot. It is defined as:

$$W = \frac{\sum_{w=w_{\min}}^{w_{\max}} w \cdot P(w)}{\sum_{w=w_{\min}}^{w_{\max}} P(w)},$$

  where $P(w)$ is the frequency distribution of white vertical line lengths w, and $w_{\min}$ is the minimal gap length considered (typically $w_{\min} = 1$). Higher values of W indicate longer periods where the system is not returning to a previous state, reflecting local instability or desynchronization.

RQA indices were computed using different time delays values, embedding dimensions, and radius thresholds to ensure robustness across parameter settings [250].

We then computed Cross Recurrence Quantification Analysis (CRQA) for all possible pairs of symptoms time series. CRQA extends traditional RQA to compare the dynamical structure of two distinct time series. The method is based on the cross recurrence plot (CRP), which visualizes the recurrence of similar states between two systems. Given

two embedded trajectories $\mathbf{x}_i$ and $\mathbf{y}_j$ from time series x and y, respectively, the cross recurrence matrix is defined as:

$$CR_{i,j} = \Theta(\varepsilon - \|\mathbf{x}_i - \mathbf{y}_j\|),$$

where $\|\cdot\|$ denotes a norm (typically Euclidean), ε is the recurrence threshold, and Θ is the Heaviside step function. A point is plotted at (i, j) in the CRP if the corresponding states $\mathbf{x}_i$ and $\mathbf{y}_j$ are sufficiently close in phase space. All standard RQA measures (e.g., recurrence rate, determinism, laminarity) can be analogously applied to the CRP to quantify inter-series dynamics. The following cross recurrence features were extracted in our analysis:

- *Cross Recurrence Rate*;
- *Cross Determinism*;
- *Cross Laminarity*;
- *Cross Trapping Time*;
- *Cross* L_{max};
- *Cross Divergence*;
- *Cross* V_{max};
- *Cross Entropy of Diagonal Line Lengths*;
- *Cross Average Diagonal Length*;
- *Cross Average White Vertical Length.*

Furthermore, we estimated Hurst Exponent, Detrended Fluctuation Analysis (DFA), Higuchi and Petrosian Fractal Dimension, characterizing long-range dependencies and self-similarity [251]–[254]:

- *Hurst Exponent*, quantifying the long-term memory of a time series. It is estimated by analyzing the scaling relationship of the rescaled range statistic:

  $$\mathbb{E}\left[\frac{R(n)}{S(n)}\right] \propto n^H,$$

  where $R(n)$ is the range of the cumulative deviation from the mean over a window of size n, $S(n)$ is the standard deviation over the same window, H is the scaling exponent estimated by log–log regression. The value of $H \in (0, 1)$ characterizes the time series: if $H = 0.5$, it is uncorrelated (random walk), else if $H > 0.5$, it is positively correlated (persistent), else if $H < 0.5$, it is negatively correlated (anti-persistent).
- *Detrended Fluctuation Analysis (DFA)*, a technique designed to detect long-range correlations in time series, even when they are non-stationary. Unlike the classical Hurst exponent, DFA separates genuine long-term memory from spurious correlations due to slow external trends. The method consists in computing the cumulative sum of deviations from the mean to obtain a profile, segmenting this profile into windows of length n, fitting a polynomial trend in each window, subtracting the trend, and then calculating the root mean square of the resulting fluctuations. The average fluctuation $F(n)$ as a function of window size n typically follows a power-law $F(n) \sim n^\alpha$. The exponent α reflects the correlation structure of the signal: values of α around 0.5 indicate uncorrelated (white noise) dynamics, values greater than 0.5 suggest persistent behavior (i.e., the tendency for increases or decreases to continue), while values below 0.5 correspond to anti-persistent dynamics, where increases are likely to be followed by decreases and vice versa. When α exceeds 1, the process is non-stationary and consistent with fractional Brownian motion.

- *Higuchi Fractal Dimension*, providing an estimate of the fractal complexity of a time series by evaluating how its curve length changes with the sampling resolution. The method constructs k different subseries from the original time series and computes the average length $L(k)$ of each resulting curve. The scaling relationship $L(k) \sim k^{-D}$ is then used to estimate the fractal dimension D as the slope of the linear fit in the log–log plot of $L(k)$ versus k. Higher values of D (approaching 2) indicate more complex and irregular dynamics, whereas lower values (closer to 1) reflect smoother or more regular signals.
- *Petrosian Fractal Dimension*, quantifying the complexity of a time series by considering the number of sign changes in its derivative. It is defined as:

$$P = \frac{\log_{10}(N)}{\log_{10}(N) + \log_{10}\left(\frac{N}{N+0.4N_\delta}\right)},$$

  where N is the length of the time series and N_δ is the number of sign changes in the signal's derivative.

Finally, we computed Correlation Dimension and Number of Zero Crossings, capturing geometric and frequency-based signal properties [255]:

- *Correlation Dimension*, a measure of the geometric complexity of a dynamical system, which, for a time series, is estimated by reconstructing its phase space using time-delay embedding and computing how the correlation sum scales with distance:

$$D_2 = \lim_{r \to 0} \frac{\log C(r)}{\log r},$$

  where $C(r)$ is the correlation sum, representing the probability that the distance between two points is less than r. If the relation between $C(r)$ and r can be described by the power law $C(r) \sim r^D$, then D is called the correlation dimension of the system.
- *Number of Zero Crossings*, the count of times the signal changes sign, indicating how often the signal passes through zero.

References

[1] Mitchell, M., *Complexity: A guided tour*. Oxford university press, 2009. DOI: 10.1093/oso/9780195124415.001.0001.

[2] Ladyman, J., Lambert, J., and Wiesner, K., "What is a complex system?" *European Journal for Philosophy of Science*, vol. 3, no. 1, pp. 33–67, 2013. DOI: 10.1007/s13194-012-0056-8.

[3] Sparrow, C., *The Lorenz equations: bifurcations, chaos, and strange attractors*. Springer Science & Business Media, 2012, vol. 41. DOI: 10.1007/978-1-4612-5767-7.

[4] Holland, J. H., *Emergence: From chaos to order*. OUP Oxford, 2000. DOI: 10.1093/oso/9780198504092.001.0001.

[5] Strogatz, S. H., "Exploring complex networks," *nature*, vol. 410, no. 6825, pp. 268–276, 2001. DOI: 10.1038/35065725.

[6] Krakauer, D. and WISCONSIN-MADISON, O., "The complexity of life," *Santa Fe Institute Bulletin*, vol. 28, pp. 1–3, 2014.

[7] Van Geert, P. L., "Dynamic systems, process and development," *Human development*, vol. 63, no. 3-4, pp. 153–179, 2020. DOI: 10.1159/000503825.

[8] Boccaletti, S., Latora, V., Moreno, Y., Chavez, M., and Hwang, D.-U., "Complex networks: Structure and dynamics," *Physics reports*, vol. 424, no. 4-5, pp. 175–308, 2006. DOI: 10.1016/j.physrep.2005.10.009.

[9] Barabási, A.-L., "Network science," *Philosophical Transactions of the Royal Society A: Mathematical, Physical and Engineering Sciences*, vol. 371, no. 1987, p. 20 120 375, 2013. DOI: 10.1098/rsta.2012.0375.

[10] Boccara, N., *Modeling complex systems*. Springer, 2004. DOI: 10.1007/b97378.

[11] Carbone, A., Jensen, M., and Sato, A.-H., "Challenges in data science: A complex systems perspective," *Chaos, Solitons & Fractals*, vol. 90, pp. 1–7, 2016. DOI: 10.1016/j.chaos.2016.04.020.

[12] Ma'ayan, A., "Complex systems biology," *Journal of the Royal Society Interface*, vol. 14, no. 134, p. 20 170 391, 2017. DOI: 10.1098/rsif.2017.0391.

[13] Arenas, A., Díaz-Guilera, A., Kurths, J., Moreno, Y., and Zhou, C., "Synchronization in complex networks," *Physics reports*, vol. 469, no. 3, pp. 93–153, 2008. DOI: 10.1016/j.physrep.2008.09.002.

[14] Arthur, W. B., "Complexity and the economy," in *Handbook of Research on Complexity*, Edward Elgar Publishing, 2009.

[15] Bonabeau, E., Dorigo, M., and Theraulaz, G., *Swarm intelligence: from natural to artificial systems*. Oxford university press, 1999. DOI: 10.1093/oso/9780195131581.001.0001.

[16] Conte, R., Gilbert, N., Bonelli, G., *et al.*, "Manifesto of computational social science," *The European Physical Journal Special Topics*, vol. 214, no. 1, pp. 325–346, 2012. DOI: 10.1140/epjst/e2012-01697-8.

[17] Goldstone, R. L. and Janssen, M. A., "Computational models of collective behavior," *Trends in cognitive sciences*, vol. 9, no. 9, pp. 424–430, 2005. DOI: 10.1016/j.tics.2005.07.009.

[18] Hmelo-Silver, C. E. and Azevedo, R., "Understanding complex systems: Some core challenges," *The Journal of the learning sciences*, vol. 15, no. 1, pp. 53–61, 2006. DOI: 10.1207/s15327809jls1501_7.

[19] Thelen, E. and Smith, L. B., *A dynamic systems approach to the development of cognition and action*. MIT press, 1994. DOI: 10.7551/mitpress/2524.001.0001.

[20] Van Gelder, T., "The dynamical hypothesis in cognitive science," *Behavioral and brain sciences*, vol. 21, no. 5, pp. 615–628, 1998. DOI: 10.1017/S0140525X98001733[Opens in a new window].

[21] Sporns, O., "Networks of the brain: Quantitative analysis and modeling," *Analysis and function of large-scale brain networks*, vol. 7, pp. 7–13, 2010.

[22] Bassett, D. S. and Sporns, O., "Network neuroscience," *Nature neuroscience*, vol. 20, no. 3, pp. 353–364, 2017. DOI: 10.1038/nn.4502.

[23] Leemput, I. A. van de, Wichers, M., Cramer, A. O., *et al.*, "Critical slowing down as early warning for the onset and termination of depression," *Proceedings of the National Academy of Sciences*, vol. 111, no. 1, pp. 87–92, 2014. DOI: 10.1073/pnas.1312114110.

[24] Kounios, J. and Beeman, M., "The cognitive neuroscience of insight," *Annual review of psychology*, vol. 65, pp. 71–93, 2014. DOI: 10.1146/annurev-psych-010213-115154.

[25] Kuppens, P., Oravecz, Z., and Tuerlinckx, F., "Feelings change: Accounting for individual differences in the temporal dynamics of affect.," *Journal of personality and social psychology*, vol. 99, no. 6, p. 1042, 2010. DOI: 10.1037/a0020962.

[26] Molenaar, P. C., "A manifesto on psychology as idiographic science: Bringing the person back into scientific psychology, this time forever," *Measurement*, vol. 2, no. 4, pp. 201–218, 2004. DOI: 10.1207/s15366359mea0204_1.

[27] Piccirillo, M. L. and Rodebaugh, T. L., "Foundations of idiographic methods in psychology and applications for psychotherapy," *Clinical psychology review*, vol. 71, pp. 90–100, 2019. DOI: 10.1016/j.cpr.2019.01.002.

[28] Borsboom, D., "A network theory of mental disorders," *World psychiatry*, vol. 16, no. 1, pp. 5–13, 2017. DOI: 10.1002/wps.20375.

[29] Fisher, A. J., Reeves, J. W., Lawyer, G., Medaglia, J. D., and Rubel, J. A., "Exploring the idiographic dynamics of mood and anxiety via network analysis.," *Journal of abnormal psychology*, vol. 126, no. 8, p. 1044, 2017. DOI: 10.1037/abn0000311.

[30] Haslbeck, J. M. and Ryan, O., "Recovering within-person dynamics from psychological time series," *Multivariate Behavioral Research*, vol. 57, no. 5, pp. 735–766, 2022. DOI: 10.1080/00273171.2021.1896353.

[31] Ryan, O., Dablander, F., and Haslbeck, J. M. B., "Toward a generative model for emotion dynamics," *Psychological Review*, vol. 132, no. 2, pp. 416–441, 2025. DOI: 10.1037/rev0000513.

[32] Schwartz, S. J., Lilienfeld, S. O., Meca, A., and Sauvigné, K. C., "The role of neuroscience within psychology: A call for inclusiveness over exclusiveness.," *American Psychologist*, vol. 71, no. 1, p. 52, 2016. DOI: 10.1037/a0039678.

[33] Borsboom, D., "Possible futures for network psychometrics," *Psychometrika*, vol. 87, no. 1, pp. 253–265, 2022. DOI: 10.1007/s11336-022-09851-z[Opens in a new window].

[34] Robinaugh, D. J., Hoekstra, R. H., Toner, E. R., and Borsboom, D., "The network approach to psychopathology: A review of the literature 2008–2018 and an agenda for future research," *Psychological medicine*, vol. 50, no. 3, pp. 353–366, 2020. DOI: 10.1017/S0033291719003404.

[35] Socci, V., Vitanza, E., and Mocenni, C., "An agent-based model to foster citizens' sustainable behavior in the italian city of siena," *The European Physical Journal B*, vol. 98, no. 4, p. 72, 2025. DOI: 10.1140/epjb/s10051-025-00910-9.

[36] Vitanza, E., Dimitri, G., Bizzarri, F., Mocenni, C., *et al.*, "Investigating the impact of extreme rainfall events on individual perception of climate change," in *2023 International Symposium on Nonlinear Theory and Its Applications NOLTA2023*, 2023, pp. 202–205. DOI: 10.34385/proc.76.A5L-42.

[37] Vitanza, E., Dimitri, G. M., and Mocenni, C., "A multi-modal machine learning approach to detect extreme rainfall events in sicily," *Scientific Reports*, vol. 13, no. 1, p. 6196, 2023. DOI: 10.1038/s41598-023-33160-9.

[38] Dimitri, G. M., Parri, L., Vitanza, E., Pozzebon, A., Fort, A., and Mocenni, C., "Weair: Wearable swarm sensors for air quality monitoring to foster citizens' awareness of climate change," *Computer Standards & Interfaces*, vol. 94, p. 104 004, 2025. DOI: 10.1016/j.csi.2025.104004.

[39] Vitanza, E., Mocenni, C., and De Lellis, P., "Egosyntonicity and emotion regulation: A probabilistic model of valence dynamics," *Royal Society Open Science*, vol. 12, no. 9, p. 250 062, 2025. DOI: 10.1098/rsos.250062.

[40] Vitanza, E., De Lellis, P., Mocenni, C., and Marin, M. R., "Complex dynamics in psychological data: Mapping individual symptom trajectories to group-level patterns," *Behavior Research Methods*, 2025, Under review (minor revision). DOI: 10.48550/arXiv.2507.14161.

[41] Railsback, S. F. and Grimm, V., *Agent-Based and Individual-Based Modeling: A Practical Introduction*. Princeton: Princeton University Press, 2011. DOI: 10.2307/jj.28274141.

[42] Bianchi, F. and Squazzoni, F., "Agent-based models in sociology," *Wiley Interdisciplinary Reviews: Computational Statistics*, vol. 7, no. 4, pp. 284–306, 2015. DOI: 10.1002/wics.1356.

[43] Bonabeau, E., "Agent-based modeling: Methods and techniques for simulating human systems," *Proceedings of the national academy of sciences*, vol. 99, no. suppl_3, pp. 7280–7287, 2002. DOI: 10.1073/pnas.082080899.

[44] Brugière, A., Nguyen-Ngoc, D., and Drogoul, A., "Handling multiple levels in agent-based models of complex socio-environmental systems: A comprehensive review," *Frontiers in Applied Mathematics and Statistics*, vol. 8, p. 1 020 353, 2022. DOI: 10.3389/fams.2022.1020353.

[45] Ferber, J. and Weiss, G., *Multi-agent systems: an introduction to distributed artificial intelligence*. Addison-wesley Reading, 1999, vol. 1.

[46] Müller, B., Bohn, F., Dreßler, G., *et al.*, "Describing human decisions in agent-based models–odd+ d, an extension of the odd protocol," *Environmental Modelling & Software*, vol. 48, pp. 37–48, 2013. DOI: 10.1016/j.envsoft.2013.06.003.

[47] Müller-Hansen, F., Schlüter, M., Mäs, M., *et al.*, "Towards representing human behavior and decision making in earth system models–an overview of techniques and approaches," *Earth System Dynamics*, vol. 8, no. 4, pp. 977–1007, 2017. DOI: 10.5194/esd-8-977-2017.

[48] DeAngelis, D. L. and Diaz, S. G., "Decision-making in agent-based modeling: A current review and future prospectus," *Frontiers in Ecology and Evolution*, vol. 6, p. 237, 2019.

[49] Adami, C., Schossau, J., and Hintze, A., "Evolutionary game theory using agent-based methods," *Physics of life reviews*, vol. 19, pp. 1–26, 2016. DOI: 10.1016/j.plrev.2016.08.015.

[50] Farooqui, A. D. and Niazi, M. A., "Game theory models for communication between agents: A review," *Complex Adaptive Systems Modeling*, vol. 4, no. 1, pp. 1–31, 2016. DOI: 10.1186/s40294-016-0026-7.

[51] Osborne, M. J. *et al.*, *An introduction to game theory*. New York: Oxford university press, 2004, vol. 3. DOI: 10.1007/978-3-031-01672-1_1.

[52] Izquierdo, L. R., Izquierdo, S. S., and Sandholm, W. H., *Agent-Based Evolutionary Game Dynamics*. University of Wisconsin Pressbooks, 2024. [Online]. Available: https://wisc.pb.unizin.org/agent-based-evolutionary-game-dynamics.

[53] Challet, D. and Zhang, Y.-C., "Emergence of cooperation and organization in an evolutionary game," *Physica A: Statistical Mechanics and its Applications*, vol. 246, no. 3-4, pp. 407–418, 1997. DOI: 10.1016/S0378-4371(97)00419-6.

[54] Santos, F. C., Pacheco, J. M., and Lenaerts, T., "Evolutionary dynamics of social dilemmas in structured heterogeneous populations," *Proceedings of the National Academy of Sciences*, vol. 103, no. 9, pp. 3490–3494, 2006. DOI: 10.1073/pnas.0508201103.

[55] Easley, D., Kleinberg, J., *et al.*, *Networks, crowds, and markets: Reasoning about a highly connected world*. Cambridge: Cambridge university press, 2010, vol. 1. DOI: 10.1111/j.1740-9713.2012.00594.x.

[56] Skyrms, B., "The stag hunt," in *Proceedings and Addresses of the American Philosophical Association*, JSTOR, vol. 75, 2001, pp. 31–41. DOI: 10.2307/3218711.

[57] Grimm, V., Railsback, S. F., Vincenot, C. E., *et al.*, "The odd protocol for describing agent-based and other simulation models: A second update to improve clarity, replication, and structural realism," *Journal of Artificial Societies and Social Simulation*, vol. 23, no. 2, 2020. DOI: 10.18564/jasss.4259.

[58] Cassandras, C. G. and Lafortune, S., *Introduction to Discrete Event Systems*, 2nd ed. Boston, MA: Springer, 2008. DOI: 10.1007/978-0-387-68612-7.

[59] Bellman, R. E. and Dreyfus, S. E., *Applied dynamic programming*. Princeton university press, 2015.

[60] Lee, T. M., Markowitz, E. M., Howe, P. D., Ko, C.-Y., and Leiserowitz, A. A., "Predictors of public climate change awareness and risk perception around the world," *Nature climate change*, vol. 5, no. 11, pp. 1014–1020, 2015. DOI: 10.1038/nclimate2728.

[61] Knight, K. W., "Public awareness and perception of climate change: A quantitative cross-national study," *Environmental Sociology*, vol. 2, no. 1, pp. 101–113, 2016. DOI: 10.1080/23251042.2015.1128055.

[62] De Silva, D. G. and Pownall, R. A., "Going green: Does it depend on education, gender or income?" *Applied Economics*, vol. 46, no. 5, pp. 573–586, 2014. DOI: 10.1080/00036846.2013.857003.

[63] Skogen, K., Helland, H., and Kaltenborn, B., "Concern about climate change, biodiversity loss, habitat degradation and landscape change: Embedded in different packages of environmental concern?" *Journal for Nature Conservation*, vol. 44, pp. 12–20, 2018. DOI: 10.1016/j.jnc.2018.06.001.

[64] Bloodhart, B. and Swim, J. K., "Sustainability and consumption: What's gender got to do with it?" *Journal of Social Issues*, vol. 76, no. 1, pp. 101–113, 2020. DOI: 10.1111/josi.12370.

[65] Baiardi, D., "What do you think about climate change?" *Journal of Economic Surveys*, vol. 37, no. 4, pp. 1255–1313, 2023. DOI: 10.1111/joes.12535.

[66] Weko, S., "Communitarians, cosmopolitans, and climate change: Why identity matters for eu climate and energy policy," *Journal of European public policy*, vol. 29, no. 7, pp. 1072–1091, 2022. DOI: 10.1080/13501763.2021.1918751.

[67] Wilensky, U., "Netlogo pd basic evolutionary model," *Center for Connected Learning and Computer-Based Modeling*, 2002. [Online]. Available: http://ccl.northwestern.edu/netlogo/models/PDBasicEvolutionary..

[68] Alstott, J., Klymko, C., Pyzza, P. B., and Radcliffe, M., "Local rewiring algorithms to increase clustering and grow a small world," *Journal of Complex Networks*, vol. 7, no. 4, pp. 564–584, Dec. 2018. DOI: 10.1093/comnet/cny032. eprint: https://academic.oup.com/comnet/article-pdf/7/4/564/29161034/cny032.pdf.

[69] Watts, D. J. and Strogatz, S. H., "Collective dynamics of 'small-world'networks," *nature*, vol. 393, no. 6684, pp. 440–442, 1998. DOI: 10.1038/30918.

[70] Telesford, Q. K., Joyce, K. E., Hayasaka, S., Burdette, J. H., and Laurienti, P. J., "The ubiquity of small-world networks," *Brain connectivity*, vol. 1 5, pp. 367–75, 2011. DOI: 10.1089/brain.2011.0038.

[71] Walker, B. and Johnson, T., "Netlogo and gis: A powerful combination.," in *CATA*, 2019, pp. 257–264. DOI: 10.29007/w8gh.

[72] Crooks, A. T. and Castle, C., "The integration of agent-based modelling and geographical information for geospatial simulation," 2012. DOI: /10.1007/978-90-481-8927-4_12.

[73] Masuda, N. and Aihara, K., "Spatial prisoner's dilemma optimally played in small-world networks," *Physics Letters A*, vol. 313, no. 1-2, pp. 55–61, 2003. DOI: 10.1016/S0375-9601(03)00693-5.

[74] McCright, A. M., "The effects of gender on climate change knowledge and concern in the american public," *Population and Environment*, vol. 32, pp. 66–87, 2010. DOI: 10.1007/s11111-010-0113-1.

[75] Bizzarri, F., Giuliani, A., and Mocenni, C., "Awareness: An empirical model," *Frontiers in Psychology*, vol. 13, p. 933 183, 2022. DOI: 10.3389/fpsyg.2022.933183.

[76] Su, Z., Meyerhenke, H., and Kurths, J., "The climatic interdependence of extreme-rainfall events around the globe," *Chaos: An Interdisciplinary Journal of Nonlinear Science*, vol. 32, no. 4, 2022. DOI: 10.1063/5.0077106.

[77] Hossain, I., Rasel, H., Imteaz, M. A., and Mekanik, F., "Long-term seasonal rainfall forecasting using linear and non-linear modelling approaches: A case study for western australia," *Meteorology and Atmospheric Physics*, vol. 132, pp. 131–141, 2020. DOI: 10.1007/s00703-019-00679-4.

[78] Kahneman, D., *Thinking, fast and slow*. macmillan, 2011.

[79] Kaufman, L. and Rousseeuw, P. J., *Finding groups in data: an introduction to cluster analysis*. John Wiley & Sons, 2009. DOI: 10.2307/2532178.

[80] Madhulatha, T. S., "An overview on clustering methods," *arXiv preprint arXiv:1205.1117*, 2012.

[81] Likas, A., Vlassis, N., and Verbeek, J. J., "The global k-means clustering algorithm," *Pattern recognition*, vol. 36, no. 2, pp. 451–461, 2003. DOI: 10.1016/S0031-3203(02)00060-2.

[82] Frey, B. J. and Dueck, D., "Clustering by passing messages between data points," *science*, vol. 315, no. 5814, pp. 972–976, 2007. DOI: 10.1126/science.1136800.

[83] Givoni, I., Chung, C., and Frey, B. J., "Hierarchical affinity propagation," *arXiv preprint arXiv:1202.3722*, 2012. DOI: 10.48550/arXiv.1202.3722.

[84] Dimitri, G. M., Spasov, S., Duggento, A., Passamonti, L., Lió, P., and Toschi, N., "Multimodal and multicontrast image fusion via deep generative models," *Information Fusion*, vol. 88, pp. 146–160, 2022. DOI: 10.1016/j.inffus.2022.07.017.

[85] Guo, X., Yang, Z., Li, C., Xiong, H., and Ma, C., "Combining the classic vulnerability index and affinity propagation clustering algorithm to assess the intrinsic aquifer vulnerability of coastal aquifers on an integrated scale," *Environmental Research*, vol. 217, p. 114 877, 2023. DOI: 10.1016/j.envres.2022.114877.

[86] Elia, M., Giannico, V., Ascoli, D., *et al.*, "Uncovering current pyroregions in italy using wildfire metrics," *Ecological Processes*, vol. 11, no. 1, p. 15, 2022. DOI: 10.1186/s13717-022-00360-6.

[87] Hornik, K., Stinchcombe, M., and White, H., "Multilayer feedforward networks are universal approximators," *Neural networks*, vol. 2, no. 5, pp. 359–366, 1989. DOI: 10.1016/0893-6080(89)90020-8.

[88] Kuan, C.-M. and White, H., "Artificial neural networks: An econometric perspective," *Econometric reviews*, vol. 13, no. 1, pp. 1–91, 1994. DOI: 10.1080/07474939408800273.

[89] Kalogirou, S. A., "Applications of artificial neural-networks for energy systems," *Applied energy*, vol. 67, no. 1-2, pp. 17–35, 2000. DOI: 10.1016/S0306-2619(00)00005-2.

[90] Rumelhart, D. E., Hinton, G. E., and Williams, R. J., "Learning representations by back-propagating errors," *nature*, vol. 323, no. 6088, pp. 533–536, 1986. DOI: 10.1038/323533a0.

[91] LeCun, Y., Bengio, Y., and Hinton, G., "Deep learning," *nature*, vol. 521, no. 7553, pp. 436–444, 2015. DOI: 10.1038/nature14539.

[92] Cortes, C. and Vapnik, V., "Support-vector networks," *Machine learning*, vol. 20, no. 3, pp. 273–297, 1995. DOI: 10.1007/BF00994018.

[93] Breiman, L., "Random forests," *Machine learning*, vol. 45, no. 1, pp. 5–32, 2001. DOI: 10.1023/A:1010933404324.

[94] Breiman, L., "Bagging predictors," *Machine learning*, vol. 24, pp. 123–140, 1996. DOI: 10.1007/BF00058655.

[95] Breiman, L., Friedman, J., Olshen, R. A., and Stone, C. J., *Classification and regression trees*. Routledge, 2017. DOI: 10.1201/9781315139470.

[96] Sutton, C. D., "Classification and regression trees, bagging, and boosting," *Handbook of statistics*, vol. 24, pp. 303–329, 2005. DOI: 10.1016/S0169-7161(04)24011-1.

[97] Spirtes, P., Glymour, C. N., and Scheines, R., *Causation, prediction, and search*. MIT press, 2000. DOI: 10.1007/978-1-4612-2748-9.

[98] Ullman, J. B. and Bentler, P. M., "Structural equation modeling," *Handbook of psychology, second edition*, vol. 2, 2012. DOI: 10.1002/9781118133880.hop202023.

[99] Zivot, E. and Wang, J., "Vector autoregressive models for multivariate time series," *Modeling financial time series with S-PLUS*, pp. 385–429, 2006. DOI: 10.1007/978-0-387-21763-5_11.

[100] Bossomaier, T., Barnett, L., Harré, M., *et al.*, *Transfer entropy*. Springer, 2016. DOI: 10.1007/978-3-319-43222-9_4.

[101] Bollen, K. A., *Structural equations with latent variables*. Wiley, 1989, vol. 25. DOI: 10.1002/9781118619179.

[102] Kim, J., Zhu, W., Chang, L., Bentler, P. M., and Ernst, T., "Unified structural equation modeling approach for the analysis of multisubject, multivariate functional mri data," *Human brain mapping*, vol. 28, no. 2, pp. 85–93, 2007. DOI: 10.1002/hbm.20259.

[103] Gates, K. M., Molenaar, P. C., Hillary, F. G., Ram, N., and Rovine, M. J., "Automatic search for fmri connectivity mapping: An alternative to granger causality testing using formal equivalences among sem path modeling, var, and unified sem," *NeuroImage*, vol. 50, no. 3, pp. 1118–1125, 2010. DOI: 10.1016/j.neuroimage.2009.12.117.

[104] Shojaie, A. and Fox, E. B., "Granger causality: A review and recent advances," *Annual Review of Statistics and Its Application*, vol. 9, no. 1, pp. 289–319, 2022. DOI: 10.1146/annurev-statistics-040120-010930.

[105] Faes, L., Nollo, G., and Porta, A., "Compensated transfer entropy as a tool for reliably estimating information transfer in physiological time series," *Entropy*, vol. 15, no. 1, pp. 198–219, 2013. DOI: 10.3390/e15010198.

[106] Runge, J., Nowack, P., Kretschmer, M., Flaxman, S., and Sejdinovic, D., "Detecting and quantifying causal associations in large nonlinear time series datasets," *Science advances*, vol. 5, no. 11, eaau4996, 2019. DOI: 10.1126/sciadv.aau4996.

[107] Runge, J., "Discovering contemporaneous and lagged causal relations in autocorrelated nonlinear time series datasets," in *Conference on uncertainty in artificial intelligence*, Pmlr, 2020, pp. 1388–1397.

[108] Runge, J., "Conditional independence testing based on a nearest-neighbor estimator of conditional mutual information," in *International Conference on Artificial Intelligence and Statistics*, Pmlr, 2018, pp. 938–947.

[109] Silfwerbrand, L., Koike, Y., Nyström, P., and Gingnell, M., "Directed causal effect with pcmci in hyperscanning eeg time series," *Frontiers in Neuroscience*, vol. 18, p. 1 305 918, 2024. DOI: 10.3389/fnins.2024.1305918.

[110] Arab, F., Ghassami, A., Jamalabadi, H., Peters, M. A., and Nozari, E., "Whole-brain causal discovery using fmri," *Network Neuroscience*, pp. 1–29, 2025. DOI: 10.1162/netn_a_00438.

[111] Trenberth, K. E., Fasullo, J. T., and Shepherd, T. G., "Attribution of climate extreme events," *Nature climate change*, vol. 5, no. 8, pp. 725–730, 2015. DOI: 10.1038/nclimate2657.

[112] Moss, R. H., Edmonds, J. A., Hibbard, K. A., *et al.*, "The next generation of scenarios for climate change research and assessment," *Nature*, vol. 463, no. 7282, pp. 747–756, 2010. DOI: 10.1038/nature08823.

[113] Baker, H. S., Millar, R. J., Karoly, D. J., *et al.*, "Higher co2 concentrations increase extreme event risk in a 1.5 c world," *Nature Climate Change*, vol. 8, no. 7, pp. 604–608, 2018. DOI: 10.1038/s41558-018-0190-1.

[114] Stott, P., "How climate change affects extreme weather events," *Science*, vol. 352, no. 6293, pp. 1517–1518, 2016. DOI: 10.1126/science.aaf7271.

[115] Cavicchia, L., Scoccimarro, E., Gualdi, S., *et al.*, "Mediterranean extreme precipitation: A multi-model assessment," *Climate Dynamics*, vol. 51, pp. 901–913, 2018. DOI: 10.1007/s00382-016-3245-x.

[116] Lavell, A., Oppenheimer, M., Diop, C., *et al.*, "Managing the risks of extreme events and disasters to advance climate change adaptation," *A special report of working groups I and II of the intergovernmental panel on climate change (IPCC)*, vol. 3, pp. 25–64, 2012. DOI: 10.13140/2.1.3117.9529.

[117] Cannarozzo, M., Noto, L. V., and Viola, F., "Spatial distribution of rainfall trends in sicily (1921–2000)," *Physics and Chemistry of the Earth, Parts a/b/c*, vol. 31, no. 18, pp. 1201–1211, 2006. DOI: 10.1016/j.pce.2006.03.022.

[118] Forestieri, A., Lo Conti, F., Blekinsop, S., Noto, L., Fowler, H., *et al.*, "Objective regional frequency analysis of extreme precipitation in sicily, italy," in *Rainfall in urban and natural systems*, Peter Molnar, Nadav Peleg, 2015, pp. 68–73. [Online]. Available: https://hdl.handle.net/10447/166833.

[119] Hosking, J. R. M. and Wallis, J. R., *Regional frequency analysis*. 1997.

[120] Sahu, R. T., Verma, M. K., and Ahmad, I., "Regional frequency analysis using l-moment methodology—a review," *Recent Trends in Civil Engineering: Select Proceedings of ICRTICE 2019*, pp. 811–832, 2021. DOI: 10.1007/978-981-15-5195-6_60.

[121] Bonaccorso, B. and Aronica, G. T., "Estimating temporal changes in extreme rainfall in sicily region (italy)," *Water Resources Management*, vol. 30, pp. 5651–5670, 2016. DOI: 10.1007/s11269-016-1442-3.

[122] Maugeri, M., Brunetti, M., Garzoglio, M., and Simolo, C., "High-resolution analysis of 1 day extreme precipitation in sicily," *Natural Hazards and Earth System Sciences*, vol. 15, no. 10, pp. 2347–2358, 2015. DOI: 10.5194/nhess-15-2347-2015.

[123] Glickman, T. S., *Glossary of meteorology*. American Meteorological Soc., 2000.

[124] Belouafa, S., Habti, F., Benhar, S., *et al.*, "Statistical tools and approaches to validate analytical methods: Methodology and practical examples," *International Journal of Metrology and Quality Engineering*, vol. 8, p. 9, 2017. DOI: 10.1051/ijmqe/2016030.

[125] Bhattacharyya, H., "Kruskal–wallis test: Theory," *Wiley StatsRef: Statistics Reference Online*, 2014. DOI: 10.1002/9781118445112.stat02748.

[126] Miller Jr, R. G., *Beyond ANOVA: basics of applied statistics*. CRC press, 1997.

[127] Levantesi, S., "Assessing italy's climate risk," *Nature*, 2021.

[128] Caccamo, M. T., Castorina, G., Colombo, F., Insinga, V., Maiorana, E., and Magazù, S., "Weather forecast performances for complex orographic areas: Impact of different grid resolutions and of geographic data on heavy rainfall event simulations in sicily," *Atmospheric Research*, vol. 198, pp. 22–33, 2017. DOI: 10.1016/j.atmosres.2017.07.028.

[129] Noto, L. V. and La Loggia, G., "Use of l-moments approach for regional flood frequency analysis in sicily, italy," *Water resources management*, vol. 23, pp. 2207–2229, 2009. DOI: 10.1007/s11269-008-9378-x.

[130] Forestieri, A., Arnone, E., Blenkinsop, S., Candela, A., Fowler, H., and Noto, L. V., "The impact of climate change on extreme precipitation in sicily, italy," *Hydrological Processes*, vol. 32, no. 3, pp. 332–348, 2018. DOI: 10.1002/hyp.11421.

[131] Dimitri, G., Parri, L., Pozzebon, A., Vitanza, E., Fort, A., Mocenni, C., *et al.*, "Weair: Wearable swarm sensors for air quality monitoring to foster citizens' awareness of climate change," in *Proceedings of 2023 IEEE International Conference on Metrology for eXtended Reality, Artificial Intelligence and Neural Engineering*, IEEE, 2023, pp. 98–103. DOI: 10.1109/MetroXRAINE58569.2023.10405724.

[132] Khomenko, S. *et al.*, "Premature mortality due to air pollution in european cities: A health impact assessment," *The Lancet Planetary Health*, vol. 5, e121–e134, 2021. DOI: 10.1016/S2542-5196(20)30272-2.

[133] Palomeque-Mangut, S. *et al.*, "Wearable system for outdoor air quality monitoring in a wsn with cloud computing: Design, validation and deployment," *Chemosphere*, vol. 307, p. 135 948, 2022. DOI: 10.1016/j.chemosphere.2022.135948.

[134] Sirbu, A., Becker, M., Caminiti, S., *et al.*, "Participatory patterns in an international air quality monitoring initiative," *PLOS one*, vol. 10, no. 8, e0136763, 2015. DOI: 10.1371/journal.pone.0136763.

[135] *Atmo*, https://atmotube.com, 2016.

[136] *Plumelabs*, https://plumelabs.com/en/flow/, 2023.

[137] Plutchik, R. and Kellerman, H., *Theories of Emotion*. Academic Press, 1980, vol. 1. DOI: 10.1016/C2013-0-11313-X.

[138] Carver, C. S. and Scheier, M. F., "Origins and functions of positive and negative affect: A control-process view.," *Psychological review*, vol. 97, no. 1, p. 19, 1990. DOI: 10.1037/0033-295X.97.1.19.

[139] Tracy, J. L., "An evolutionary approach to understanding distinct emotions," *Emotion Review*, vol. 6, no. 4, pp. 308–312, 2014. DOI: 10.1177/1754073914534478.

[140] Kuppens, P. and Verduyn, P., "Emotion dynamics," *Current Opinion in Psychology*, vol. 17, pp. 22–26, 2017. DOI: 10.1016/j.copsyc.2017.06.004.

[141] Mauss, I. B., Bunge, S. A., and Gross, J. J., "Automatic emotion regulation," *Social and Personality Psychology Compass*, vol. 1, no. 1, pp. 146–167, 2007. DOI: 10.1111/j.1751-9004.2007.00005.x.

[142] Kuppens, P. and Verduyn, P., "Looking at emotion regulation through the window of emotion dynamics," *Psychological Inquiry*, vol. 26, no. 1, pp. 72–79, 2015. DOI: 10.1080/1047840X.2015.960505.

[143] Mesquita, B. and Boiger, M., "Emotions in context: A sociodynamic model of emotions," *Emotion Review*, vol. 6, no. 4, pp. 298–302, 2014. DOI: 10.1177/1754073914534480.

[144] Gross, J. J., "Emotion regulation: Current status and future prospects," *Psychological inquiry*, vol. 26, no. 1, pp. 1–26, 2015. DOI: 10.1080/1047840X.2014.940781.

[145] Tamir, M., "Why do people regulate their emotions? a taxonomy of motives in emotion regulation," *Personality and social psychology review*, vol. 20, no. 3, pp. 199–222, 2016. DOI: 10.1177/1088868315586325.

[146] Cunningham, W. A., Dunfield, K. A., and Stillman, P. E., "Emotional states from affective dynamics," *Emotion Review*, vol. 5, no. 4, pp. 344–355, 2013. DOI: 10.1177/1754073913489749.

[147] Lench, H. C., Flores, S. A., and Bench, S. W., "Discrete emotions predict changes in cognition, judgment, experience, behavior, and physiology: A meta-analysis of experimental emotion elicitations," *Psychological Bulletin*, vol. 137, no. 5, pp. 834–855, 2011. DOI: 10.1037/a0024244.

[148] Adolphs, R. and Anderson, D. J., *The Neuroscience of Emotion: A New Synthesis*. Princeton University Press, 2018. DOI: 10.23943/9781400889914.

[149] Behnke, M., Kreibig, S. D., Kaczmarek, L. D., Assink, M., and Gross, J. J., "Autonomic nervous system activity during positive emotions: A meta-analytic review," *Emotion Review*, vol. 14, no. 2, pp. 132–160, 2022. DOI: 10.1177/17540739211073084.

[150] Eronen, M. I. and Romeijn, J.-W., "Philosophy of science and the formalization of psychological theory," *Theory & Psychology*, vol. 30, no. 6, pp. 786–799, 2020. DOI: 10.1177/0959354320969876.

[151] Lange, J., Dalege, J., Borsboom, D., Kleef, G. A. van, and Fischer, A. H., "Toward an integrative psychometric model of emotions," *Perspectives on Psychological Science*, vol. 15, no. 2, pp. 444–468, 2020. DOI: 10.1177/1745691619895057.

[152] Scherer, K. R., "Emotions are emergent processes: They require a dynamic computational architecture," *Philosophical Transactions of the Royal Society B: Biological Sciences*, vol. 364, no. 1535, pp. 3459–3474, 2009. DOI: 10.1098/rstb.2009.0141.

[153] Gershenson, C., "Modelling emotions with multidimensional logic," in *18th international conference of the north american fuzzy information processing society-nafips (cat. no. 99th8397)*, IEEE, 1999, pp. 42–46. DOI: 10.1109/NAFIPS.1999.781649.

[154] Della Rossa, F., Menditto, G., and De Lellis, P., "Early warning signals for psychopathology," in *2024 IEEE Workshop on Complexity in Engineering (COMPENG)*, IEEE, 2024, pp. 1–5. DOI: 10.1109/COMPENG60905.2024.10741467.

[155] Cipresso, P., Borghesi, F., and Chirico, A., "Affects affect affects: A markov chain," *Frontiers in Psychology*, vol. 14, p. 1 162 655, 2023. DOI: 10.3389/fpsyg.2023.1162655.

[156] Thornton, M. A. and Tamir, D. I., "Mental models accurately predict emotion transitions," *Proceedings of the National Academy of Sciences*, vol. 114, no. 23, pp. 5982–5987, 2017. DOI: 10.1073/pnas.1616056114.

[157] Strauss, G. P., Esfahlani, F. Z., Raugh, I. M., Luther, L., and Sayama, H., "Markov chain analysis indicates that positive and negative emotions have abnormal temporal interactions during daily life in schizophrenia," *Journal of Psychiatric Research*, vol. 164, pp. 344–349, 2023. DOI: 10.1016/j.jpsychires.2023.06.025.

[158] Rowland, Z. and Wenzel, M., "Mindfulness and affect-network density: Does mindfulness facilitate disengagement from affective experiences in daily life?" *Mindfulness*, vol. 11, pp. 1253–1266, 2020. DOI: 10.1007/s12671-020-01335-4.

[159] Russell, J. A., "A circumplex model of affect.," *Journal of personality and social psychology*, vol. 39, no. 6, p. 1161, 1980. DOI: 10.1037/h0077714.

[160] Freud, S., "1991." on narcissism: An introduction.","*On Metapsychology: The Theory of Psychoanalysis*, vol. 11, pp. 165–97, 1914.

[161] Sandia, I. and Baptista, T., "Ego-dystonia: A review in search of definitions," *Revista Colombiana de Psiquiatría (English ed.)*, vol. 51, no. 3, pp. 240–244, 2022. DOI: 10.1016/j.rcpeng.2022.08.006.

[162] Purdon, C., Cripps, E., Faull, M., Joseph, S., and Rowa, K., "Development of a measure of egodystonicity," *Journal of Cognitive Psychotherapy*, vol. 21, no. 3, pp. 198–216, 2007. DOI: 10.1891/088983907781494537.

[163] O'Connor, B. P. and St. Pierre, E. S., "Personality disorders," *Diagnostic Interviewing: Fourth Edition*, pp. 201–226, 2010. DOI: 10.1007/978-1-4419-1320-3_10.

[164] Belloch, A., Roncero, M., and Perpiñá, C., "Ego-syntonicity and ego-dystonicity associated with upsetting intrusive cognitions," *Journal of Psychopathology and Behavioral Assessment*, vol. 34, pp. 94–106, 2012. DOI: 10.1007/s10862-011-9255-4.

[165] Yiend, J., "The effects of emotion on attention: A review of attentional processing of emotional information," *Cognition and emotion*, pp. 221–285, 2010. DOI: 10.1080/02699930903205698.

[166] Gross, J. J. and John, O. P., "Individual differences in two emotion regulation processes: Implications for affect, relationships, and well-being," *Journal of Personality and Social Psychology*, vol. 85, no. 2, pp. 348–362, 2003. DOI: 10.1037/0022-3514.85.2.348.

[167] Rogers, C. R., *Client-centered therapy: Its current practice, implications, and theory, with chapters*. Houghton Mifflin Oxford, United Kingdom, 1951.

[168] Sheldon, K. M., Ryan, R. M., Rawsthorne, L. J., and Ilardi, B., "Trait self and true self: Cross-role variation in the big-five personality traits and its relations with psychological authenticity and subjective well-being," *Journal of Personality and Social Psychology*, vol. 73, no. 6, pp. 1380–1393, 1997. DOI: 10.1037/0022-3514.73.6.1380.

[169] Roncero, M., Belloch, A., Perpiñá, C., and Treasure, J., "Ego-syntonicity and ego-dystonicity of eating-related intrusive thoughts in patients with eating disorders," *Psychiatry Research*, vol. 208, no. 1, pp. 67–73, 2013. DOI: 10.1016/j.psychres.2013.01.006.

[170] Hyland, M. E., *The origins of health and disease*. Cambridge University Press, 2011. DOI: 10.1017/CBO9780511976216.

[171] Kessler, R. C., Cox, B. J., Green, J. G., *et al.*, "The effects of latent variables in the development of comorbidity among common mental disorders," *Depression and Anxiety*, vol. 28, no. 1, pp. 29–39, 2011. DOI: 10.1002/da.20760.

[172] Borsboom, D., Cramer, A. O., Schmittmann, V. D., Epskamp, S., and Waldorp, L. J., "The small world of psychopathology," *PloS one*, vol. 6, no. 11, e27407, 2011. DOI: 10.1371/journal.pone.0027407.

[173] Borsboom, D. and Cramer, A. O., "Network analysis: An integrative approach to the structure of psychopathology," *Annual review of clinical psychology*, vol. 9, no. 1, pp. 91–121, 2013. DOI: 10.1146/annurev-clinpsy-050212-185608.

[174] Kendler, K. S., Zachar, P., and Craver, C., "What kinds of things are psychiatric disorders?" *Psychological medicine*, vol. 41, no. 6, pp. 1143–1150, 2011. DOI: 10.1017/S0033291710001844.

[175] Kendler, K. S., "The dappled nature of causes of psychiatric illness: Replacing the organic–functional/hardware–software dichotomy with empirically based pluralism," *Molecular psychiatry*, vol. 17, no. 4, pp. 377–388, 2012. DOI: 10.1038/mp.2011.182.

[176] Hofmann, S. G. and Curtiss, J., "A complex network approach to clinical science," *European journal of clinical investigation*, vol. 48, no. 8, e12986, 2018. DOI: 10.1111/eci.12986.

[177] Wichers, M., Riese, H., Hodges, T. M., Snippe, E., and Bos, F. M., "A narrative review of network studies in depression: What different methodological approaches tell us about depression," *Frontiers in psychiatry*, vol. 12, p. 719 490, 2021. DOI: 10.3389/fpsyt.2021.719490.

[178] Bringmann, L. F., Albers, C., Bockting, C., *et al.*, "Psychopathological networks: Theory, methods and practice," *Behaviour Research and Therapy*, vol. 149, p. 104 011, 2022. DOI: 10.1016/j.brat.2021.104011.

[179] Contreras, A., Nieto, I., Valiente, C., Espinosa, R., and Vazquez, C., "The study of psychopathology from the network analysis perspective: A systematic review," *Psychotherapy and psychosomatics*, vol. 88, no. 2, pp. 71–83, 2019. DOI: 10.1159/000497425.

[180] Groen, R. N., Ryan, O., Wigman, J. T., *et al.*, "Comorbidity between depression and anxiety: Assessing the role of bridge mental states in dynamic psychological networks," *BMC medicine*, vol. 18, pp. 1–17, 2020. DOI: 10.1186/s12916-020-01738-z.

[181] Ren, L., Wang, Y., Wu, L., *et al.*, "Network structure of depression and anxiety symptoms in chinese female nursing students," *BMC psychiatry*, vol. 21, pp. 1–12, 2021. DOI: 10.1186/s12888-021-03276-1.

[182] Cramer, A. O., Waldorp, L. J., Van Der Maas, H. L., and Borsboom, D., "Comorbidity: A network perspective," *Behavioral and brain sciences*, vol. 33, no. 2-3, pp. 137–150, 2010. DOI: 10.1017/S0140525X09991567.

[183] Burger, J., Isvoranu, A.-M., Lunansky, G., *et al.*, "Reporting standards for psychological network analyses in cross-sectional data.," *Psychological methods*, vol. 28, no. 4, p. 806, 2023. DOI: 10.1037/met0000471.

[184] Borsboom, D., Deserno, M. K., Rhemtulla, M., *et al.*, "Network analysis of multivariate data in psychological science," *Nature Reviews Methods Primers*, vol. 1, no. 1, p. 58, 2021. DOI: 10.1038/s43586-021-00055-w.

[185] Piccirillo, M. L. and Rodebaugh, T. L., "Personalized networks of social anxiety disorder and depression and implications for treatment," *Journal of Affective Disorders*, vol. 298, pp. 262–276, 2022. DOI: 10.1016/j.jad.2021.10.034.

[186] Howe, E., Bosley, H. G., and Fisher, A. J., "Idiographic network analysis of discrete mood states prior to treatment," *Counselling and Psychotherapy Research*, vol. 20, no. 3, pp. 470–478, 2020. DOI: 10.1002/capr.12295.

[187] Epskamp, S., Borkulo, C. D. van, Veen, D. C. van der, *et al.*, "Personalized network modeling in psychopathology: The importance of contemporaneous and temporal connections," *Clinical Psychological Science*, vol. 6, no. 3, pp. 416–427, 2018. DOI: 10.1177/2167702617744325.

[188] Bringmann, L. F., "Person-specific networks in psychopathology: Past, present, and future," *Current opinion in psychology*, vol. 41, pp. 59–64, 2021. DOI: 10.1016/j.copsyc.2021.03.004.

[189] Fisher, A. J., Bosley, H. G., Fernandez, K. C., *et al.*, "Open trial of a personalized modular treatment for mood and anxiety," *Behaviour research and therapy*, vol. 116, pp. 69–79, 2019. DOI: 10.1016/j.brat.2019.01.010.

[190] Jeronimus, B. F., "Dynamic system perspectives on anxiety and depression," *Psychosocial Development in Adolescence*, pp. 100–126, 2019. DOI: 10.4324/9781315165844-7.

[191] Wright, A. G. and Woods, W. C., "Personalized models of psychopathology," *Annual review of clinical psychology*, vol. 16, no. 1, pp. 49–74, 2020. DOI: 10.1146/annurev-clinpsy-102419-125032.

[192] Haslbeck, J. M., Epskamp, S., and Waldorp, L. J., "Testing for group differences in multilevel vector autoregressive models," *Behavior Research Methods*, vol. 57, no. 3, p. 100, 2025. DOI: 10.3758/s13428-024-02541-x.

[193] Hosenfeld, B., Bos, E. H., Wardenaar, K. J., *et al.*, "Major depressive disorder as a nonlinear dynamic system: Bimodality in the frequency distribution of depressive symptoms over time," *Bmc psychiatry*, vol. 15, pp. 1–9, 2015. DOI: 10.1186/s12888-015-0596-5.

[194] Haslbeck, J., Ryan, O., Robinaugh, D. J., Waldorp, L. J., and Borsboom, D., "Modeling psychopathology: From data models to formal theories.," *Psychological Methods*, vol. 27, no. 6, p. 930, 2022. DOI: 10.1037/met0000303.

[195] Eaton, N. R., Bringmann, L. F., Elmer, T., *et al.*, "A review of approaches and models in psychopathology conceptualization research," *Nature Reviews Psychology*, vol. 2, no. 10, pp. 622–636, 2023. DOI: 10.1038/s44159-023-00218-4.

[196] McNally, R. J., "Network analysis of psychopathology: Controversies and challenges," *Annual review of clinical psychology*, vol. 17, no. 1, pp. 31–53, 2021. DOI: 10.1146/annurev-clinpsy-081219-092850.

[197] Fisher, A. J., Medaglia, J. D., and Jeronimus, B. F., "Lack of group-to-individual generalizability is a threat to human subjects research," *Proceedings of the National Academy of Sciences*, vol. 115, no. 27, E6106–E6115, 2018. DOI: 10.1073/pnas.1711978115.

[198] Hoekstra, R. H., Epskamp, S., and Borsboom, D., "Heterogeneity in individual network analysis: Reality or illusion?" *Multivariate Behavioral Research*, vol. 58, no. 4, pp. 762–786, 2023. DOI: 10.1080/00273171.2022.2128020.

[199] Borsboom, D. and Haslbeck, J., "Integrating intra-and interindividual phenomena in psychological theories," *Multivariate Behavioral Research*, vol. 59, no. 6, pp. 1290–1309, 2024. DOI: 10.1080/00273171.2024.2336178.

[200] Izard, C. E., *Patterns of emotions: A new analysis of anxiety and depression*. Academic Press, 2013.

[201] Dobson, K. S., "The relationship between anxiety and depression," *Clinical Psychology Review*, vol. 5, no. 4, pp. 307–324, 1985. DOI: 10.1016/0272-7358(85)90010-8.

[202] Kalin, N. H., *The critical relationship between anxiety and depression*, 2020. DOI: 10.1176/appi.ajp.2020.20030305.

[203] Katon, W. and Roy-Byrne, P. P., "Mixed anxiety and depression.," *Journal of abnormal Psychology*, vol. 100, no. 3, p. 337, 1991. DOI: 10.1037/0021-843X.100.3.337.

[204] Eysenck, M., Payne, S., and Santos, R., "Anxiety and depression: Past, present, and future events," *Cognition & Emotion*, vol. 20, no. 2, pp. 274–294, 2006. DOI: 10.1080/02699930500220066.

[205] Baldwin, D. S., Evans, D. L., Hirschfeld, R., and Kasper, S., "Can we distinguish anxiety from depression?" *Psychopharmacology Bulletin*, vol. 36, pp. 158–165, 2002.

[206] Pollack, M. H., "Comorbid anxiety and depression," *Journal of Clinical Psychiatry*, vol. 66, p. 22, 2005.

[207] Hagmann, P., Cammoun, L., Gigandet, X., *et al.*, "Mapping the structural core of human cerebral cortex," *PLoS biology*, vol. 6, no. 7, e159, 2008. DOI: 10.1371/journal.pbio.0060159.

[208] Freeman, L. C. *et al.*, "Centrality in social networks: Conceptual clarification," *Social network: critical concepts in sociology. Londres: Routledge*, vol. 1, no. 3, pp. 238–263, 2002.

[209] Kriege, N. M., Johansson, F. D., and Morris, C., "A survey on graph kernels," *Applied Network Science*, vol. 5, pp. 1–42, 2020. DOI: 10.1007/s41109-019-0195-3.

[210] Vishwanathan, S. V. N., Schraudolph, N. N., Kondor, R., and Borgwardt, K. M., "Graph kernels," *The Journal of Machine Learning Research*, vol. 11, pp. 1201–1242, 2010.

[211] Yaveroğlu, Ö. N., Milenković, T., and Pržulj, N., "Proper evaluation of alignment-free network comparison methods," *Bioinformatics*, vol. 31, no. 16, pp. 2697–2704, 2015. DOI: 10.1093/bioinformatics/btv170.

[212] Sugiyama, M., Ghisu, M. E., Llinares-López, F., and Borgwardt, K., "Graphkernels: R and python packages for graph comparison," *Bioinformatics*, vol. 34, no. 3, pp. 530–532, 2018. DOI: 10.1093/bioinformatics/btx602.

[213] Shervashidze, N., Schweitzer, P., Van Leeuwen, E. J., Mehlhorn, K., and Borgwardt, K. M., "Weisfeiler-lehman graph kernels.," *Journal of Machine Learning Research*, vol. 12, no. 9, 2011.

[214] Goldberger, A. L., Amaral, L. A., Hausdorff, J. M., Ivanov, P. C., Peng, C.-K., and Stanley, H. E., "Fractal dynamics in physiology: Alterations with disease and aging," *Proceedings of the National Academy of Sciences*, vol. 99, no. suppl 1, pp. 2466–2472, 2002. DOI: 10.1073/pnas.012579499.

[215] Kantz, H. and Schreiber, T., *Nonlinear time series analysis*. Cambridge university press, 2003. DOI: 10.1017/CBO9780511755798.

[216] Marwan, N., Carmen Romano, M., Thiel, M., and Kurths, J., "Recurrence plots for the analysis of complex systems," *Physics Reports*, vol. 438, no. 5-6, pp. 237–329, 2007. DOI: 10.1016/j.physrep.2006.11.001.

[217] Guyon, I. and Elisseeff, A., "An introduction to variable and feature selection," *Journal of machine learning research*, vol. 3, no. Mar, pp. 1157–1182, 2003.

[218] Tang, J., Alelyani, S., and Liu, H., "Feature selection for classification: A review," *Data classification: Algorithms and applications*, p. 37, 2014.

[219] Kursa, M. B. and Rudnicki, W. R., "Feature selection with the boruta package," *Journal of statistical software*, vol. 36, pp. 1–13, 2010. DOI: 10.18637/jss.v036.i11.

[220] Krieke, L. van der, Emerencia, A. C., Bos, E. H., *et al.*, "Ecological momentary assessments and automated time series analysis to promote tailored health care: A proof-of-principle study," *JMIR research protocols*, vol. 4, no. 3, e4000, 2015. DOI: 10.2196/resprot.4000.

[221] Nitschke, J. B., Heller, W., Imig, J. C., McDonald, R. P., and Miller, G. A., "Distinguishing dimensions of anxiety and depression," *Cognitive Therapy and Research*, vol. 25, pp. 1–22, 2001. DOI: 10.1023/A:1026485530405.

[222] Barlow, D. H., "The nature of anxiety: Anxiety, depression, and emotional disorders.," 1991.

[223] Watson, D., Clark, L. A., and Carey, G., "Positive and negative affectivity and their relation to anxiety and depressive disorders.," *Journal of abnormal psychology*, vol. 97, no. 3, p. 346, 1988. DOI: 10.1037/0021-843X.97.3.346.

[224] Ryan, O., Haslbeck, J. M., and Waldorp, L. J., "Non-stationarity in time-series analysis: Modeling stochastic and deterministic trends," *Multivariate Behavioral Research*, vol. 60, no. 3, pp. 556–588, 2025. DOI: 10.1080/00273171.2024.2436413.

[225] Marinazzo, D., Van Roozendaal, J., Rosas, F. E., *et al.*, "An information-theoretic approach to build hypergraphs in psychometrics," *Behavior Research Methods*, vol. 56, no. 7, pp. 8057–8079, 2024. DOI: 10.3758/s13428-024-02471-8.

[226] Brosch, T., "From individual to collective climate emotions and actions: A review," *Current Opinion in Behavioral Sciences*, vol. 61, p. 101 466, 2025. DOI: 10.1016/j.cobeha.2024.101466.

[227] Doell, K. C., Conte, B., and Brosch, T., "Interindividual differences in environmentally relevant positive trait affect impacts sustainable behavior in everyday life," *Scientific Reports*, vol. 11, no. 1, p. 20 423, 2021. DOI: 10.1038/s41598-021-99438-y.

[228] Vlasceanu, M., Doell, K. C., Bak-Coleman, J. B., *et al.*, "Addressing climate change with behavioral science: A global intervention tournament in 63 countries," *Science advances*, vol. 10, no. 6, eadj5778, 2024. DOI: 10.1126/sciadv.adj5778.

[229] Ogunbode, C. A., Doran, R., Hanss, D., *et al.*, "Climate anxiety, wellbeing and pro-environmental action: Correlates of negative emotional responses to climate change in 32 countries," *Journal of Environmental Psychology*, vol. 84, p. 101 887, 2022. DOI: 10.1016/j.jenvp.2022.101887.

[230] Helmold, M., "Prisoners' dilemma and negotiation types," *Successful International Negotiations: A Practical Guide for Managing Transactions and Deals*, pp. 25–29, 2020. DOI: 10.1007/978-3-030-33483-3_2.

[231] Poundstone, W., *Prisoner's dilemma: John von Neumann, game theory, and the puzzle of the bomb*. United States: Anchor, 1993.

[232] Maynard Smith, J., *On evolution*, eng. Edinburgh: Edinburgh University Press, 1972.

[233] Blomquist, G. C. and Whitehead, J. C., "Resource quality information and validity of willingness to pay in contingent valuation," *Resource and Energy Economics*, vol. 20, no. 2, pp. 179–196, 1998. DOI: 10.1016/S0928-7655(97)00035-3.

[234] Brécard, D., Hlaimi, B., Lucas, S., Perraudeau, Y., and Salladarré, F., "Determinants of demand for green products: An application to eco-label demand for fish in europe," *Ecological economics*, vol. 69, no. 1, pp. 115–125, 2009. DOI: 10.1016/j.ecolecon.2009.07.017.

[235] Klineberg, S. L., McKeever, M., and Rothenbach, B., "Demographic predictors of environmental concern: It does make a difference how it's measured," *Social science quarterly*, pp. 734–753, 1998. [Online]. Available: https://www.jstor.org/stable/42863844.

[236] Torgler, B. and Garcia-Valiñas, M. A., "The determinants of individuals' attitudes towards preventing environmental damage," *Ecological economics*, vol. 63, no. 2-3, pp. 536–552, 2007. DOI: 10.1016/j.ecolecon.2006.12.013.

[237] Milfont, T. L., Zubielevitch, E., Milojev, P., and Sibley, C. G., "Ten-year panel data confirm generation gap but climate beliefs increase at similar rates across ages," *Nature communications*, vol. 12, no. 1, p. 4038, 2021. DOI: 10.1038/s41467-021-24245-y.

[238] Andor, M. A., Schmidt, C. M., and Sommer, S., "Climate change, population ageing and public spending: Evidence on individual preferences," *Ecological economics*, vol. 151, pp. 173–183, 2018. DOI: 10.1016/j.ecolecon.2018.05.003.

[239] Commissione europea, "Il cambiamento climatico - eurobarometro speciale 538 (2023)," 2023.

[240] Peritia, "Public perceptions on climate change (2022)," EU-funded PERITIA project, 2022.

[241] Vorontsov, I. E., Kulakovskiy, I. V., and Makeev, V. J., "Jaccard index based similarity measure to compare transcription factor binding site models," *Algorithms for Molecular Biology*, vol. 8, pp. 1–11, 2013. DOI: 10.1186/1748-7188-8-23.

[242] McKight, P. E. and Najab, J., "Kruskal-wallis test," *The corsini encyclopedia of psychology*, pp. 1–1, 2010. DOI: 10.1002/9780470479216.corpsy0491.

[243] Hecke, T. V., "Power study of anova versus kruskal-wallis test," *Journal of Statistics and Management Systems*, vol. 15, no. 2-3, pp. 241–247, 2012. DOI: 10.1080/09720510.2012.10701623.

[244] Ostertagova, E., Ostertag, O., and Kováč, J., "Methodology and application of the kruskal-wallis test," *Applied mechanics and materials*, vol. 611, pp. 115–120, 2014. DOI: 10.4028/www.scientific.net/AMM.611.115.

[245] Bandt, C. and Pompe, B., "Permutation entropy: A natural complexity measure for time series," *Physical review letters*, vol. 88, no. 17, p. 174 102, 2002. DOI: 10.1103/PhysRevLett.88.174102.

[246] Richman, J. S. and Moorman, J. R., "Physiological time-series analysis using approximate entropy and sample entropy," *American journal of physiology-heart and circulatory physiology*, vol. 278, no. 6, H2039–H2049, 2000. DOI: 10.1152/ajpheart.2000.278.6.H2039.

[247] Richman, J. S., Lake, D. E., and Moorman, J. R., "Sample entropy," in *Methods in enzymology*, vol. 384, Elsevier, 2004, pp. 172–184. DOI: 10.1016/S0076-6879(04)84011-4.

[248] Eckmann, J.-P., Kamphorst, S. O., and Ruelle, D., "Recurrence plots of dynamical systems," in *Turbulence, Strange Attractors and Chaos*, World Scientific, 1995, pp. 441–445. DOI: 10.1142/9789812833709_0030.

[249] Rawald, T., Sips, M., and Marwan, N., "Pyrqa—conducting recurrence quantification analysis on very long time series efficiently," *Computers & Geosciences*, vol. 104, pp. 101–108, 2017. DOI: 10.1016/j.cageo.2016.11.016.

[250] Webber Jr, C. L. and Zbilut, J. P., "Recurrence quantification analysis of nonlinear dynamical systems," *Tutorials in contemporary nonlinear methods for the behavioral sciences*, vol. 94, no. 2005, pp. 26–94, 2005.

[251] Hurst, H. E., "The problem of long-term storage in reservoirs," *Hydrological Sciences Journal*, vol. 1, no. 3, pp. 13–27, 1956. DOI: 10.1080/02626665609493644.

[252] Kantelhardt, J. W., Koscielny-Bunde, E., Rego, H. H., Havlin, S., and Bunde, A., "Detecting long-range correlations with detrended fluctuation analysis," *Physica A: Statistical Mechanics and its Applications*, vol. 295, no. 3-4, pp. 441–454, 2001. DOI: 10.1016/S0378-4371(01)00144-3.

[253] Higuchi, T., "Approach to an irregular time series on the basis of the fractal theory," *Physica D: Nonlinear Phenomena*, vol. 31, no. 2, pp. 277–283, 1988. DOI: 10.1016/0167-2789(88)90081-4.

[254] Petrosian, A., "Kolmogorov complexity of finite sequences and recognition of different preictal eeg patterns," in *Proceedings eighth IEEE symposium on computer-based medical systems*, IEEE, 1995, pp. 212–217. DOI: 10.1109/CBMS.1995.465426.

[255] Grassberger, P. and Procaccia, I., "Characterization of strange attractors," *Physical review letters*, vol. 50, no. 5, p. 346, 1983. DOI: 10.1103/PhysRevLett.50.346.